공학박사학위논문

Heterogeneous Iron and Ruthenium Catalysts for Carbohydrate Based Biomass Transformations

탄수화물기반 바이오매스 전환을 위한 불균일계 철과 루테늄 촉매에 관한 연구

2015년 2월

서울대학교 대학원

화학생물공학부

김 요 한

탄수화물기반 바이오매스 전환을 위한

불균일계 철과 루테늄 촉매에 관한 연구

Heterogeneous Iron and Ruthenium Catalysts for Carbohydrate Based Biomass Transformations

지도 교수 이 윤 식

이 논문을 공학박사 학위논문으로 제출함

2014년 12월

서울대학교 대학원

화학생물공학부

김 요 한

김요한의 공학박사 학위논문을 인준함

2015년 1월

위 원 장 _____ (인)

부위원장 _____ (인)

위 원 _____ (인)

위 원 _____ (인)

위 원 _____ (인)

ABSTRACT

Heterogeneous Iron and Ruthenium Catalysts for Carbohydrate Based Biomass Transformations

(Supervisor: Yoon-Sik Lee, Ph.D.)

Yo-Han Kim

School of Chemical and Biological Engineering
The Graduate School
Seoul National University

Heterogeneous catalyst applications have increased attention in green chemistry. Polymer, metal oxide, and carbon are used as universal support materials to fabricate heterogeneous catalysts. Because the heterogeneous catalyst is generally insoluble in solvent, it can be separated easily from the reaction media by filtration and recycled numerous times. Moreover, it is possible to design the property of catalysts through chemical processes. Despite these advantages, the use of heterogeneous catalysts has not been increased in biomass conversion to produce value-added chemicals because of lower activities than homogeneous catalysts. Thus, the development of highly efficient heterogeneous catalyst still remains a challenge in biomass transformation.

In this thesis, two types of heterogeneous transition metal catalysts were utilized for efficient carbohydrate transformations: iron catalyst for fructose dehydration and ruthenium catalyst for 5-hydroxymethyl furfural (HMF) hydrogenation/oxidation.

In chapter 1, fructose dehydration into HMF by heterogeneous NHC-Fe catalyst is described. Developing HMF production process has been the most important task in C6 biomass transformation. So far, numerous HMF production methods from carbohydrates have been reported using various catalysts such as Bronsted and Lewis acid, and ionic liquids. *N*-heterocyclic carboene (NHC)-Fe complex grafted heterogeneous catalysts were prepared from polystyrene and graphene oxide support. NHC ligand provided a stable and strong metal-ligand bonding environment to form an efficient active site. Polystyrene supported NHC-Fe^{III} catalyst showed excellent fructose dehydration activity comparing to other supported NHC-metal catalysts. Graphene oxide grafted with NHC-Fe^{III} catalyst showed better catalytic performance than polystyrene supported one. Futhermore, the NHC-Fe^{III} grafted catalysts could be reused for 5 cycles without significant loss of activity.

In chapter 2, synthesis of HMF derivatives by heterogeneous ruthenium catalyst is described. HMF derivatives such as 2,5-furandicarboxylic acid (FDCA) and 2,5-bis(hydroxymethyl)furan (BHMF) have received a lot of attention because of their applicability. Zirconia was chosen as a suitable solid support with unique surface features, which can improve the catalytic ability of the metal active sites. Ruthenium active sites were immobilized on the surface

of zirconia without forming Ru(0) metal or RuO_2 nanoparticles (NPs). The well deposited Ru active site resulted in enhanced HMF hydrogenation and oxidation activity. The zirconia supported ruthenium catalyst showed excellent catalytic ability for oxidation of HMF into FDCA with molecular oxygen as a green oxidant. HMF was selectively reduced to BHMF with excellent yield under pressured hydrogen gas condition. Moreover, the zirconia supported ruthenium catalyst could be recycled over 10 times without significant loss of activity.

Keywords: biomass transformation, fructose dehydration, HMF oxidation, HMF reduction, FDCA, BHMF, NHC, iron catalyst, ruthenium catalyst, green chemistry, molecular oxygen, heterogeneous catalyst

Student Number: 2010-20985

TABLE OF CONTENTS

ABSTRACT.....i

TABLE OF CONTENTS.....iv

LIST OF TABLES.....vii

LIST OF FIGURES viii

LIST OF SCHEME.....xii

LIST OF ABBREVIATIONS xiv

Introduction

1. Concept of Green Chemistry 1

2. Biomass and Bio-refinery 4

2.1 Biomass: Renewable Carbon Source 4

2.2 Bio-refinery 6

2.2.1 Strategies of Biomass Transformation Processes..... 8

2.2.2 Biomass Based Platform Chemicals..... 10

2.3 Carbohydrate Biomass Conversion to Produce Platform Chemicals 12

2.3.1 Carbohydrate based Platform Chemicals 12

2.3.2 Synthesis of HMF from Carbohydrates..... 14

2.3.3 Synthesis of FDCA from HMF 17

2.3.4 Synthesis of BHMF from HMF 21

3. Catalysts.....23

3.1 Heterogeneous Catalysts 23

3.2 Catalytic Dehydration Reaction 25

3.3 Catalytic Oxidation Reaction 26

3.4 Catalytic Reduction Reaction.....31

3.5 Iron Catalyst in Organic Synthesis.....33

3.6 Ruthenium Catalyst in Organic Synthesis.....36

4. Research Objectives.....38

Chapter 1 Fructose Dehydration for Producing HMF

1. Experimental Section.....39

1.1. Chemicals and Materials 39

1.2 Characterization 41

1.3. Preparation of *N*-Heterocyclic Carbene (NHC)─Fe^{III} Catalyst.....43

1.3.1 Immobilization of 1-Methyl Imidazole on Chloromethyl Polystyrene..... 43

1.3.2 Preparation of PS-NHC-Fe^{III} Catalyst 44

1.3.3 Synthesis of NHC Ligand 45

1.3.4. Preparation of Graphene Oxide (GO) 47

1.3.5 Preparation of GO-NHC-Fe^{III} 48

1.4. Fructose Dehydration Reaction Catalyzed by NHC-Fe^{III} 49

1.4.1. General Experimental Procedure for Fructose Dehydration Reaction Catalyzed by PS-NHC-Fe^{III} 49

1.4.2 General Experimental Procedure for Fructose Dehydration Reaction Catalyzed by GO-NHC-Fe^{III} 50

1.4.3 Reusability Test of PS-NHC-Fe^{III} Catalysts for Fructose Dehydration Reaction..... 51

1.4.4 Reusability Test of GO-NHC-Fe^{III} Catalysts for Fructose Dehydration Reaction..... 52

1.5 Separation of HMF from DMSO 53

2. Result and Discussion 54

2.1. Characterization of PS-NHC-Fe^{III} 54

2.2. Dehydration of Fructose to HMF Catalyzed by PS-NHC-Metal Catalysts 65

2.3. Characterization of GO-NHC-Fe^{III}.....71

2.4. Dehydration of fructose to HMF catalyzed by GO-NHC-Fe^{III} catalysts..83

2.5. Separation of HMF from DMSO 89

3. Conclusion 91

Chapter 2. Conversion of HMF to Value Added Chemicals

1. Experimental Section.....92

1.1. Chemicals and Materials.....92

1.2. Characterization.....93

1.3. Oxidation of HMF into FDCA Catalyzed by $Ru(OH)_x/ZrO_2$.....95

1.4. Reduction of HMF into BHMF Catalyzed by $Ru(OH)_x/ZrO_2$.....96

2. Results and Discussion.....97

2.1. Characterization of $Ru(OH)_x/ZrO_2$ Catalyst.....97

2.2. Oxidation HMF into FDCA Catalyzed by $Ru(OH)_x/ZrO_2$.....103

2.3. Reduction HMF into BHMF Catalyzed by $Ru(OH)_x/ZrO_2$.....118

2.3.1. Reaction Optimization in Reduction HMF into BHMF..... 118

2.3.2. Hydrogenation of HMF into BHMF..... 123

3. Conclusion.....129

References.....130

Appendix.....151

Abstract in Korean.....161

LIST OF TABLES

Table 1. The 12 Principles of Green Chemistry 3
Table 2. Production of Biomass Based Chemicals 11
Table 3. The Top 12 Carbohydrate-based Building Blocks 13
Table 4. Atom Efficiency of Various Oxygen Containing Oxidants 27
Table 5. Dehydration of Fructose into HMF in The Presence of Various Heterogeneous Catalysts 68
Table 6. Difference in Dehydration Activity Depending on Metals 69
Table 7. Recycling Test of PS-NHC-Fe^{III} in Dehydration of Fructose into HMF 70
Table 8. Dehydration of Fructose into HMF in The Presence of Various Heterogeneous Catalysts 86
Table 9. Recycling Test of Fructose Dehydration into HMF Catalyzed by GO-NHC-Fe^{III} 88
Table 10. The Effect of Reaction Solvent on The Aerobic Oxidation of HMF 107
Table 11. The Effect of Base on Aerobic Oxidation of HMF 108
Table 12. The Effect of Reaction Temperature, Pressure of Molecular Oxygen, and Catalyst Amount on The Aerobic Oxidation of HMF 110
Table 13. The Results of The Aerobic Oxidation of HMF into HMF Derivatives Using Different Catalysts 113
Table 14. Recycle Test of $Ru(OH)_x/ZrO_2$ in Oxidation of HMF 117
Table 15. Hydrogenation of HMF Result Depending on Various Solvent 119
Table 16. Hydrogenation of HMF Result Depending on Reaction Temperature 120
Table 17. Hydrogenation of HMF Result Depending on Various Hydrogen Pressure 121
Table 18. Hydrogenation of HMF Result Depending on Amount of Catalyst 122
Table 19. The Results of The Aerobic Oxidation of HMF into HMF

Derivatives Using Different Catalysts 127
Table 20. Recycling Test of $Ru(OH)_x/ZrO_2$ in Hydrogenation of HMF ... 128

LIST OF FIGURES

Figure 1. Chemical structure of biomass feedstocks. 5
Figure 2. Overview of the processing of crude feedstocks to refined products in a sustainable bio-refinery. 7
Figure 3. Strategies of biomass conversion processes. 9
Figure 4. Scheme of HMF synthesis and their derivatives. 16
Figure 5. Oxidation of HMF to 2,5-furandicarboxylic acid (FDCA). 19
Figure 6. Oxidation of HMF in methanol. 20
Figure 7. Reduction of 5-hydroxymethyl furfural (HMF) to various intermediates. 22
Figure 8. Number of publications from 1997 to 2013, according to a search in the Web of Science database of ISI Web of Knowledge. 24
Figure 9. Reaction of triplet oxygen and formation of Metal-oxygen species. 29
Figure 10. Divergent products in the hydrogenation of cis-jasmone catalytzed by copper or palladium. 32
Figure 11. Iron species in the biological system. 34
Figure 12. Common synthetic routes toward NHC-Fe complex. 35
Figure 13. Extraction procedure for the separation of HMF from DMSO. 53
Figure 14. Swelling properties of CM PS and PS-IM with various solvent. 57
Figure 15. Fourier-transform infrared spectroscopy spectra. (a) CM PS, (b) PS-IM, (c) PS-NHC-Fe^{III}. 58
Figure 16. Scanning electron microscope image of (a) PS-IM, (b) freshly prepared PS-NHC-Fe^{III} and (c) reused PS-NHC-Fe^{III}. 58
Figure 17. X-ray diffraction patterns of (a) PS-IM, (b) freshly prepared PS-NHC-Fe^{III}, and (c) reused PS-NHC-Fe^{III}. 60
Figure 18. X-ray photoelectron spectra of (a) PS-IM and PS-NHC-Fe^{III} (wide scan), (b) Fe 2p from PS-NHC-Fe^{III}, N 1s from (c) PS-IM and (d) PS-NHC-Fe^{III}, and Cl 2p from (e) PS-NHC-Fe^{III} 62
Figure 19. Transmission electron microscopy images of (a) GO, (b) GO-IM,

(c) GO-NHC-Fe^{III}. 76
Figure 20. FT-IR spectra of GO, Go-IM, and GO-NHC-Fe^{III}. 76
Figure 21. X-ray photoelectron (a) C 1s of Go, (b) C 1s of GO-IL, (c) C 1s of GO-NHC-Fe^{III}, (d) N 1s of GO-IM, (e) N 1s of Go-NHC-Fe^{III}, and (f) Fe 2p of Go-NHC-Fe^{III}, (g) Cl 2p of Go-NHC-Fe^{III}. 82
Figure 22. X-ray diffraction patterns of (a) Natural graphite, (b) Graphene xide, and (c) GO-NHC-Fe^{III}. 82
Figure 23. Recovery of HMF from DMSO using extraction method with various organic solvents after (a) 4 times and (b) 10 times dilution with distilled water (red line indicates the theoretical recovery yield of HMF at 100%). 90
Figure 24. Surface morphologies of (a) ZrO2 (b) Ru(OH)x/ZrO2 and (c) used Ru(OH)x/ZrO2 obtained from high resolution transmission electon microscope (HR-TEM), which shows d-spacing of (a) 0.29 nm, (b) 0.29 nm (ZrO2 as a reference: 0.29 nm). 98
Figure 25. X-ray diffraction patterns (XRD) of Ru(OH)x/ZrO2 (red) and ZrO2 (black). 100
Figure 26. XPS spectra of $Ru(OH)_x/ZrO_2$. (a) Peaks of ruthenium 3d from $Ru(OH)_x/ZrO_2$, (b) peaks of oxygen 1s from $Ru(OH)_x/ZrO_2$. O 1s peak around 531 eV came from carbon tape background. 102
Figure 27. Time course of HMF conversion and product distribution during the aerobic oxidation of HMF using $Ru(OH)_x/ZrO_2$. Reaction conditions: HMF (0.5 mmol), water (3 mL), $Ru(OH)_x/ZrO_2$ (2 mol%), NaOH (2 mmol), O_2 1 bar. 105

LIST OF SCHEMES

Scheme 1. Scheme of transition metal catalyzed oxidation mechanism with molecular oxygen. (a) Metal nanoparticle catalyzed oxidation reaction (b) Metal-Ligand complex catalyzed oxidation reaction.. 30

Scheme 2. The strategy to develop fructose based biomass transformation processes. 38

Scheme 3. Preparation of polystyrene-supported NHC metal catalysts. 55

Scheme 4. Dehydration of fructose into HMF catalyzed by the PS-NHC-Fe^{III} catalyst. 66

Scheme 5. Synthetic scheme of imidazolium based ionic liquid. 72

Scheme 6. Synthetic scheme of GO-NHC-Fe^{III}. 75

Scheme 7. Dehydration of fructose into HMF catalyzed by GO-NHC-Fe^{III}. 85

Scheme 8. The oxidation of HMF into the FDCA by two routes. Route A: the aldehyde group of HMF is oxidized to form a carboxylic acid. Route B: the hydroxyl group of HMF is oxidized to yield the dialdehyde. 103

Scheme 9. A possible reaction mechanism for $Ru(OH)_x/ZrO_2$ catalyzed oxidation of HMF in water. 115

Scheme 10. A possible reaction mechanism for Ru(OH)x/ZrO2 catalyzed hydrogenation of HMF in presince of 2-propanol. 126

LIST OF ABBREVIATIONS

API	1-(3-aminopropyl)imidazole
ATR	attenuated total reflection
BHMF	2,5-bis(hydroxylmethyl)furan
BHMTHF	2,5-bis(hydroxymethyl)tetrahydrofuran
Boc	tert-butyloxycarbony
$CDCl_3$	chloroform-d
CM PS	chloromethyl polystyrene resin
CPME	cyclopentyl methyl ether
DCM	dichloromethane
DEE	diethyl ether
DFF	2,5-diformylfuran
DIC	*N, N'*-diisopropylcarbodiimide
2,5-DMF	2,5-dimethylfuran
DMF	*N, N*-dimethyl formamide
DMSO	dimethyl sulfoxide
DMTHF	2,5-dimethyltetrahydrofuran
EA	ethyl acetate
EDS	energy dispersive X-ray spectroscopy
EtOH	ethanol

FDCA	2,5-furandicarboxylic acid
FDMC	2,5-furandimehylcarbonate
FFCA	2-formylfurancarboxylic acid
FHMTHF	2-formyl-5-(hydroxylmethyl)tetrahydrofuran
FT-IR	Fourier-transform infrared
GC	gas chromatography
GC/MS	gas chromatography/mass spectrometry
GO	graphene oxide
GO-IL	ionic liquid grafted graphene oxide
GO-NHC-Fe^{III}	*N*-heterocyclic carbene-Fe grafted graphene oxide
^{1}H NMR	proton nuclear magnetic resonance
H_2SO_4	surfuric acid
H_3PO_4	phosphoric acid
HMF	5-hydroxylmethyl furfural
HMFCA	5-hydroxylmethyl furancarboxylic acid
HMMF	5-hydroxylmethyl methylfuranate
HOBt	1-hydroxybenzotriazole
HPLC	high performance liquid chromatography
HR-TEM	high resolution-transmission electron microscope
ICP-AES	inductively coupled plasma-atomic emission spectroscopy
ILs	ionic liquids

MeOH	methanol
MIBK	4-methyl-2-pentanone
MS	mass spectrometry
n.d.	not detected
NHC	*N*-heterocyclic carbene
PS-IM	ionic liquid grafted polystyrene
PS-NHC-Fe^{III}	*N*-heterocyclic carbene-Fe^{III} grafted polystyrene
$Ru(OH)_x/ZrO_2$	ruthenium hydroxide deposited zirconium oxide
SEM	scanning electron microscope
TEA	triethyl amine
TEM	transmission electron microscope
TFA	trufluoroacetic acid
THF	tetrahydrofuran
TLC	thin layer chromatography
TMS	tetramethylsilane
TOF	turnover frequency
TON	turnover number
XPS	X-ray photoelectron spectrometry
XRD	X-ray diffraction

Introduction

1. Concept of Green Chemistry

Modern human society has gained benefits from chemical industries due to their chemical product versatility and capability of mass production. This prosperity has been obtained at the cost of low fossil fuels prices and has had adverse effects on the environment.[1] In this regard, scientist communities have developed more environmentally benign processes in the chemical industry to reduce undesirable side effects. This has led to a paradigm shift of chemical processes from traditional concepts to environmentally acceptable ones, known as Green Chemistry, to achieve sustainable technology. Green Chemistry can reduce dependency on petroleum-based chemical industries, as well as reduce the emission of greenhouse gases to the environment.[2] Furthermore, Green Chemistry can substitute biomass based chemicals for petrochemicals, and will reduce the carbon footprint from the petrochemical based products.[3]

The concept of green chemistry is related to chemical processes, which utilize renewable materials and reduce or avoid substances hazardous to humans.

Furthermore, atom economy is one goal of green chemistry, removing inefficient steps from conventional processes, and introducing new technologies such as bio-catalysis, heterogeneous catalysis and renewable carbon sources.[4] As Anatase suggested, this view is embedded in the 12 principles of Green Chemistry listed in Table 2.[5] To achieve greening chemical approaches in the chemical industry, Sheldon has suggested several methodologies: (i) developing catalysis (avoiding stoichiometric reagents), (ii) introducing renewable carbon sources (reducing CO_2 emission), and (iii) reducing E-factor (the weight of waste per unit weight of desired product).

Table 1. The 12 Principles of Green Chemistry[5]

1.	It is better to **prevent waste** than to treat or clean up waste after it is formed.
2.	Synthetic methods should be designed to maximize the incorporation of all materials used into the final product.
3.	Wherever practicable, synthetic methodologies should be designed to use and generate substances that **processes little or no toxicity to human health and the environment.**
4.	Chemical products should be designed to preserve efficacy of function while **reducing toxicity**.
5.	The use of auxiliary substances (e.g. solvents, separation agents, etc.) should be made unnecessary wherever possible, and innocuous when used.
6.	**Energy requirements should be recognized for their environmental and economic impacts** and should be minimized. Synthetic methods should be conducted at ambient temperature and pressure.
7.	A raw material of feedstock should be renewable rather than depleting wherever technically and economically practicable.
8.	Unnecessary derivatization (blocking group, protection/deprotection, and temporary modification of physical/chemical processes) should be avoided whenever possible.
9.	**Catalytic reagents** (as selective as possible) are superior to stoichiometric reagents.
10.	Chemical products should be designed to preserve efficacy of function while reducing toxicity.
11.	Analytical methodologies need to be developed to allow for real-time, in-process monitoring and control prior to the formation of hazardous substances.
12.	Substances and the form of a substance used in a chemical process should be chosen so as to minimize the potential for chemical accidents, including releases, explosions and fires.

2. Biomass and Bio-refinery

2.1 Biomass: Renewable Carbon Source

As global warming is now threatening the prosperity of human civilization, developing sustainable green energy has become a crucial worldwide issue. The Kyoto protocol for reducing society's dependence on petroleum has drawn the attention of scientists to the use of renewable and sustainable sources of energy for transportation and fine chemicals production.[6] Consequently, biomass, generated from CO_2, H_2O and sunlight, has been considered as a renewable source of both energy and carbon in current industries, replacing fossil-based ones. As illustrated in Figure 1, three classes of biomass feedstocks are appropriate for the production of energy and chemicals: lignocellulose, triglyceride, and starch. Lignocellosic feedstock is the most abundant biomass not involved in food chains. Triglyceride feedstocks, comprised of fatty acid and glycerol, are major sources of biofuel. Starch feedstocks are biopolymers of glucose joined by a glycosidic linkage, which amounts to 75 % of annually regenerated biomass. In this sense, glucose and starch are considered to be the most abundant bio-refinery starters.[7]

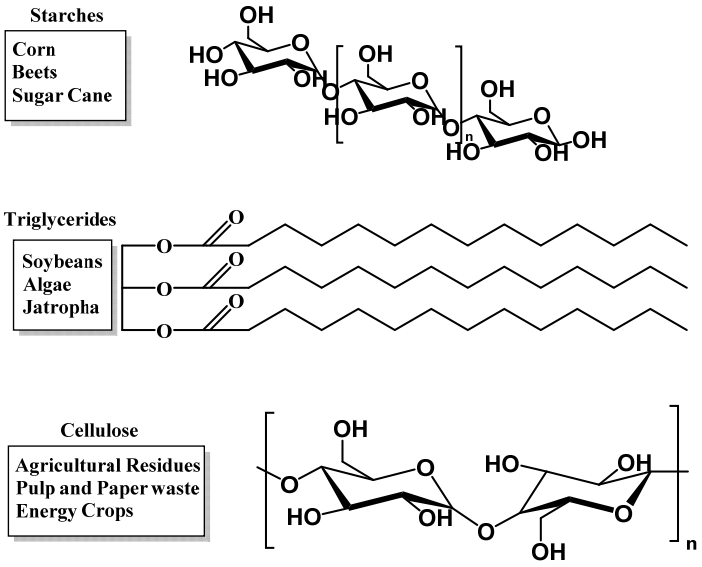

Figure 1. Chemical structure of biomass feedstocks.[7]

2.2 Bio-refinery

Bio-refinery has been described as a facility that produces power, fuels, and chemicals from biomass, including biomass conversion processes and supplies. In the current petrochemical industry, crude oil is refined to produce various hydrocarbon feedstocks that can be transformed into chemical intermediates and fine chemicals. Similarly, the transformation of biomass into chemical products and/or energy involves a series of feed streams, interconnected processes, and chemical intermediates illustrated in Figure 2.[8] Because the carbon cycle of bio-refinery is quite different from the petrochemical system, the release of greenhouse gases is decreased through cycles of biomass regeneration and utilization. The US Department of Energy Accession has a political vision to dramatically reduce the greenhouse gases, with 51% transportation fuel and 55 % chemicals produced from biomass by 2030.[9]

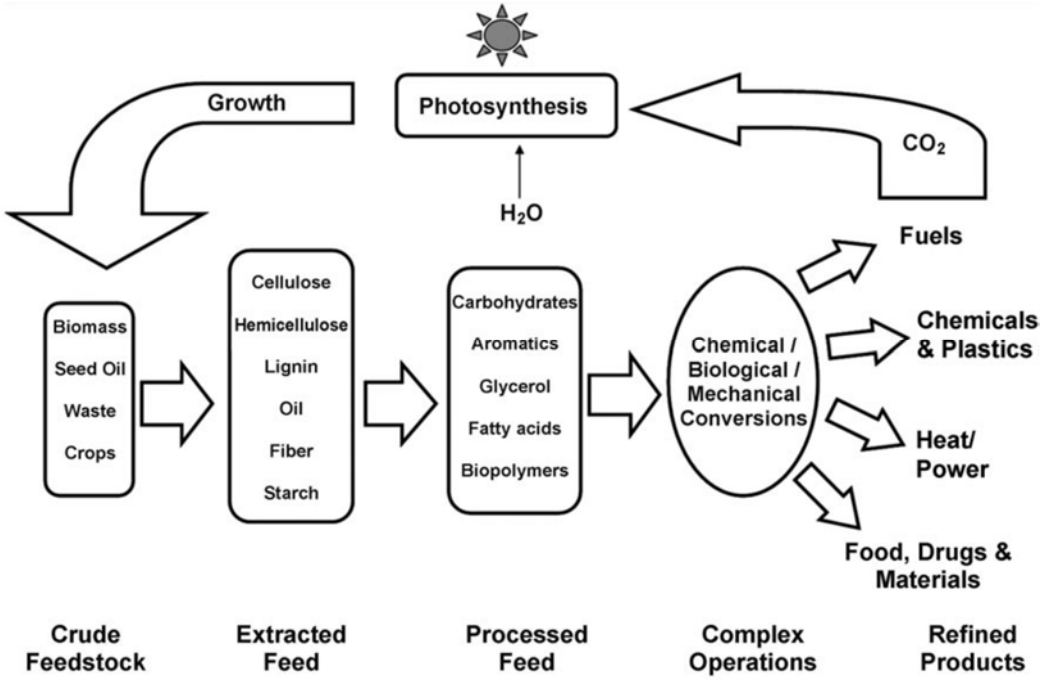

Figure 2. Overview of the processing of crude feedstocks to refined products in a sustainable bio-refinery.[8]

2.2.1 Strategies of Biomass Transformation Processes.

Although abundant literature on biomass conversion methodologies and processes have been published, they can be classified into three categories (Figure 3). First, manufacturing platform chemicals by depolymerization and/or fermentation of biomass as building blocks for fine chemicals and fine chemical intermediates. Second, production of large amounts of end-products that are a mixture of chemicals with similar functionalities. Third, introducing new functionalities to the biomass by chemical modification.[10] For example, thermal treatment of biomass can produce a complex mixture of molecules connected to hydroprocessing to improve product quality.[11] The catalytic depolymerization of carbohydrates[12] and transesterification[13] can lead to the production of platform chemicals. Modified cellulose fiber[14] is an example of introducing new functionalities. From the green chemistry point of view, the strategies described above can be combined with each other to develop the desired product. Furthermore, they are inevitably involved with the “catalytic process”.[15]

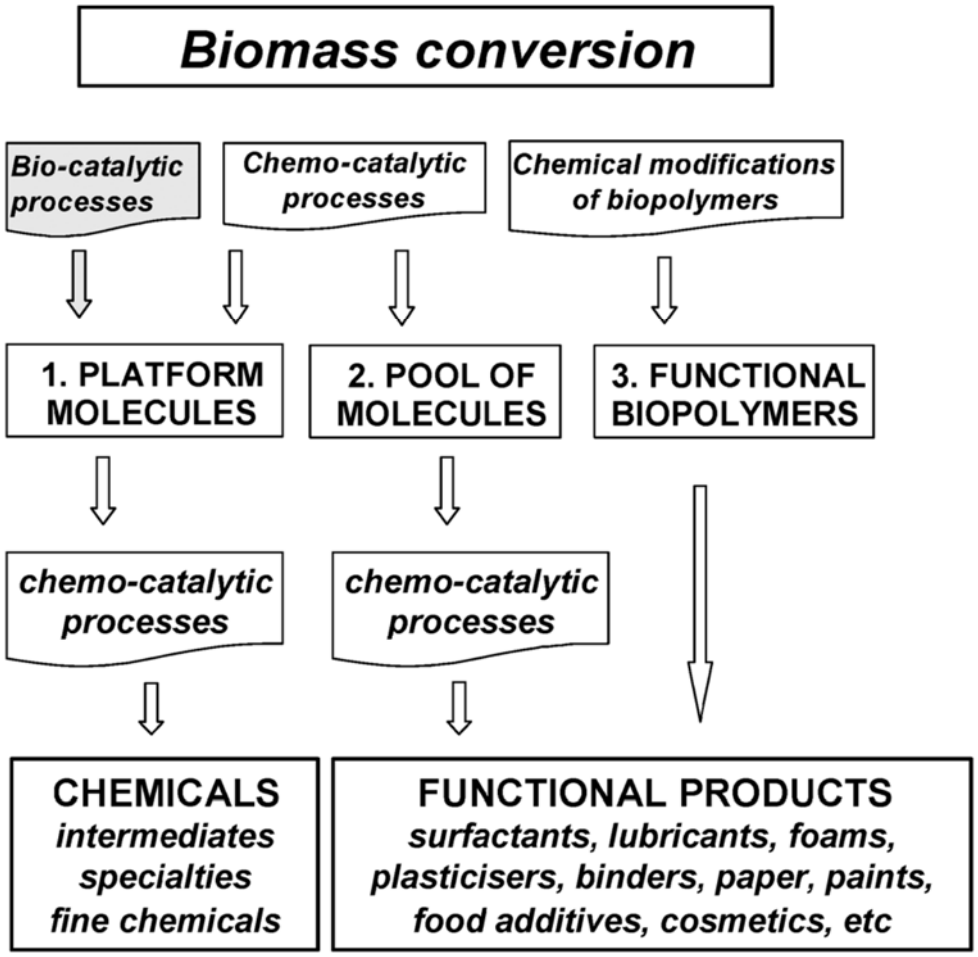

Figure 3. Strategies of biomass conversion processes.[10]

2.2.2 Biomass Based Platform Chemicals

Recently, the renewable arena has been widened by the involvement of many researchers and companies.[16] As shown in Table 3, a wide range of chemicals have been manufactured that possess strong growth potential in the chemical industry. Among the listed chemicals, C6 and C3 based chemicals are predominant due to abundance of C6 feedstocks in biomass. Although most of the chemicals on the list were already manufactured from petrochemicals, they now can be produced by enzymatic fermentation and catalytic reaction with biomass.

Table 2. Production of Biomass Based Chemicals[16]

	Products with strong growth potential		Bio-based Chemicals in the pipeline	
Number of carbon	Chemical	Company	Chemical	Company
1	Methanol	BioMCN	Formic acid	Maine BioProducts
2	Ehtylene	DOW, Braskem	Ethyl acetate	Zeachem
	Ethanol	Many	Glycolic acid	Metabolix Explorer
	Ethylene glycol	JBF industries, Greencol Taiwan	Acetic acid	Wacker
3	Lactic acid	Purac, Henan Jindan	Acrylic acid	Gargil, Perstorp, DOW
	Glycerol	Many	Propylene	Mitsui Chemicals, Toyota Tsusho
	Epichlorohydrin	DOW, Solvay	3-hydroxypropionic acid	Cargil
	1,3-propanediol	DuPont/Tate&Lyle	n-propanol	Braskem
	Ethyl lactate	Vertec BioSolvents	Isopropanol	Mitsui Chemicals
	Propylene glycol	ADM, DuPont		
4	n-butanol	Buramax, Butalco	1,4-Butanediol	Mitsubishi Chemical
	Iso-butanol	Gevo, Butamax	Methyl metacrylate	Lucite, Mitsubishi Rayon
	Succinic acid	BASF, Reverdia	Iso-butene	Gevo/Lanxess
5	Furfural	Many	Itaconic acid	Itaconix
	Xylitol	Lenzing	Isoprene	Goodyear, Amyris
	Glutamic acid	Global Biotech, Juhua	Levulinic acid	Avantium, Maine BioProducts
6	Sorbitol	Roquette, ADM	Adipic acid	Verdezyne, BioAmber
	Isosorbide	Roquette	2,5-Furandicarboxylic acid	Avantium
	Lysine	Global Biotech, BBCA	Glucaric acid	Rivertop Renewables
	Citric acid	DSM, Cargil	Caprolactam	DSM

2.3 Carbohydrate Biomass Conversion to Produce Platform Chemicals

2.3.1 Carbohydrate based Platform Chemicals

The most abundant, fastest-growing, and major composition of plant based biomass are carbohydrates, and these represent 75 % of annually regenerated feedstocks.[17] Especially, hexoses and pentoses, such as glucose, fructose and xylose, are the most abundant and readily available biomass. As shown in Table 4, Werpy and Petersen have listed 12 top potential platform chemicals from glucose, fructose and xylose.[18] Comparing Table 2 and Table 3, although most of the chemicals listed are overlapped, it is clear that carbohydrate-derived platform chemicals have become major marketable bio-refinery products. Especially, 5-hydroxymethyl furfural (HMF) is major platform chemical for manufacturing value-added products, such as 2,5-furandicarboxylic acid, and levulinic acid.[19]

Table 3. The Top 12 Carbohydrate-based Building Blocks[16]

Succinic, Fumaric, and Maleic	Itaconic acid
2,5-Furandicarboxylic acid	Levulinic acid
3-Hydroxyl propionic acid	3-Hydroxybutyrolactone
Aspartic acid	Glycerol
Glutaric acid	Sorbitol
Glutamic acid	Xylitol/Arabinitol

2.3.2 Synthesis of HMF from Carbohydrates

HMF is synthesized by the dehydration of fructose in the presence of acid catalysts or by more complex catalytic systems from glucose and polysaccharides.[20] As a being synthesized from C6 carbohydrate unit, HMF is the most important and promising platform chemical due to its valuable derivatives such as levulinic acid, 2,5-bis(hydoxymethyl)furan (2,5-BHF), 2,5-diformylfuran (2,5-DFF) and 2,5-furandicarboxylic acid (2,5-FDCA) (Figure 4). Since HMF derivatives are listed in the "Top 10 valuable chemicals" by the US Department of Energy, the key issue is to develop economically acceptable manufacturing processes that can be scaled up at industrial scale.[18]

HMF production technologies have been advanced in the dehydration process of fructose. Aqueous fructose solution acidified with HCl has yielded 63 % of HMF at 52 % fructose conversion.[21] Although there are risks of sulfur contamination and difficulty of DMSO removal, high HMF yield was obtained in DMSO with the least amount of side product such as humin, formic acid, and levulinic acid.[22-27] Dumesic et al. have developed an advanced biphasic HMF production system that

could extract HMF to organic phase, enhancing conversion and yield.[28, 29] The use of ionic liquids (ILs) was intensively investigated because ILs are compatible with catalysts and give much higher HMF yield from not only fructose,[30, 31] but also other conventionally available carbohydrates such as glucose,[32-35] sucrose,[36, 37] inulin,[38] cellulose,[32, 36] and starch[34]. Even though various solvent systems and agents have been utilized for the conversion of fructose into HMF, the majority of catalysts are still homogeneous acid catalysts.

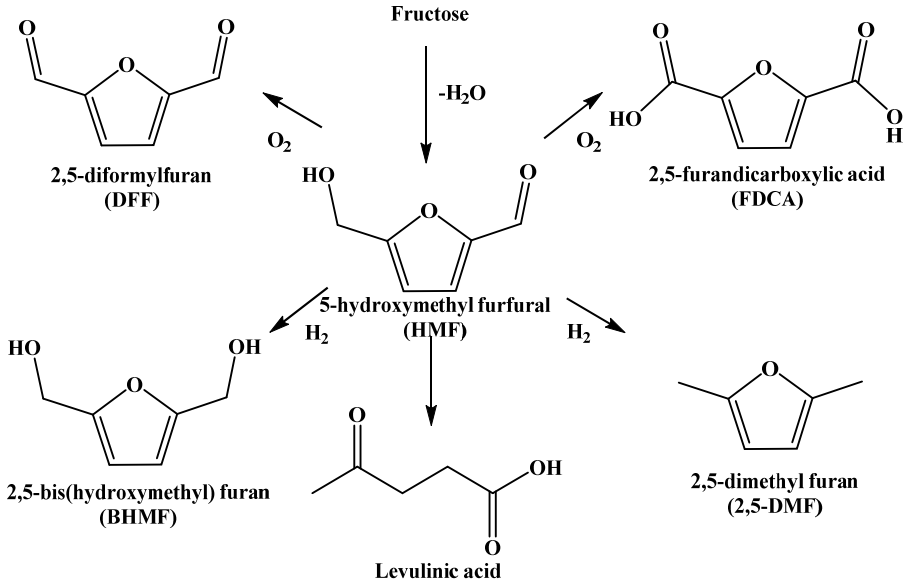

Figure 4. Scheme of HMF synthesis and their derivatives.

2.3.3 Synthesis of FDCA from HMF

HMF contains a carbonyl group, a furan ring, and a hydroxyl group, and can be transformed into a wide range of chemical intermediates including mono- and diacids, dicarbonyls, tetrahydrofurans, diols, anhydrides, and esters.[16] The HMF derivatives can be applied as polymer monomers,[39-41] chemical intermediates,[42] fine chemicals,[43] solvents,[44, 45] fuel additives,[46] and bio-fuels.[47-49] Due to the presence of aldehyde and hydroxyl group in HMF, oxidation of each functional group can yield different types of oxidized products: 5-hydroxymethyl furancarboxylic acid (HMFCA), 2,5-diformylfuran (DFF), 5-formyl furancarboxylic acid (FFCA), and 2,5-furandicarboxylic acid (FDCA) (Figure 5). 2,5-furandicarboxylic acid (FDCA), as one of the 12 chemical building blocks, is a suitable substitute for terephthalic or isophthalic acids used in the production of polyesters, polyamides, and polyurethanes.[22] FDCA can be easily obtained by using stoichiometric amounts of oxidants (e.g. $KMnO_4$). However, from the green chemistry point of view, the use of molecular oxygen with heterogeneous catalyst is obviously preferred.[50] In addition, many efforts have been tried to develop the

oxidation process of HMF to FDCA with heterogeneous catalyst and molecular oxygen under basic condition. Previous reports on the oxidation of HMF to FDCA describe the use of supported metal catalysts such as Pt/C,[51, 52] Pt/Al_2O_3,[53] and Pt/ZrO_2[54]. Aqueous aerobic oxidation reactions by supported gold catalysts such as gold Au/TiO_2,[55, 56] Au/CeO_2,[57] Au/Fe_2O_3,[58] and Au/C[58] have been recently reported. The reaction profile of HMF oxidation shows that HMF is converted quickly to HMFCA and transformed slowly to FDCA under basic condition. To avoid the use of bases, hydrotalcite was used as a supporting material and recoverable base.[59] When the oxidation of HMF is carried out in alcohol solvents (Figure 6),[60] the corresponding esters are obtained and side reactions are inevitable, unlike with aqueous reactions. Thus, when considering HMF oxidation to FDCA, the use of an aqueous system is preferable.

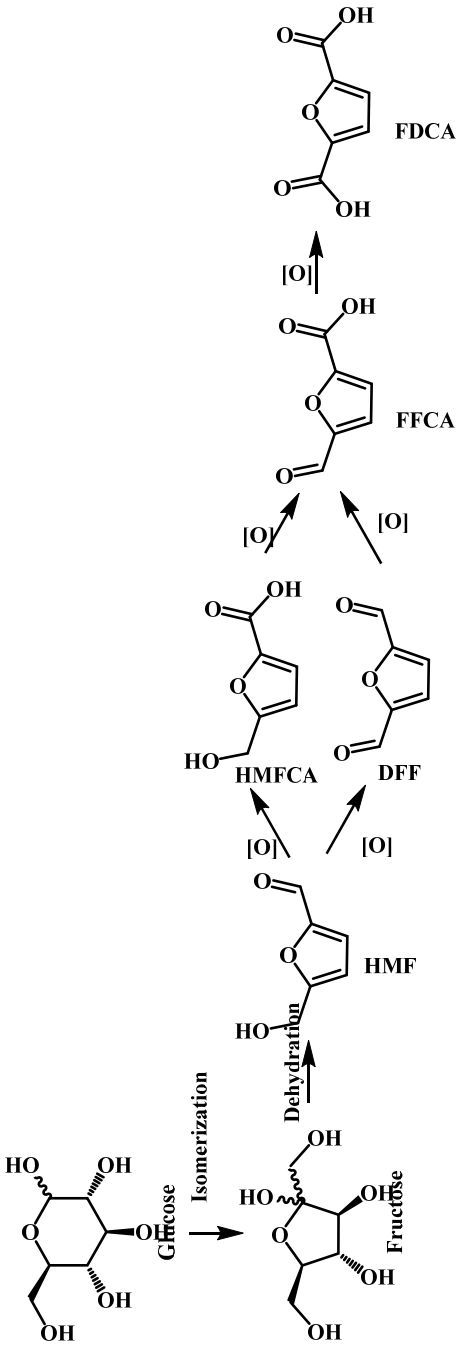

Figure 5. Oxidation of HMF to 2,5-furandicarboxylic acid (FDCA).

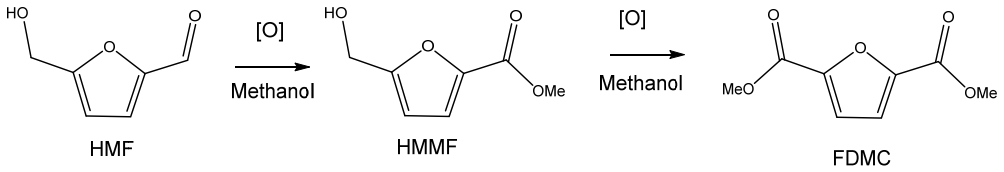

Figure 6. Oxidation of HMF in methanol.

2.3.4 Synthesis of BHMF from HMF

The selective hydrogenation of HMF can lead to interesting products, which can be applied for bio-fuel, solvents, and polymer intermediates.[61, 62] As shown in Figure 7, hydrogenation of HMF can yield 2,5-bis-(hyroxymethyl)furan (BHMF), 2-formyl-5-(hydroxymethyl)tetrahydrofuran (FHMTHF), 2,5-bis(hydroxymethyl)tetrahydro-furan (BHMTHF) depending on the reduction condition. When hydrogenolysis of hydroxyl groups of BHMF and BHMTHF occurs, 2,5-dimethylfuran (DMF) and 2,5-dimethyltetrahydrofuran (DMTHF) are produced. These hydrogenated HMF derivatives are attractive as potential alternatives to petrochemicals. Especially, the diol groups in BHMF and BHMTHF can be directly utilized as monomers in the preparation of polyesters, polyamide, and polyurethane.[63]

The catalytic hydrogenation of HMF to BHMF and BHMTHF have been reported with silica supported Ni and Co catalysts,[64] conventional Pd, Pt, Ru, Ir, Re catalysts,[65] supported Ru, Pd, and Pt catalysts.[66] Although many catalysts have been reported, selective hydrogenation has yet to be achieved.

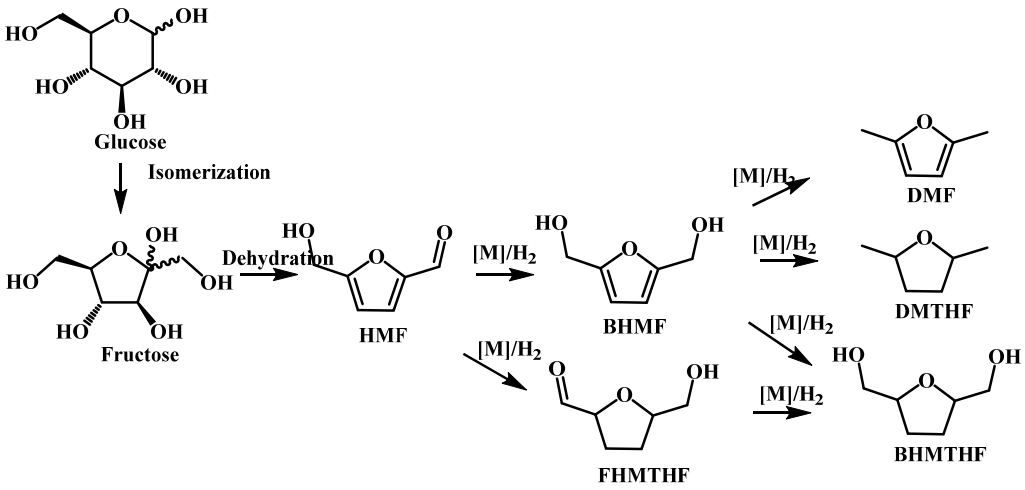

Figure 7. Reduction of 5-hydroxymethyl furfural (HMF) to various intermediates.

3. Catalysts

3.1 Heterogeneous Catalysts

As mentioned in section 1.2, heterogeneous catalysts are incorporated into the 12 principles of green chemistry. It is not only a particular scientific approach for breakthroughs, but also a change in the framework dictating strategies on how to conduct organic synthesis. In particular, heterogeneous catalysts can address the goals of green chemistry by providing easy separation of product and catalyst, thereby eliminating additional processes.[2] This change can be recognized in the number of publications during the last decade. As shown in Figure 8, ‘green’ topics have been increasing in chemistry and are linked with heterogeneous catalysis in green chemistry.

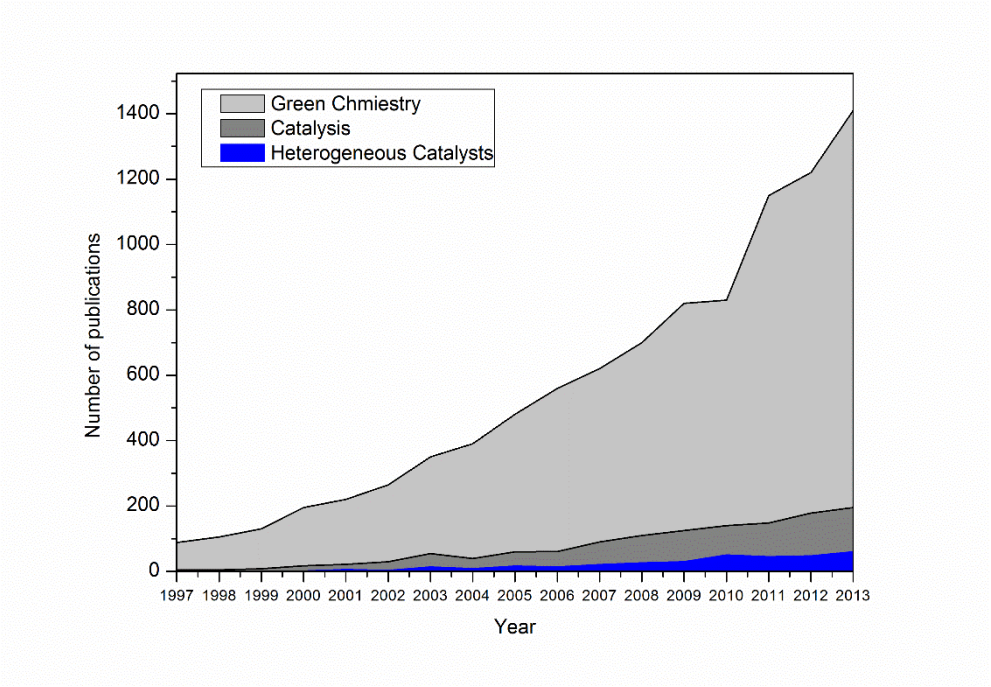

Figure 8. Number of publications from 1997 to 2013, according to a search in the Web of Science database of ISI Web of Knowledge.

3.2 Catalytic Dehydration Reaction

A major issue in dehydration reactions is how to create a better leaving group from the hydroxyl group on a molecule. Generally, Brønsted acid enhances the reaction rate by protonation of the hydroxyl group.[20] Liquid acids as well as solids acids have been applied for dehydration reactions such as glycerol to acrolein[67], alcohols to alkenes,[68] anhydrous, and rearranged products. Currently, dehydration reactions have received much attention due to the important reaction that produces HMF via carbohydrate dehydration. Like other dehydration reactions, carbohydrate dehydrations have been carried out under liquid acids and solid acids. However, corrosive conditions and separation difficulties have caused serious environmental issues and high operation costs when liquid acids and sulfur containing solid acids are utilized. Meanwhile, Lewis acids such as ruthenium, iron, aluminum, tin catalyzed dehydration methodology are becoming popular as an alternatives to overcome the above mentioned drawbacks.[69] However, most of the transition metals still cause side reactions due to their inferior catalytic performances. Thus, heterogeneous Lewis acid catalysts have been suggested to achieve selective dehydration reactions.

3.3 Catalytic Oxidation Reaction

A catalytic selective oxidation reaction has received notable attention and is one of the most important reactions in the chemical industry for producing fine chemicals.[70, 71] Traditional oxidation methods for oxidation reactions require stoichiometric amounts of oxidants (e.g., inorganic salt, Oxone, and 2-iodoxybenzoic acid), which are highly toxic, and produce large amounts of harmful metal salts as a waste. For economic reasons and atom efficiency, using environmentally friendly oxidants, such as molecular oxygen or hydrogen peroxide as the primary oxidant, is very important to reduce chemical waste.[72, 73] . In an aspect of green and sustainable chemistry, molecular oxygen is believed as an ideal oxidant because of its environmentally friendly characters and highly atom-efficient oxidant per weight (50% in Table 3). Generally, there are two fundamental challenges when the transition metal catalyzed oxidation reaction with molecular oxygen as the oxidant: (i) The molecular oxygen is hard to activate at mild conditions in the direct oxidation of organic substrate. (ii) The chemoselectivity is required to achieve in the oxidation reaction. In addition, replacement noble metal catalysts such as Pt, Pd, and Au is

required due to their expensive cost and decaying activity. Fortunately, there have been significant advances in non-noble metal catalyzed oxidation reactions employing molecular oxygen as the sole oxidant.[74]

Table 4. Atom Efficiency of Various Oxygen Containing Oxidants[73]

Donor	**Active Oxygen (%)**	**Co-product**
O_2	50	H_2O
H_2O_2	14.1	H_2O
NaOCl	21.6	NaCl
$NaIO_4$	7.5	$NaIO_3$
tert-BuO_2H	17.8	*tert*-BuOH
O_3	33.3	O_2

The activation mechanism of molecular oxygen is described in Figure 9. Due to parallel spin of unpaired electrons in molecular oxygen (triplet state), direct reaction of molecular oxygen ($^3O_2$) with singlet organic substrates has a spin hindrance that results in very low reaction. The reaction of triplet molecular oxygen with a transition metal ion produces a superoxometal complex and subsequent inter- or intra-molecular electron-transfer leads to the formation of a variety of metal-oxygen species that can provide oxygen species on organic substrates. Generally, in the presence of metal catalysts, oxidation reaction with molecular oxygen involves free radical processes. Due to this ubiquity of free radicals, the oxidation mechanism with molecular oxygen is harder to interpret than that of hydrogenation.[73] As shown in Scheme 1, different catalytic cycle showed in molecular oxygen mediated chemical oxidation between noble metal nanoparticle catalysts (e.g.Au, Pt, and Pd) and transition metal-ligand complex. In case of noble metal nanoparticle catalyst, the oxidation state of metal active site on the surface of metal NPs can be changed during the substrate oxidation, subsequently, generating of metal-hydride. The metal-oxo species (M=O) can occur during the oxidation of hydride species on the metal-hydride by molecular oxygen.

the metal active site (metal(0)) can be regenerated by reduction of oxo species by another metal-hydride. Metal-hydride species also can generate in case of metal ligand complex catalyzed oxidation and can be oxidized by molecular oxygen. Otherwise, metal-oxo species did not occurred and the oxidation state of metal did not change.

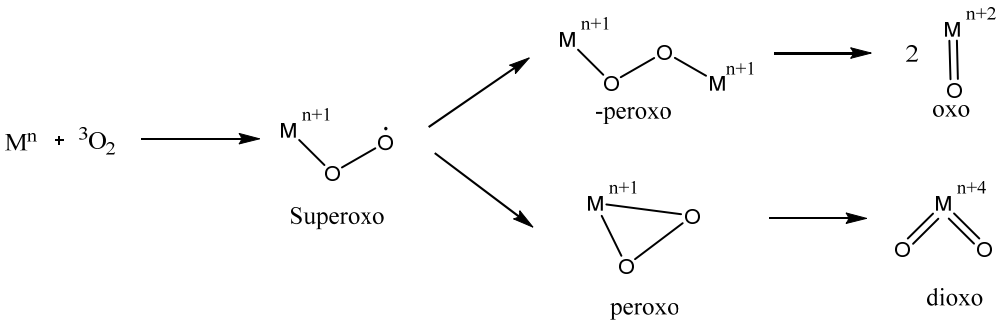

Figure 9. Reaction of triplet oxygen and formation of Metal-oxygen species.

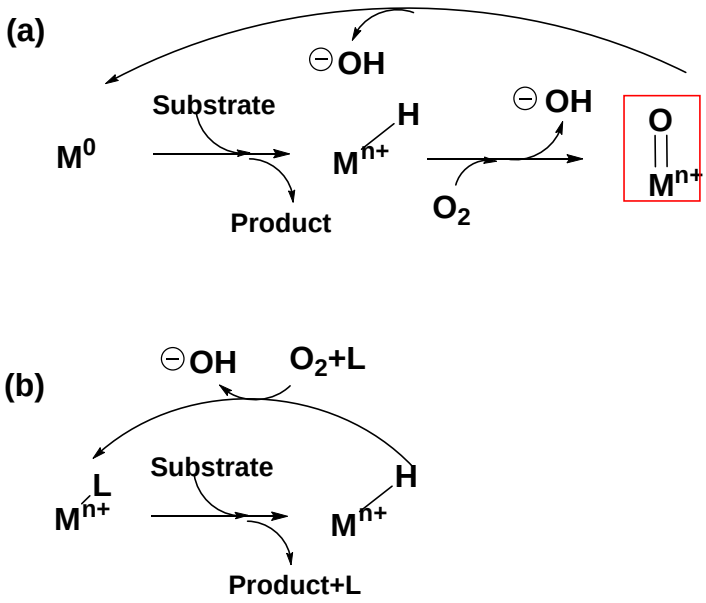

Scheme 1. Scheme of transition metal catalyzed oxidation mechanism with molecular oxygen. (a) Metal nanoparticle catalyzed oxidation reaction (b) Metal-Ligand complex catalyzed oxidation reaction.

3.4 Catalytic Reduction Reaction

Catalytic hydrogenation using hydrogen gas with heterogeneous catalysts is considered to be the most important reaction both in the chemical industry and in organic chemistry for production of fine chemicals. Since hydrogen is obviously a clean reducing agent, heterogeneous catalytic hydrogenation has several advantages: (i) highly selective in a broad range of chemicals, (ii) products can be obtained under mild conditions, (iii) quite popular in industry. In addition, the reaction can achieve generally highly selectivity atom efficiency, reusability, and economically viable processes in the presence of heterogeneous catalyst. Thus, Heterogeneous catalytic hydrogenation is used to produce chemicals between 10-20% of organic synthesis. Hydrogenation reaction is carried out with supported transition metal catalysts such as Cu, Pd, Rh, Co, Ru, Ni and even with enzymes. [73] Depending on the metal catalyst the selectivity of the product can be changed. Because metal influences the strength of adsorption of reductant, the rate of desorption of product and the rate of chemical transformation, the choice of metal is crucial for activity and selectivity of catalytic hydrogenation (Figure 10).

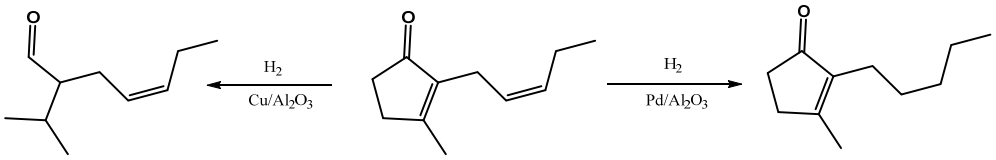

Figure 10. Divergent products in the hydrogenation of cis-jasmone catalytzed by copper or palladium.[75]

3.5 Iron Catalyst in Organic Synthesis

Iron (Fe) is one of the most important elements in nature due to its environmentally benign character and involvement in a multitude of biological processes. As a result, it has become a practical catalyst for a variety of chemical reactions.[76, 77] Fe can have oxidation states ranging from 0 to +5 and has been applied to both the Haber-Bosch and the Fischer-Tropsch Processes.[78] In biological system, Fe has utilized as a co-factor and catalyst, showed excellent ability but always ligand-Fe system (Figure 11). Nowadays, due to intensive efforts to develop Fe catalysis, various reactions such as reductions, oxidations, dehydrations, isomerizations, cycloadditions, and polymerizations use ligand-Fe catalysts.[79]

Since *N*-heterocyclic carbenes (NHCs)-Fe complexes were reported in 1969, NHC-Fe compounds have played a significant role in organic synthesis. Although many advances have been achieved in the field of NHC-Fe complexes, catalytic applications still remain in early stages. Since imidazolium-based HNC ligands was first reported in the 1990's, they have been widely adopted because the NHC ligands have neutral two-electron σ donors, which provide strong and stable ligand-metal

bonding.[80] As shown in Figure 12, NHC-Fe complexes can be synthesized by six methods: early synthetic methods (A, B), through piano-stool type complex (C), deprotonation (D, F), and transmetallation (E). Among them, route D (deprotonation by base) is the most simple and suitable, and side reactions rarely occur.[81]

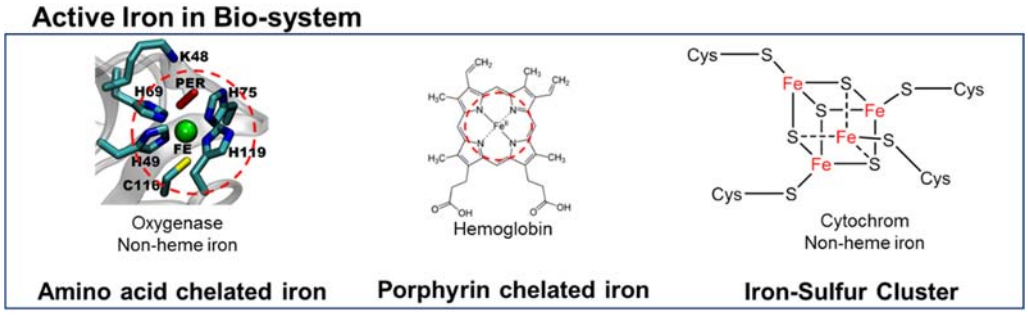

Figure 11. Iron species in the biological system.

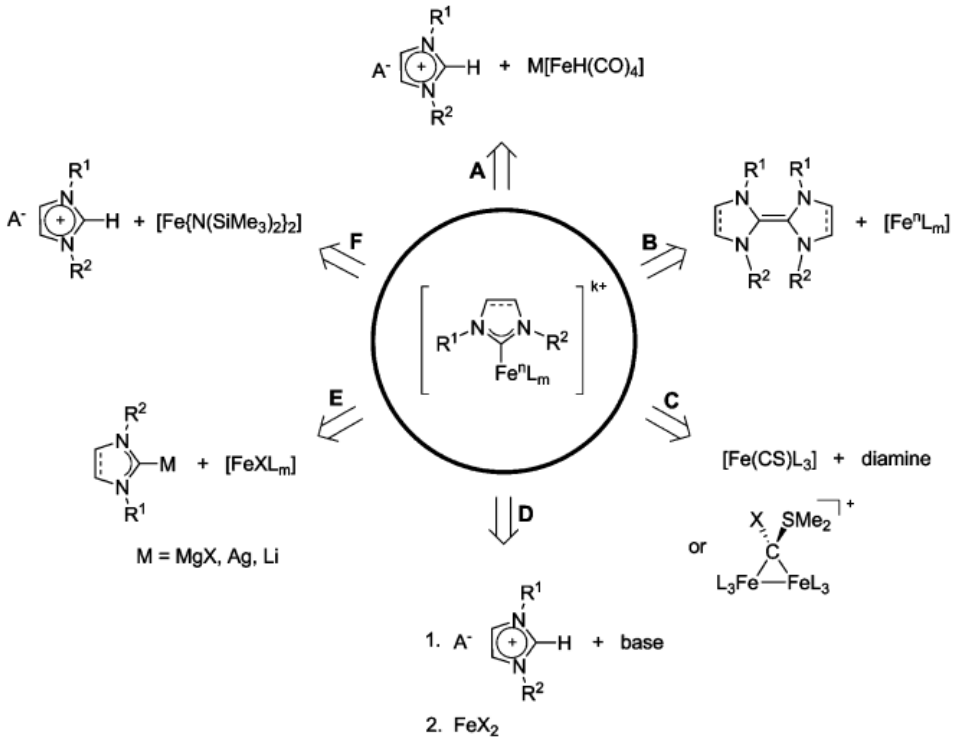

Figure 12. Common synthetic routes toward NHC-Fe complex.[81]

3.6 Ruthenium Catalyst in Organic Synthesis

Ruthenium (Ru) has been considered as a substitutable transition metal catalyst, compared to other transition metals such as Rh, Ir, Pd, and Pt, because it is relatively cheap. Ru has a very wide range of oxidation states, from -2 to +7, with various coordination geometries, which can provide a wide variety of catalytic ability. Formation of Ru complexes is generally favored with trigonal-bypyramidal and octahedral structures in the lower 0, +2, and +3 oxidation states.[82] Due to the useful characteristics including high electron transfer ability, low redox potential, Lewis acid ability, and high coordination ability to heteroatoms, Ru catalysts are applicable in various organic reactions such as hydrogenation, oxidation, and isomerization by the precise control of active sites.[83, 84]

Ru-H and Ru-Cl are well known Ru active sites in their catalytic mechanism.[85] However, Ru-OH, combined form of a Lewis acid and hydroxide, was discovered rather recently as an active site.[86, 87] The superior catalytic ability of hydrous RuO_2 NPs was originated from the existence of Ru-OH, which was confirmed by the Ru K-edge X-ary absorption fine structure (RuO_2-FAU).[87] There was an attempt to

immobilize the $Ru(OH)_3$ active site on a solid support to harness the Ru-OH active site for oxidation reaction.[88] However, there have been relatively few reports on Ru-OH catalyzed hydrogenation reactions.

4. Research Objectives

The main purpose of this thesis was to develop heterogeneous iron and ruthenium catalysts with the goal of achieving fructose based biomass transformation processes (Scheme 2). First, heterogeneous ligand-Fe catalysts were fabricated using polystyrene or graphene oxide as a support. HMF was successfully recovered from the reaction mixture by extraction. Second, zirconia supported Ru catalyst was developed for HMF oxidation/hydrogenation. The Ru catalyst can selectively transform functional groups on HMF to obtain the desired products.

As heterogeneous catalysts, the Fe and Ru catalysts can contribute to the increasing demands for green chemical processes which are based on renewable feedstock

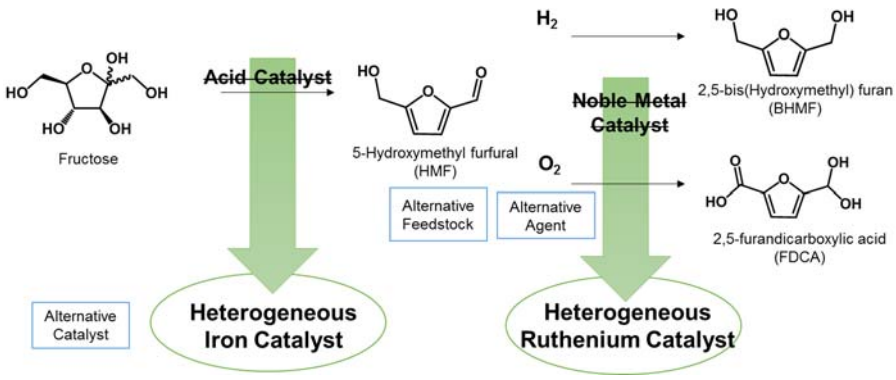

Scheme 2. The strategy to develop fructose based biomass transformation processes.

Chapter 1 Fructose Dehydration for Producing HMF

1. Experimental Section

1.1. Chemicals and Materials

D-(-)-fructose (≥99%), dimethyl sulfoxide (DMSO, ≥99.9%), 1-(3-aminopropyl)imidazole (API), 2,4,6-trimethylbenzyl chloride, trifluoroacetic acid (TFA), potassium permanganate ($KMnO_4$), *N*,*N*'-diisopropylcarbodiimide (DIC), potassium tert-butoxide (KO^tBu), *N*,*N*-dimethylformamide (DMF, ≥99.9%, HPLC grade), 4-methyl-2-pentanone (MIBK), sulfuric acid solution (0.5 mol/L), iron(II) chloride tetrahydrate ($FeCl_2 \cdot 4H_2O$, 99%), iron(III) chloride hexahydrate ($FeCl_3 \cdot 6H_2O$, ≥98%), tin(IV) chloride pentahydrate ($SnCl_4 \cdot 5H_2O$, 98%), chromium(III) chloride ($CrCl_3$, 95%), aluminum(III) chloride ($AlCl_3$, anhydrous, 99.99%), 1-methylimidazole (99%), and Amberlyst 15 (H^+ form, 4 mmol/g resin) were purchased from Sigma-Aldrich. Tetrahydrofuran (THF, ≥99.9%) was purchased from BASF PETRONAS Chemicals. Chloromethyl polystyrene resin (CM PS, bead shape, 150 μm in diameter, 2.1 mmol of 'Cl'/g resin), 1-hydroxybenzotriazole (HOBt) were purchased from BeadTech Inc. Graphite flake (median 7-10 micron, 99% (metals

basis)) was purchased from Alfa Aesar (England). All other reagents and solvents were used as received without further purification.

1.2 Characterization

High performance liquid chromatography (HPLC, Agilent 1200 series) was equipped with an auto sampler (G1329A, Agilent), a column temperature controller (G1316A, Agilent), detectors (G1315D for UV and G1362A for RID, Agilent) and an ion-exchange column (Bio-Rad Aminex HPX-87H 300 × 7.8 mm). HPLC analysis was performed under the following conditions: eluent, 0.01 *N* H_2SO_4; flow rate, 0.6 mL/min; column temperature, 45 °C. Gas chromatography (GC) analyses were performed on Younglin GC-6500 using a flame ionization detector (FID) equipped with a HP-INNOWAX capillary column (internal diameter = 0.25 mm, length = 30 m). Mass spectra (GC/MS) were recorded on Hewlett Packard 6850 gas chromatograph system with 5973 MS detector (Hewlett Packard, USA) at an ionization voltage of 70 eV equipped with a DB-5 capillary column (internal diameter = 0.25 mm, length = 30 m). The ^{1}H NMR spectra were obtained on Ascend^{TM} 400 (Bruker, USA). The infra-red (IR) analysis was carried out on a Nicolet 6700 (Thermo Scientific, USA) operating at ATR mode. The X-ray photoelectron spectra (XPS) was obtained on a SIGMA PROBE (ThermoVG, U.K) equipped with a full 180 degree

spherical sector analyzer to examine the chemical composition of the elements. The photon source was from an Al anode at 15 kV. The X-ray diffraction (XRD) patterns were obtained on a Bruker D8 DISCOVER (Bruker, USA) equipped with a full 180 degree spherical sector analyzer to examine the chemical composition of the elements. Elemental analysis was conducted using an elemental analyzer (LECO Corp US/CHNS-932). The amount of metal loadings on solid support was measured using an inductively coupled plasma emission spectrometer (ICP, Shimadzu ICPS-7510). The transmission electron microscope (TEM) analysis was performed on a JEM1010 (JEOL, Japan) operating at 80 kV, the high resolution transmission electron microscope (HR-TEM) analysis was performed on a JEOL JEM-3010 operating at 300 kV, for which samples were deposited on a 300 mesh holey carbon grid. Mass spectrometry (MS) was performed on a LCQ (Thermo Finnigan, USA) operating at a low resolution to analyze the molecular weight.

1.3. Preparation of *N*-Heterocyclic Carbene (NHC)─Fe^{III} Catalyst

1.3.1 Immobilization of 1-Methyl Imidazole on Chloromethyl Polystyrene

To fabricate ionic liquid immobilized PS beads, 1-methylimidazole-coupled polystyrene (PS-IM) beads were prepared by reactions 1-methylimidazole with a gel type CM PS beads (2.1 mmol of 'Cl'/g resin). 1-Methylimidazole (3.5 mL, 30 mmol) and CM PS beads (10 g) were stirred in DMF (200 mL) at 80 °C for 24 h. The beads was filtered and washed to remove excess 1-methylimidazole, affording PS-IM beads (12 g).

1.3.2 Preparation of PS-NHC-Fe^{III} Catalyst

To prepare the polymer-supported NHC-metal complex, the PS-IM beads (1 g, 1.9 mmol of 'N'/g resin) was placed in a 100 mL 3-neck round-bottomed flask equipped with overhead stirrer, and then, iron(III) chloride (0.5 equiv, 0.9 mmol), potassium *tert*-butoxide (0.55 equiv, 1 mmol), and THF/DMF (1:1) (100 mL) were added. The reaction mixture was stirred at 80 °C for 8 h under nitrogen purging condition. The resulting resin was filtered and thoroughly washed with DMF, MeOH, and brine and dried in vacuum, yielding polystyrene-supported NHC-Fe^{III} (PS-NHC-Fe^{III}) catalysts (1 g, 0.2 mmol of 'Fe'/g resin).

1.3.3 Synthesis of NHC Ligand

Synthesis of 1-[(*N*-tert-butoxycarbonyl)aminopropyl] imidazole (1)

N-Protected alkyl 1-(3-aminopropyl) imidazole was prepared as a NHC ligand for GO. 1-(3-Aminopropyl)imidazole (API, 2.4 mL, 20 mmol), $NaHCO_3$ (4.0 g, 48 mmol), and dried DCM (25 mL) were charged into a 100 ml two-neck round bottom flask with an egg stirring bar under anhydrous condition. Di-*tert*-butyl dicarbonate (5.2 g, 24 mmol) solution in DCM (25 mL) was added dropwise with vigorous stirring. The reaction was proceeded for 4 h and the progress of reaction was checked by TLC (1:1 DCM/MeOH eluent). The resulting product (**1**) was washed with diethyl ether (yield : 18 mmol, 90 %). ^{1}H-NMR of **1** (400 MHz, $CDCl_3$, TMS): δ (ppm) = 7.5 (s, 1H), 7.0 (s, 1H), 6.9 (s, 1H), 4.7 (s, 1H), 4.0 (t, 2H), 3.1 (q, 2H), 1.9 (quin, 2H), 1.4 (s, 9H). Mass: m/z: 226.1 (M^+) (see Figure A1 in Appendix).

Synthesis of methyl (3-aminopropyl) imidazolium chloride (3)

Compound **1** was transformed to methyl (3-aminopropyl) imidazole (**3**) by iodomethane. Compound **1** (2.25 g, 10 mmol), was reacted with iodomethane (850 μL, 12 mmol) in chloroform (50 mL) into a 250 mL two-neck round bottom flask

with stirrings at 50 ^{o}C for 12 h. Then, the resulting product (**2**) was washed with DCM and diethyl ether solution and dried in *vacuo* (yield : 3.2 g, 84%). ^{1}H-NMR of compound **3** (400 MHz, $CDCl_3$, TMS): δ (ppm) = 7.5 (s, 1H), 7.0 (s, 1H), 6.9 (s, 1H), 4.6 (t, 1H), 3.9 (q, 2H), 3.7 (s, 3H), 3.1 (q, 2H), 1.9 (quin. 2H), 1.4 (s, 9H) (see Figure A2 in Appendix). Mass: m/z : 240.02 (M^+) (see Figure A4 in Appendix).

1.3.4. Preparation of Graphene Oxide (GO)

Graphene oxide (GO) was exfoliated from graphite flake by the modified Hummer's method.[89] Graphite flake (2 g, median 7-10 micron, 99% (metals basis) was suspended in 9:1 mixture of H_2SO_4/H_3PO_4 (400 mL) in a 500mL round bottom flask with an egg stirring bar. $KMnO_4$ (12 g, 6 equiv.) was slowly added into the red reaction mixture and the resulting solution was stirred at room temperature for 1 h and further stirred at 50 ^oC. After cooling down to room temperature, the resulting solution was mixed with water (400 mL) and 30% H_2O_2 (5 mL) in an ice-bath. The yellow solution was rinsed with 6*N* HCl (x2), EtOH (x5), and water (x5) by ultracentrifugation at 10000 rpm for 40 min. The resulting product was dried in *vacuo*.

1.3.5 Preparation of GO-NHC-Fe^{III}

Before grafting methyl (3-aminopropyl)imidazolium chloride **(3)**, the Boc group was removed from **(3)** by 5% TFA/DCM. TFA and DCM were evaporated to obtain the resulting product. GO (0.5 g, 1.2 mmol/g, 7~10 μm), *N*,*N*'-diisopropylcarbodiimide (DIC) (387 μL, 2.5 mmol), 1-hydroxybenzotriazole (HOBt) (338 mg, 2.5 mmol), and *N*,*N*-diisopropylethylamine (DIPEA) (865 μL, 5 mmol) were dissolved in DMF (200 mL), and methyl (3-aminopropyl) imidazolium chloride (335 mg, 2.5 mmol) in DMF (50 mL) was added under magnetic stirring at room temperature for 12 h. The resulting product was rinsed with DMF (×5), EtOH (×3), and acetone (×2) by ultracentrifugation at 10000 rpm for 40 min. The residue was dried in *vacuo*. The resulting catalyst was analyzed with FT-IR, TEM, XPS, XRD, and elemental analyzer.

1.4. Fructose Dehydration Reaction Catalyzed by NHC-Fe^{III}

1.4.1. General Experimental Procedure for Fructose Dehydration Reaction Catalyzed by PS-NHC-Fe^{III}

Dehydration of fructose was performed using PS-NHC-metal catalysts. Fructose (180 mg, 1 mmol), PS-NHC-metal catalyst (0.02 mmol, 2 mol% of catalyst to fructose) and DMSO (2 mL) were placed into tubular type reactors (10 mL) equipped with cross-shaped magnetic stirring bar. Then, the reaction mixture was stirred at 100 °C for 3 h. A control reaction was performed using Amberlyst 15 (20 mg corresponding to 0.02 mmol of H^+) under the same conditions. After the reaction, the catalysts were filtered, and the filtrates was diluted (×10) by water (HPLC grade) and analyzed by HPLC.

1.4.2 General Experimental Procedure for Fructose Dehydration Reaction Catalyzed by GO-NHC-Fe^{III}

Fructose (18 mg, 0.1 mmol), GO-NHC-Fe^{III} catalyst, and various solvents (2 mL) were added in a cylinder type glass tube (10 mL) with a cross-shaped magnetic stirring bar. The reaction mixture was stirred at 100 °C for 12 h. After the reaction, the resulting solution was filtered and diluted (×10) by water (HPLC grade) for HPLC analysis.

1.4.3 Reusability Test of PS-NHC-Fe^{III} Catalysts for Fructose Dehydration Reaction

Reusability of PS-NHC-Fe^{III} catalyst was tested with fructose (180 mg, 1 mmol) in DMSO (2 mL). The reaction was performed in a cylinder type reactor (10 mL) with cross-shaped magnetic stirring bar at 100 ^{o}C. After the reaction, the catalyst was separated by filtration, and washed with DMSO and acetone and dried in *vacuo* before being recycled.

1.4.4 Reusability Test of GO-NHC-Fe^{III} Catalysts for Fructose Dehydration Reaction

Reusability of GO-NHC-Fe^{III} catalyst was tested with fructose (18 mg, 0.1 mmol) in DMSO (2 mL). The reaction was performed in a cylinder type reactors (10mL) with cross-shaped magnetic stirring bar at 100 ^{o}C. After the reaction, the catalyst was separated by filtration, and washed with DMSO and acetone, and dried in *vacuo* before being recycled.

1.5 Separation of HMF from DMSO

After fructose dehydration reaction, the catalystswere removed by filtration and the DMSO solution containing HMF was diluted with deionized water (×4 and ×10 in volume), and extracted (×3) with the same volume of various organic solvents including dichloromethane (DCM), ethyl acetate (EA), methyl isobutyl ketone (MIBK), and diethyl ether (DEE). The organic layer was separated and evaporated under reduced pressure to yield crude product, which was analyzed by HPLC (Figure 13).

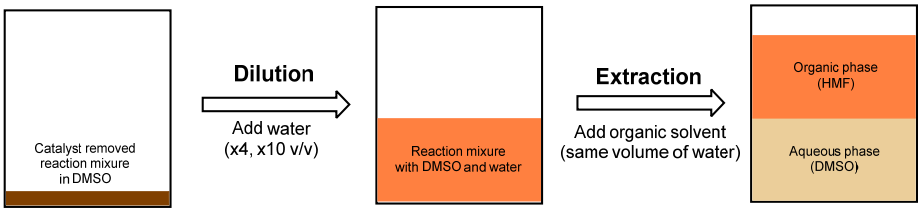

Figure 13. Extraction procedure for the separation of HMF from DMSO.

2. Result and Discussion

2.1. Characterization of PS-NHC-Fe^{III}

Polymer-supported NHC ligand precursor, imidazolium grafted polystyrene (PS-IM) resin, was readily prepared by previously reported methods (Scheme 3).[90] Chloromethyl polystyrene (CM PS) beads were used as a support, and a substitution reaction of CM PS with 1-methylimidazole afforded PS-IM. Imidazolium immobilized the solid supports could provide an ion liquid like environment and a semi-homogeneous phase to be miscible with substrates.[91] Unlike CM PS, PS-IM was highly compatible with hydrophilic solvents such as methanol, ethanol and even water, despite of the hydrophobic polystyrene backbone (Figure 14). This solvent compatibility enables hydrophilic compounds like carbohydrates to diffuse into the polymer matrix and react with the metal catalysts. In addition, the covalently bonded imidazolium salt in PS-IM provides ionic liquid like moiety within the polymer matrix, which would improve the accessibility of a substrate and the stability of the supported catalyst. As illustrated in Scheme 3, imidazolium groups on PS-IM can act as a NHC ligand precursor for the metal catalyst as well as an ionic liquid phase.

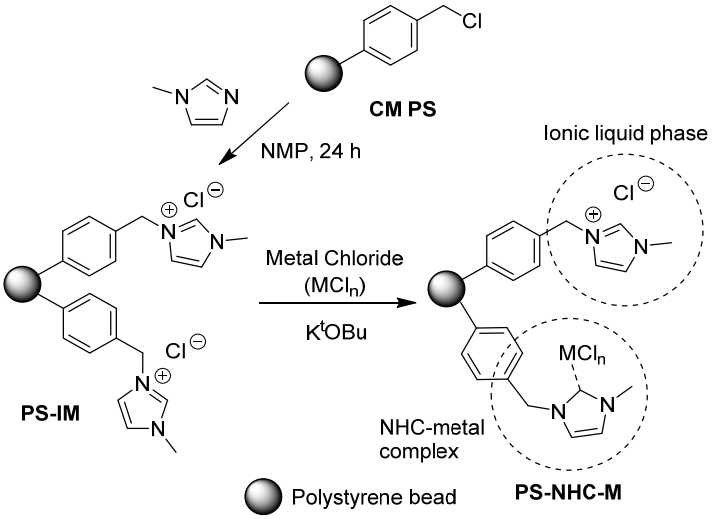

Scheme 3. Preparation of polystyrene-supported NHC metal catalysts.

After coordination of metals, the resulting PS-NHC-metal catalysts were still compatible with the hydrophilic solvents. As shown in Figure 15, the formation of NHC-Fe^{III} complexes was confirmed by ATR FT-IR analysis. The peak intensity at 1156 cm^{-1} corresponding to the quaternary ammonium of imidazolium decreased, which indicates that the metals were coordinated to the NHC ligand.

SEM images, taken after each reaction step, show that the morphological homogeneity of the polymeric supports was maintained during the attachment of 1-methylimidazole onto the CM PS and after the coordination of the metals to PS-IM (Figure 16). EDS analysis proved that PS-NHC-metal catalysts properly contained the metals and the counter anions (Cl^-), which was further confirmed by ICP-AES. The loading percentage of the metals on the NHC ligand was 1.6 – 16 mol% of the total imidazolium (30 – 300 μmol of metal from 1.9 mmol of imidazolium/g resin).

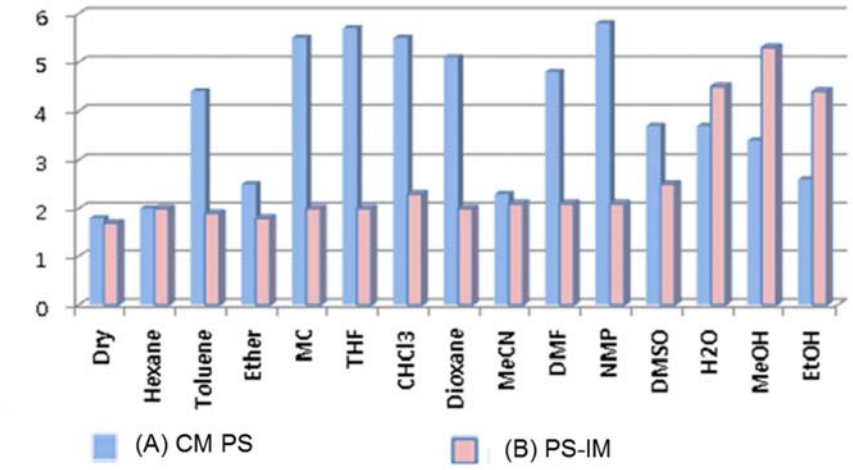

Figure 14. Swelling properties of CM PS and PS-IM with various solvent.

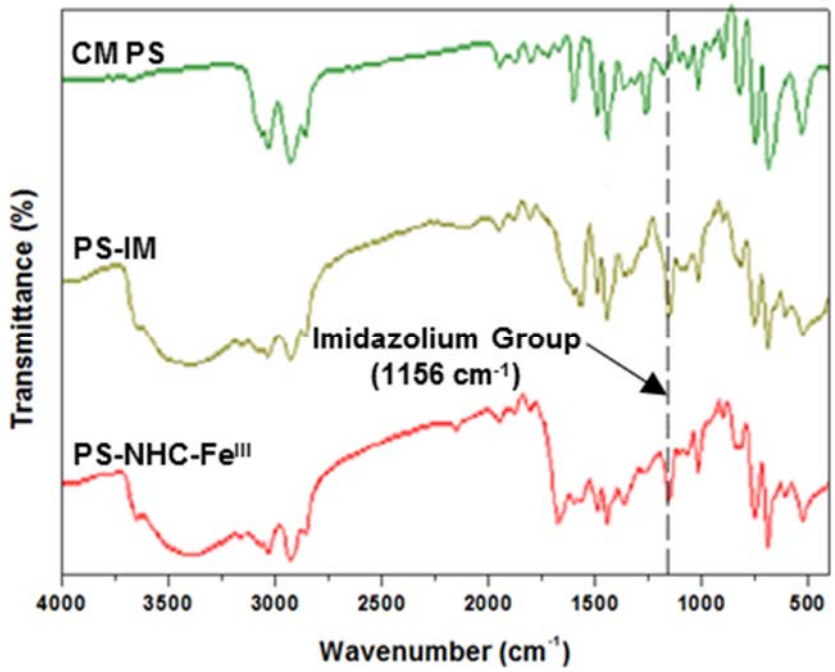

Figure 15. Fourier-transform infrared spectroscopy spectra. (a) CM PS, (b) PS-IM, (c) PS-NHC-Fe^{III}.

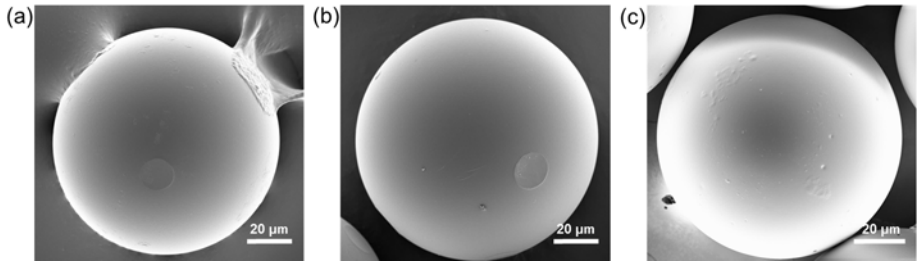

Figure 16. Scanning electron microscope image of (a) PS-IM, (b) freshly prepared PS-NHC-Fe^{III} and (c) reused PS-NHC-Fe^{III}.

The powder XRD patterns of PS-NHC-Fe^{III} catalysts showed only a broad peak (2θ = 20) for the amorphous polymer support. No peaks for crystalline iron nanoparticles or iron oxides (Fe_2O_3 or Fe_3O_4) were observed from the freshly prepared PS-NHC-Fe^{III} catalyst or even from reused PS-NHC-Fe^{III} catalyst (red versus black pattern in Figure 17). From the XRD result, we could confirmed that Fe^{III} was successfully coordinated to the polymer-supported NHC ligand on an atomic level.

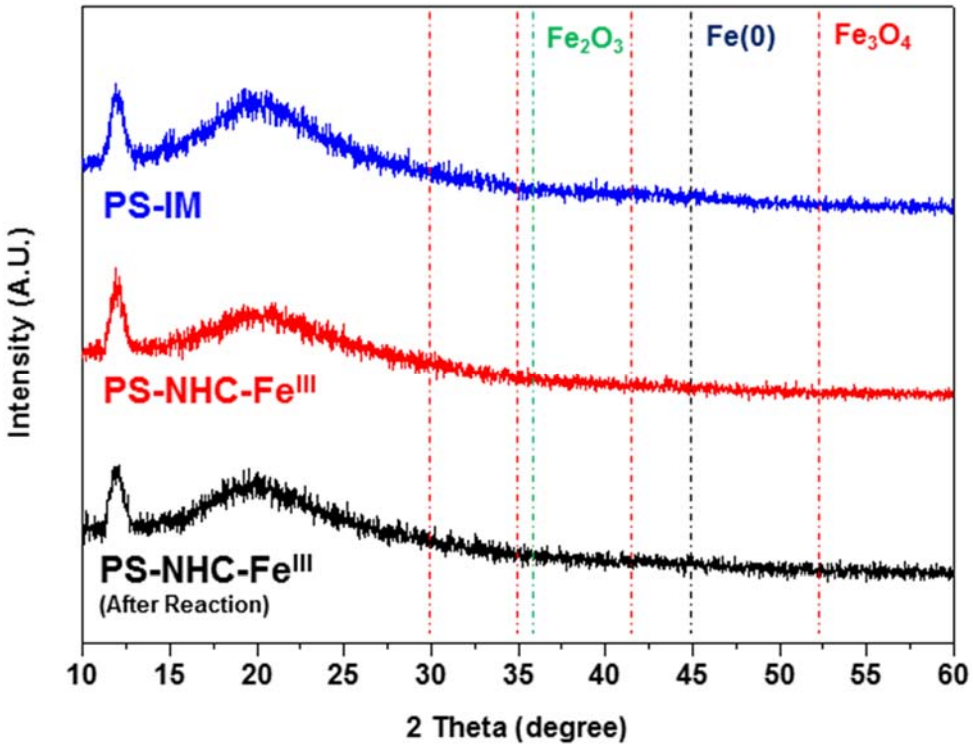

Figure 17. X-ray diffraction patterns of (a) PS-IM, (b) freshly prepared PS-NHC-Fe^{III}, and (c) reused PS-NHC-Fe^{III}.

To validate the coordination of Fe^{III} to the polymer-supported NHC ligand, the binding energies of PS-NHC–Fe^{III} catalyst were investigated by XPS (Figure 18). Comparing PS-IM with PS-NHC-Fe^{III}, iron species were found on PS-NHC-Fe^{III} (Figure 18a). Peaks from Fe^{III} $2p_{3/2}$ and Fe^{III} $2p_{1/2}$ were observed at 710.7 eV and 724.3 eV, respectively. The satellite peak for Fe^{III} $2p_{3/2}$ appeared at 718.8 eV (Figure 18b). A small peak for Fe^{II} $2p_{3/2}$ was also found at 708.2 eV. It is believed that a little part of Fe^{III} was reduced to Fe^{II} during the coordination step in the presence of a strong base (*tert*-butoxide in this case). The XPS spectra of N 1s indicate that the peaks at 401.4 eV and 402.2 eV correspond to the N 1s of the quaternary ammoniums, and the peaks at 389.9 eV and 399.9 eV correspond to the N 1s of the trialkylamines (Figure 18c). After coordination of Fe^{III} to the polymer-supported NHC ligand, the peak intensity for N 1s of the quaternary ammoniums was dramatically reduced. This indicates that the imidazolium ring was changed to *N*-heterocyclic carbene by complex formation with the Fe^{III} atom (Figure 18c versus Figure 18d).[92] The spectrum of Cl $2p_{3/2}$ proved the coordination of Fe-Cl complex on PS-NHC-Fe^{III} catalyst. The peak at 199.6 eV is a strong evidence of metal-Cl bond (Figure 18e).

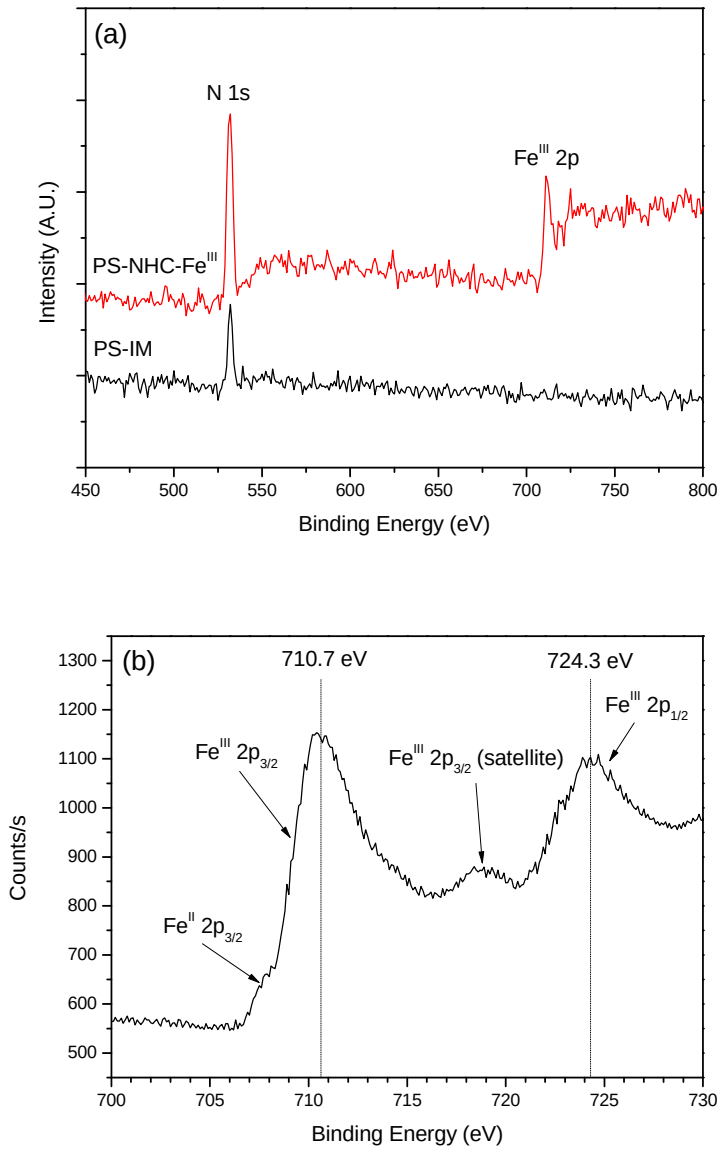

Figure 18. X-ray photoelectron spectra of (a) PS-IM and PS-NHC-Fe^{III} (wide scan), (b) Fe 2p from PS-NHC-Fe^{III}, N 1s from (c) PS-IM and (d) PS-NHC-Fe^{III}, and Cl 2p from (e) PS-NHC-Fe^{III} (continue).

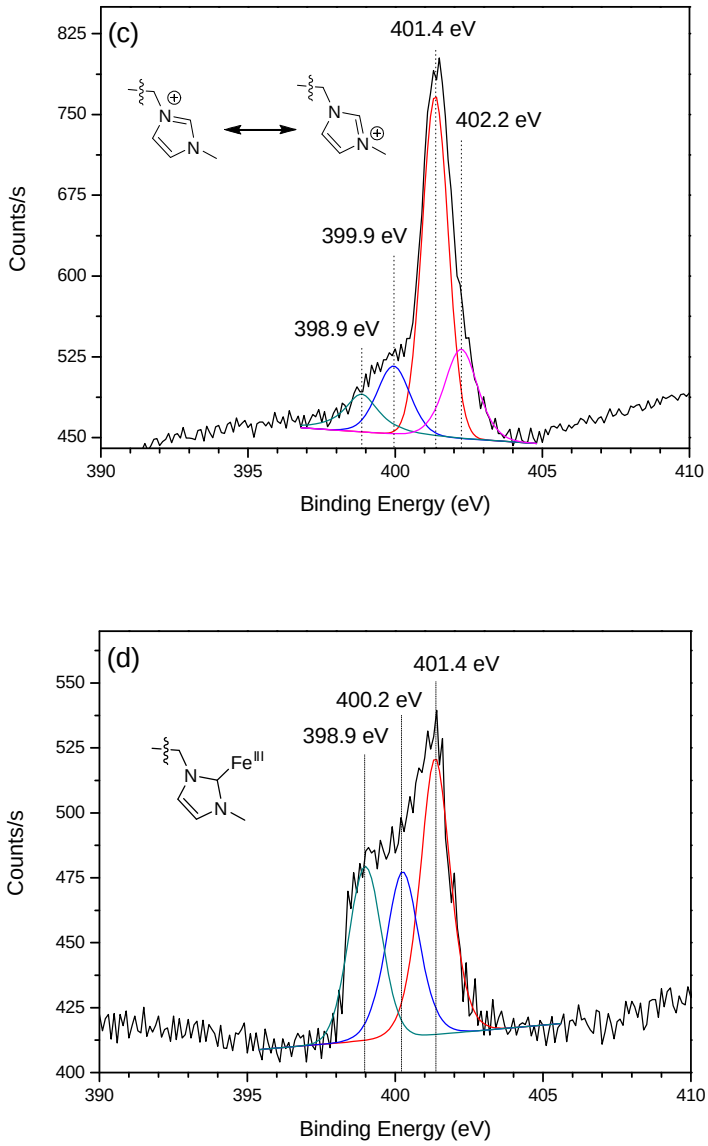

Figure 18. X-ray photoelectron spectra of (a) PS-IM and PS-NHC-Fe^{III} (wide scan), (b) Fe 2p from PS-NHC-Fe^{III}, N 1s from (c) PS-IM and (d) PS-NHC-Fe^{III}, and Cl 2p from (e) PS-NHC-Fe^{III} (continue).

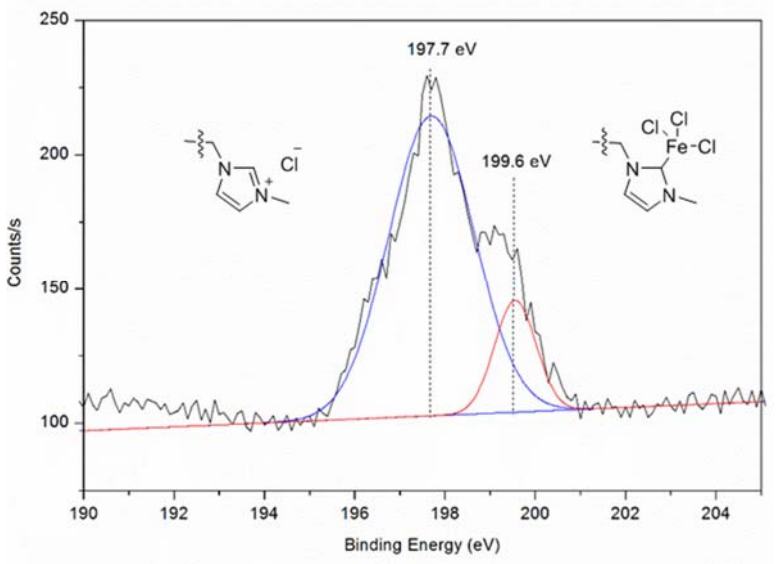

Figure 18. X-ray photoelectron spectra of (a) PS-IM and PS-NHC-Fe^{III} (wide scan), (b) Fe 2p from PS-NHC-Fe^{III}, N 1s from (c) PS-IM and (d) PS-NHC-Fe^{III}, and Cl 2p from (e) PS-NHC-Fe^{III}.

2.2. Dehydration of Fructose to HMF Catalyzed by PS-NHC-Metal Catalysts

Various transition metal catalysts have been previously applied to the dehydration of biomass-derived fructose into HMF in a homogeneous phase.[33-35, 93] However, the metal catalysts as a Lewis acid in a homogeneous phase have intrinsic disadvantages: (i) the use of toxic transition metals in most cases and (ii) the difficulty in recycling the metals. In this respect, dehydration of the fructose into HMF was studied using heterogeneous PS-NHC–metal catalysts. In particular, Fe^{III} was selected as a candidate for a metal catalyst for the dehydration of fructose into HMF (Scheme 4). Although iron has great potential as a metal catalyst because of its low cost and low toxicity, not much effort has been given for its use in the field of biomass transformation. Other PS-NHC–metal catalysts were also prepared including Al^{III}, Sn^{IV} and Cr^{III}, which are well-known as efficient metal catalysts for the dehydration of fructose into HMF.[33]

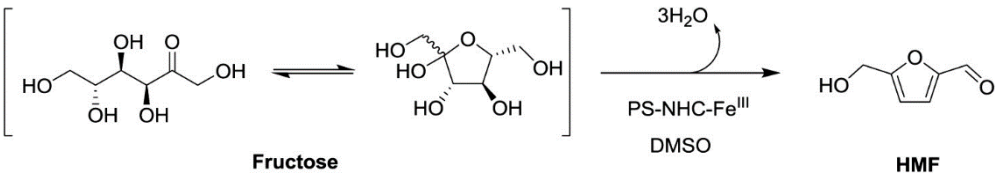

Scheme 4. Dehydration of fructose into HMF catalyzed by the PS-NHC-Fe^{III} catalyst.

Table 5 shows the effect of various catalysts on the dehydration of fructose to HMF. When the dehydration of fructose was carried out in DMSO without any catalyst, very low level of selectivity (15%) for HMF was observed although the conversion of fructose was 75% (Entry 1). PS-IM showed a considerable selectivity for HMF (70%) but the reaction was slow (Entry 2). The reaction rates increased when PS-NHC–metal catalysts were used. PS-NHC–Al^{III}, PS-NHC–Sn^{IV}, and PS-NHC–Cr^{III} showed a turnover frequency (TOF) of 10–12 h^{-1} (Entry 3–5), which is greater than Amberlyst 15 (TOF = 8 h^{-1}) and other previously reported heterogeneous catalysts such as Sn–W oxide (TOF = 6 h^{-1}),[94], LPSnP-1 (TOF = 0.1 h^{-1}),[95], WO_3/ZrO_2 (TOF = 10 h^{-1}),[96], $H_3PW_{12}O_{40}$ (TOF = 7 h^{-1}),[97]. On the other hand, the PS-NHC–Fe^{III} catalyst showed better results. The yield of HMF was 73% and the TOF was 12 h^{-1}. Major byproduct was levulinic acid, which was generated by deformylation of

HMF. The catalytic activity of PS-NHC–Fe^{III} in dehydration of fructose into HMF was comparable to the homogeneous NHC–$FeCl_3$ complex,[98] which was prepared from 1-benzyl-3-methylimidazolium chloride and $FeCl_3$ (yield of HMF in 73% with PS-NHC–Fe^{III} vs 80% with NHC–$FeCl_3$ complex). The good catalytic activity of heterogeneous PS-NHC–Fe^{III} could be also attributed to the imidazolium groups on polymer support, because the ammonium group, which is similar to the imidazolium group, enhances the activity of Fe^{III} catalyst in dehydration of fructose into HMF.[99] Comparing with Lewis acid value of the metals in Table 6, the Lewis acid value of the metal seemed to be critical for the activity in acid-catalyzed dehydration reactions because PS-NHC–Fe^{II} is a weak Lewis acid (Entry 1,3, and 4 in Table 6).

Table 5. Dehydration of Fructose into HMF in The Presence of Various Heterogeneous Catalysts[a]

Entry	Catalyst	Conversion (%)	HMF Selectivity (%)	HMF Yield (%)	TOF (h^{-1})
1	None	75	15	20	-
2	PS-IM	76	70	51	0.1
3	PS-NHC-Al^{III}	93	75	70	11
4	PS-NHC-Sn^{IV}	89	80	71	12
5	PS-NHC-Cr^{III}	83	76	64	10
6	PS-NHC-Fe^{III}	97	75	73	12
7	PS-NHC-Fe^{II}	3	n/d	0	-
8	Amberlyst 15	79	83	65	8

a Conversion, selectivity and yield were determined by HPLC. Reaction conditions: fructose (0.5 mmol), catalyst (2 mol%), DMSO (2 mL), 3 h, and 100 ^{o}C.

The PS-NHC–Fe^{III} catalyst was successfully recycled. During recycling, the activity of the catalyst was maintained up to 10 times of recycling with similar HMF yields (~70%) and reaction rates (TOF 11–12 h^{-1}) (Table 7). Based on ICP analysis, the metals did not leach. In addition, humins, a byproduct, were not seen on the surface of the catalyst and the color of the catalyst was not significantly changed compared to that of freshly prepared catalyst.

Table 6. Difference in Dehydration Activity Depending on Metals

Entry	Core Metal on PS-NHC-metal Catalyst	Average Coordination Number	Lewis Acidic Value[a]	Selectivity of HMF (%)
1	Sn^{IV}	5.86	0.68	80
2	Al^{III}	5.26	0.57	75
3	Cr^{III}	6	0.50	76
4	Fe^{III}	5.69	0.53	75
5	Fe^{II}	5.89	0.34	n.d.

a: Lewis Acidity Value = V/N, V: the oxidation state of the cation, N: the average of the coordination numbers.

Table 7. Recycling Test of PS-NHC-Fe^{III} in Dehydration of Fructose into HMF

Cycle Number	Fructose Conversion (%)	HMF Yield (%)	ICP-AES (mmol 'Fe'/g)
1	91	73	0.21
2	97	71	0.20
3	97	70	0.20
4	93	73	0.21
5	95	67	0.20
6	95	72	0.21
7	97	70	0.21
8	92	67	0.20
9	94	71	0.20
10	96	69	0.21

Reaction conditions: fructose (0.5 mmol), PS-NHC-Fe^{III} (2 mol%), DMSO (2 mL), 3 h, and 100 ^{o}C.

2.3. Characterization of GO-NHC-Fe^{III}

A grafting method of ILs on a solid surface is well known in the field of heterogeneous catalysis applications.[100-102] Depending on the substituted alkyl group and the counter anion of imidazolium based IL can be tunable surface properties (c.f. hydrophobicity) on the solid support.[103] In terms of tunability, imidazolium based IL was synthesized to introduce HNC ligand to GO. For this, the free amino group of 1-(3-aminopropyl)imidazole (API) was protected by Boc group to prevent undesired side reaction during the alkyl group substitution reaction. The Boc-API (**1**) was obtained in 99% yield (Scheme 5). Then, alkyl group substitution reaction on IL (**2**) gave 90% yield. Because compound 2 was less soluble in diethyl ether compared to API and di-*tert* butyl dicarbonate, it was well obtained by simple washing step. The compound **2** was treated with 5% TFA solution in DCM to remove Boc group and to generate free amino group. Before grafting the compound **3** onto GO, the compound **2** and **3** were analyzed by ^{1}H NMR, and the molecular weights were confirmed by mass spectrometry (Appendix Figure A2–A4).

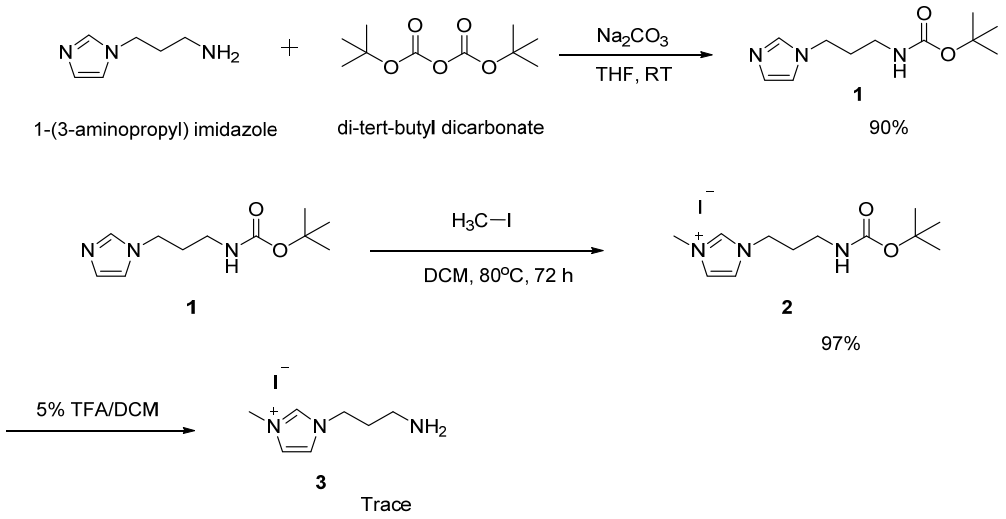

Scheme 5. Synthetic scheme of imidazolium based ionic liquid.

GO-NHC-Fe^{III} catalyst was prepared as illustrated in Scheme 6. The surface of GO, which contains carboxyl groups, was grafted with compound **2** to introduce NHC ligand moiety. The coupling of compound **2** with carboxylic acid on GO was successfully proceeded by the DIC coupling method in DMF. The IL group loading was found to be 1.2 mmol/g of GO by elemental analysis. Then, iron was coordinated with the NHC ligand on GO by the *in situ* deprotonation of the azolium C–H by potassium *tert*-butoxide, both exogenous in the metal precursor, and the subsequent metal-complexation. The iron loading level on the catalyst was afforded to 0.2 mmol/g of GO-NHC-Fe^{III}. The loading percentage of the iron on the NHC ligand was 16 mol% of the total imidazolium. This indicates that imidazolium groups within the GO can provide precursor for the metal catalyst as well as the ionic liquid phase.

The morphological changes of GO, during IL grafting iron coordination on GO, were investigated using transmission electron microscopy (TEM). The natural graphite was chemically exfoliated to obtain GO of below 10 μm size (Figure 19a). After the ligand grafting step, no morphology changes were observed (Figure 19b). As shown in Figure 19c, the nanoparticles such as Fe metal, Fe_3O_4 or Fe_2O_3 were not observed

throughout the surface of the GO. The functional group change was confirmed by FT-IR analysis after coupling of imidazolium based IL on GO and iron coordination (Figure 20). IR spectrum of GO sheet showed typical functional groups: peak at 3184 cm^{-1} (O–H bonds), 2980 cm^{-1} (C–H stretch), 1739 cm^{-1} (C=O bonds), 1225 cm^{-1} (C–OH), and 1058 cm^{-1} (C–O (epoxy)). After imidazolium based IL grafting on GO surface, the peaks at 1615 cm^{-1} (carbonyl group of amide), 1361 cm^{-1} (imidazolium), 1152 cm^{-1} (imidazolium), and 746 cm^{-1} (aromatic) newly appeared, which are quite different of pristine GO. Especially, the peak at 1152 cm^{-1} indicated the presence of quaternary ammonium, meaning that imidazolium based IL was successfully coupled to GO surface.

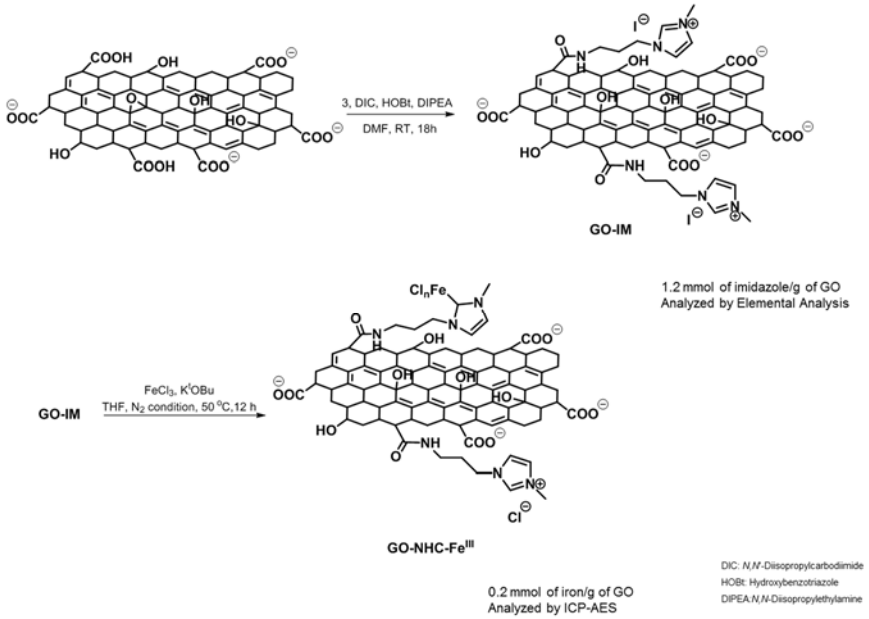

Scheme 6. Synthetic scheme of GO-NHC-Fe^{III}.

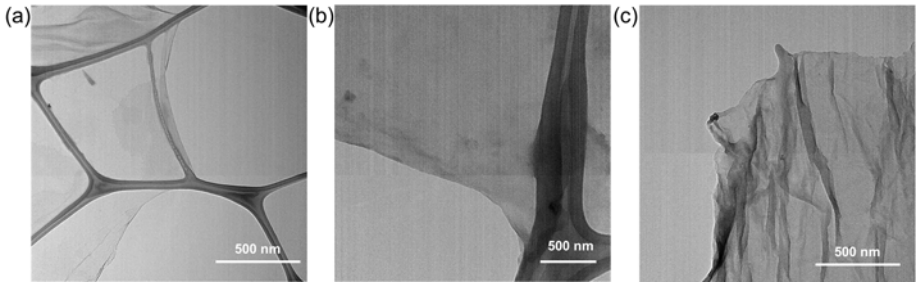

Figure 19. Transmission electron microscopy images of (a) GO, (b) GO-IM, (c) GO-NHC-Fe^{III}.

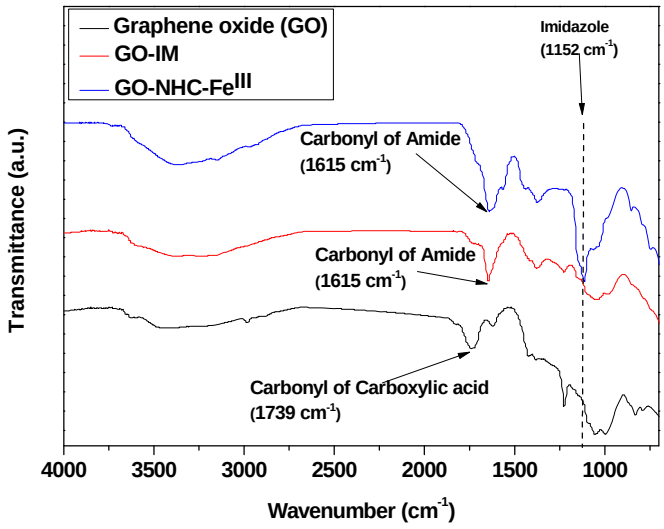

Figure 20. FT-IR spectra of GO, Go-IM, and GO-NHC-Fe^{III}.

To identify the surface modification on GO surface, XPS analysis was carried out on GO, GO-IM, and GO-NHC-Fe^{III}. As shown in C 1s XPS spectrum in Figure 21a, GO was well exfoliated from the natural graphite and contained oxygen functional groups such as C–O (286.5 eV) and C=O (288.7 eV) originated from carboxylic groups.[104] After IL grafting on GO surface, the ratio of carbon species was dramatically changed and the peaks of nitrogen newly observed, because IL contained C=N bond, which is shown in C 1s XPS spectrum (286.0 eV in Figure 21b and Figure 21c). Two peaks at 399.3 and 401.3 eV correspond to the N 1s of the imidazolium from GO-IM. Iron coordination on GO-IM surface led to significant change in C, N, and Fe species (Figure 21d and Figure 21e). Comparing the peaks of N 1s from GO-IM with those from GO-NHC-Fe^{III}, the proportion of trialkylamines at 399.3 eV increased from 39% to 71%. Peaks of Fe^{III} $2p_{3/2}$ were observed at 710.8 eV (Figure 21f). After the coordination of Fe^{III} to the GO-IM, the peaks for N 1 s of the quaternary ammoniums were dramatically reduced. This indicates that the imidazolium ring was changed into *N*-heterocyclic carbene by complex formation with the Fe^{III} atom (Figure 21d versus Figure 21e).[92] Moreover, the spectrum of Cl $2p_{3/2}$ proved existence of Fe-Cl

bonding on GO-NHC-Fe^{III} catalyst (peak at 199.6 eV in Figure 21g). Therefore, it confirmed that NHC-Fe complex was well formed on GO.

(a)

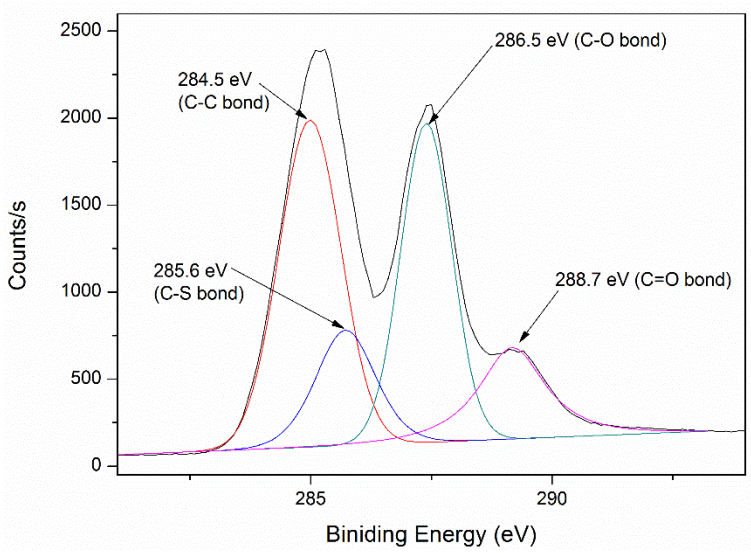

(b)

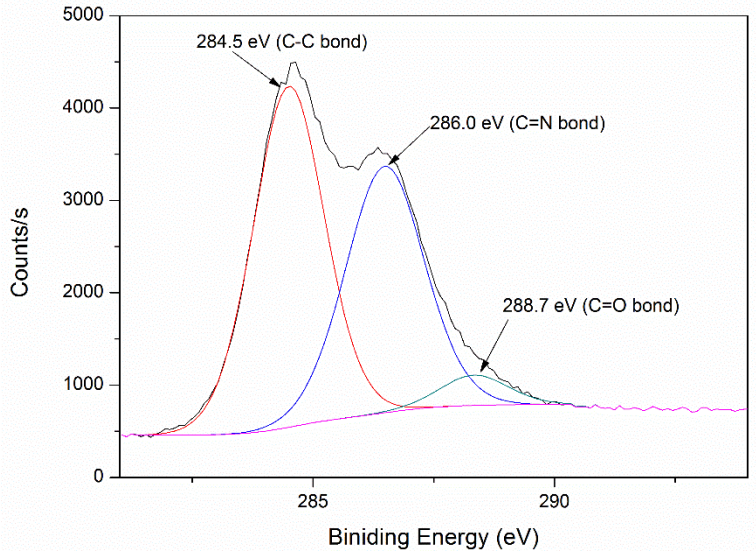

Figure 21. X-ray photoelectron spectra of (a) C 1s of GO, (b) C 1s of GO-IL, (c) C 1s of GO-NHC-Fe^{III}, (d) N 1s of GO-IM, (e) N 1s of Go-NHC-Fe^{III}, and (f) Fe 2p of Go-NHC-Fe^{III}, (g) Cl 2p of Go-NHC-Fe^{III} (continue).

(c)

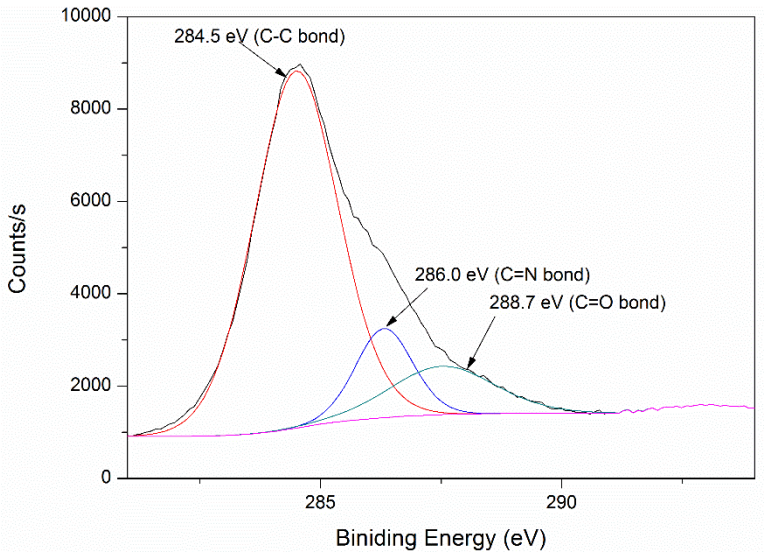

(d)

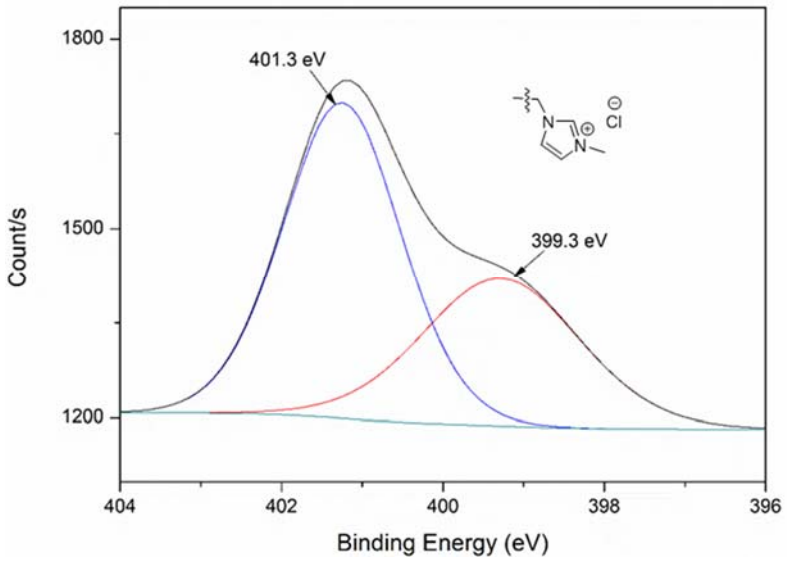

Figure 21. X-ray photoelectron spectra of (a) C 1s of Go, (b) C 1s of GO-IL, (c) C 1s of GO-NHC-Fe^{III}, (d) N 1s of GO-IM, (e) N 1s of Go-NHC-Fe^{III}, and (f) Fe 2p of Go-NHC-Fe^{III}, (g) Cl 2p of Go-NHC-Fe^{III} (continue).

(e)

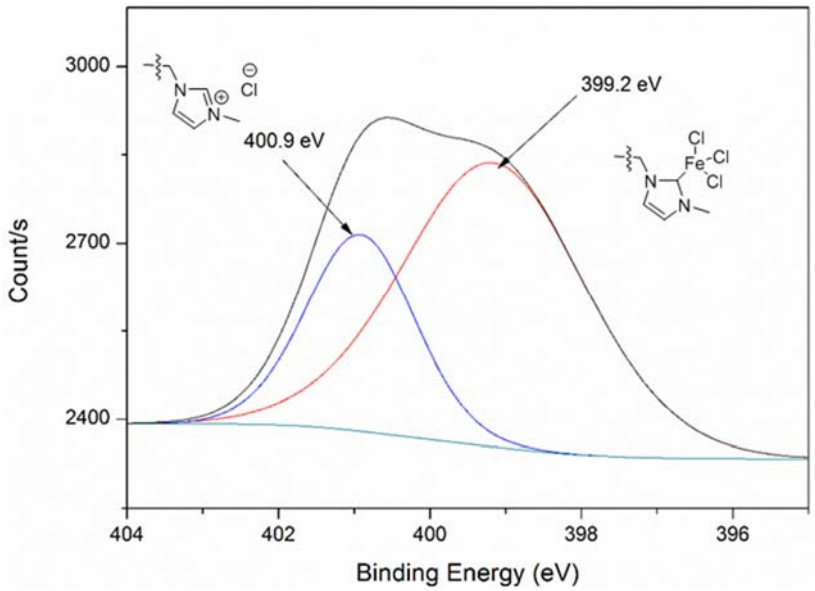

(f)

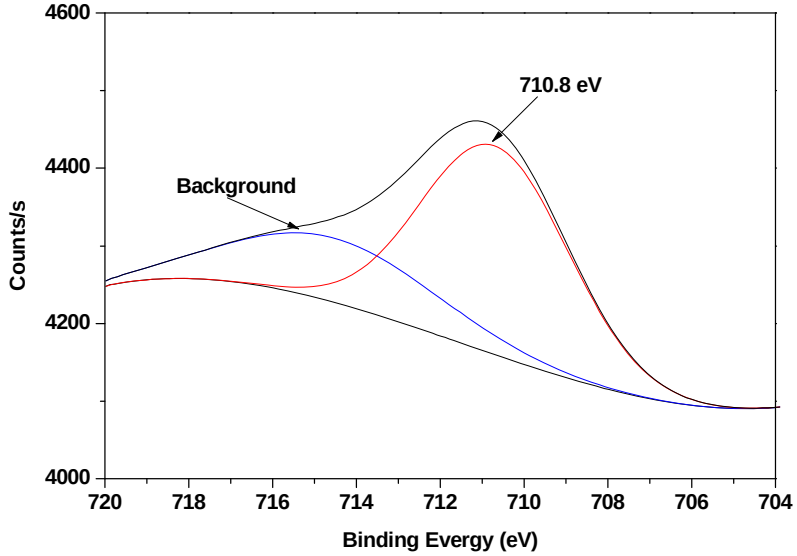

Figure 21. X-ray photoelectron spectra of (a) C 1s of Go, (b) C 1s of GO-IL, (c) C 1s of GO-NHC-Fe^{III}, (d) N 1s of GO-IM, (e) N 1s of Go-NHC-Fe^{III}, and (f) Fe 2p of Go-NHC-Fe^{III}, (g) Cl 2p of Go-NHC-Fe^{III} (continue).

(g)

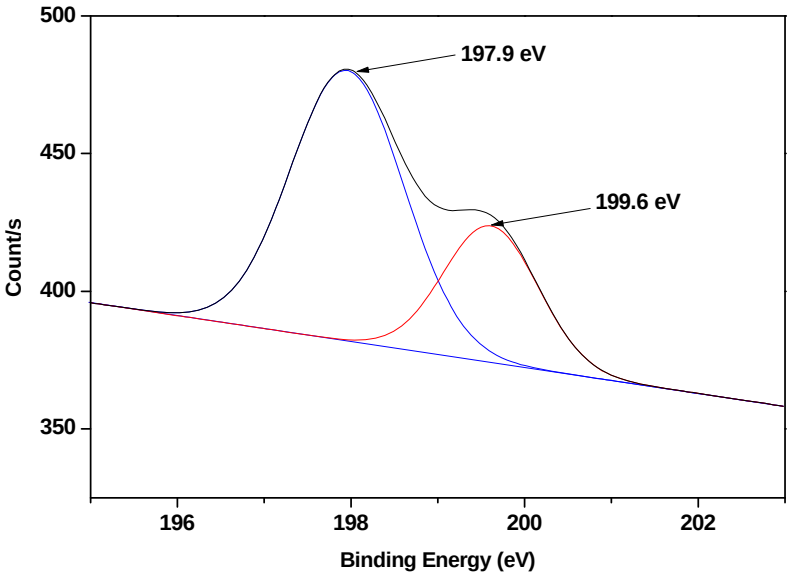

Figure 21. X-ray photoelectron (a) C 1s of Go, (b) C 1s of GO-IL, (c) C 1s of GO-NHC-Fe^{III}, (d) N 1s of GO-IM, (e) N 1s of Go-NHC-Fe^{III}, and (f) Fe 2p of Go-NHC-Fe^{III}, (g) Cl 2p of Go-NHC-Fe^{III}.

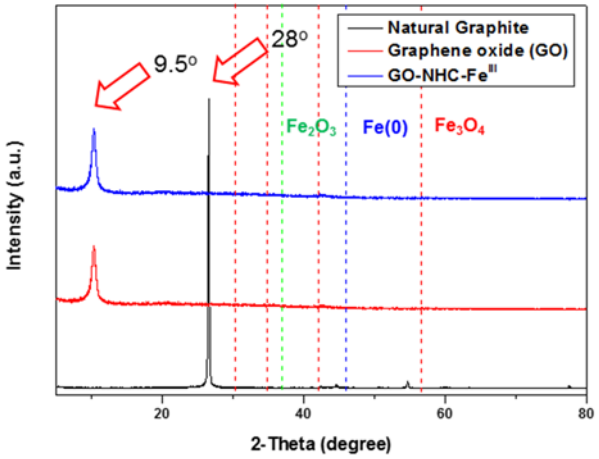

Figure 22. X-ray diffraction patterns of (a) Natural graphite, (b) Graphene xide, and (c) GO-NHC-Fe^{III}.

2.4. Dehydration of fructose to HMF catalyzed by GO-NHC-Fe^{III} catalysts

Although heterogeneous PS-NHC-Fe^{III} catalyst was fabricated for dehydration of fructose reaction into HMF, polymer support has intrinsic disadvantages: (i) slow reaction rate due to the diffusional constraints and (ii) poor stability of the polymer matrix under harsher reaction conditions (c.f. high temperature, strong acid or base conditions). In this sense, GO was chosen as a solid support, which had excellent physical properties such as thermal stability, high surface area, ease of modification, and little solvent limitation. To determine the catalytic ability of GO-NHC-Fe^{III}, various heterogeneous Lewis acid catalysts and GO-NHC-Fe^{III} were compared in the transformation of fructose to HMF as illustrated in Scheme 7. The fructose was dominantly transformed into levulinic acid without any catalysts (15% of selectivity to HMF). In literally, DMSO can act as a catalyst in dehydration reaction in high temperatures (> 160 ^{o}C).[105] It was believed that DMSO had the ability for fructose dehydration at 100 ^{o}C (entry 1 in Table 8). Because the fructose dehydration reaction is an endothermic reaction, the reaction temperature in this study was enough to

trigger the dehydration reaction.

As it is observable from Table 8, GO-NHC-Fe^{III} catalyst exhibited the highest catalytic activity with respect to conversion and selectivity (Entry 3). When the dehydration of fructose was carried out in DMSO without any catalyst, a very low level of selectivity (15%) for HMF was observed although the conversion of fructose was 76% (Entry 1). GO-IM showed a similar conversion of fructose (76%), but selectivity for HMF (16%) (Entry 2). The selectivity to HMF was too low in spite of the high conversion of the fructose because over dehydration to levulinic acid occurred as the dominant reaction. Based on these, NHC-Fe^{III} complex was performed as an active site for dehydration of fructose. The catalytic activity of Fe catalyst was compared with other immobilized Lewis acid such as Al^{III}, Sn^{IV}, and Cr^{III}, which previously showed efficient catalytic activity for dehydration of fructose (Entry 3 and 4–6). GO-NHC–Al^{III}, GO-NHC–Sn^{IV}, and GO-NHC–Cr^{III} showed a turnover frequency (TOF) of 12–14 h^{-1} (Entry 4–6), which was greater than Amberlyst 15 (TOF = 10 h^{-1}). Although Amberlyst 15 had been shown good catalytic performance as known from previous literal and industrial process, catalysts

regeneration step was required to be recycle. Thus, our catalyst is more suitable for fructose dehydration reactions than Amberlyst 15. GO-NHC-Fe^{III} showed a turnover frequency (TOF) of 15 h^{-1} (Entry 3), which was greater than the Amberlyst 15 (TOF = 10 h^{-1}) and other previously reported heterogeneous catalysts such as Sn–W oxide (TOF = 6 h^{-1}),[94] $H_3PW_{12}O_{40}$ (TOF = 7 h^{-1}),[97] supported ionic liquid silica nanoparticles (TOF = 0.1 h^{-1}),[106] and sulfonated ZrO_2 (TOF = 7 h^{-1}),[23].

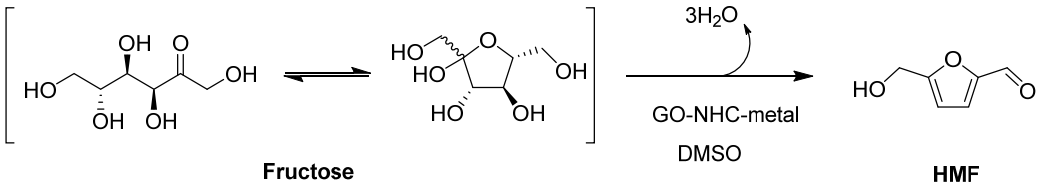

Scheme 7. Dehydration of fructose into HMF catalyzed by GO-NHC-Fe^{III}.

Table 8. Dehydration of Fructose into HMF in The Presence of Various Heterogeneous Catalysts[a]

Entry	Catalyst	Conversion (%)	HMF Selectivity (%)	HMF Yield (%)	TOF (h^{-1})
1[b]	None	75	15	11	
2	GO-IM	76	16	12	2
3	GO-NHC-Fe^{III}	>99	90	90	15
4	GO-NHC-Sn^{IV}	>99	85	85	14
5	GO-NHC-Cr^{III}	>99	71	71	12
6	GO-NHC-Al^{III}	>99	76	76	13
7	Amberlyst 15	>99	58	58	10

a. Conversion, selectivity and yield were determined by HPLC. Reaction condition: fructose (18 mg, 0.1 mmol), GO-NHC-Fe^{III} (2 mol%), DMSO (2 mL), 100 ^{o}C, 3h b: byproduct was levulinic acid.

In order to confirm the catalytic reproducibility, reusability was performed during 5 times of recycling. As shown in Table 9, the yield of HMF was maintained about 90% up to 5 times of recycling, and the active site did not leach despite of washing and catalytic reaction steps. The selectivity of HMF was above 99 %. After the 5 times of recycling, the used catalyst was confirmed by TEM, XPS. As a result of TEM image, it was confirmed that the morphology of used catalyst GO remained unchanged and iron particles were not newly formed either. (Figure 19). In the XRD patterns, the crystallization pattern of GO remained the same compared with the fresh GO-NHC-Fe^{III} (Figure 22).

Table 9. Recycling Test of Fructose Dehydration into HMF Catalyzed by GO-NHC-Fe^{III}

Cycle Number	Fructose Conversion (%)	HMF Yield (%)	ICP-AES (mmol 'Fe'/g)
1	99	90	0.22
2	95	86	0.21
3	96	85	0.20
4	94	85	0.20
5	95	84	0.20

Reaction condition: fructose (18 mg, 0.1 mmol), GO-NHC-Fe^{III} (2 mol%), DMSO (2 mL), 100 ^{o}C, 3h**.**

2.5. Separation of HMF from DMSO

Although DMSO is the most efficient solvent for the dehydration of fructose into HMF in the presence of heterogeneous catalysts, its separation is still problematic especially when scale-up process is needed. The boiling point of DMSO (189 °C) is too high for evaporation since HMF is not quite stable at high temperatures. Although a large number of studies for HMF synthesis have been conducted, there have been relatively few reports on the isolation of HMF. Therefore, we investigated a systematic extraction method in order to recover HMF from DMSO under mild conditions. Readily evaporable organic solvents such as DCM, EA, MIBK, and DEE have been used for the extraction of HMF. From the results, we found that the order of extracting ability was DCM > > EA > MIBK > DEE (Figure 23). Even though DCM quantitatively recovered HMF, a considerable amount of DMSO was also extracted compared with the other extraction solvents. Due to the purity of the recovered HMF, MIBK and DEE showed good performance. In particular, DEE extracted HMF more selectively compared with the other solvents.

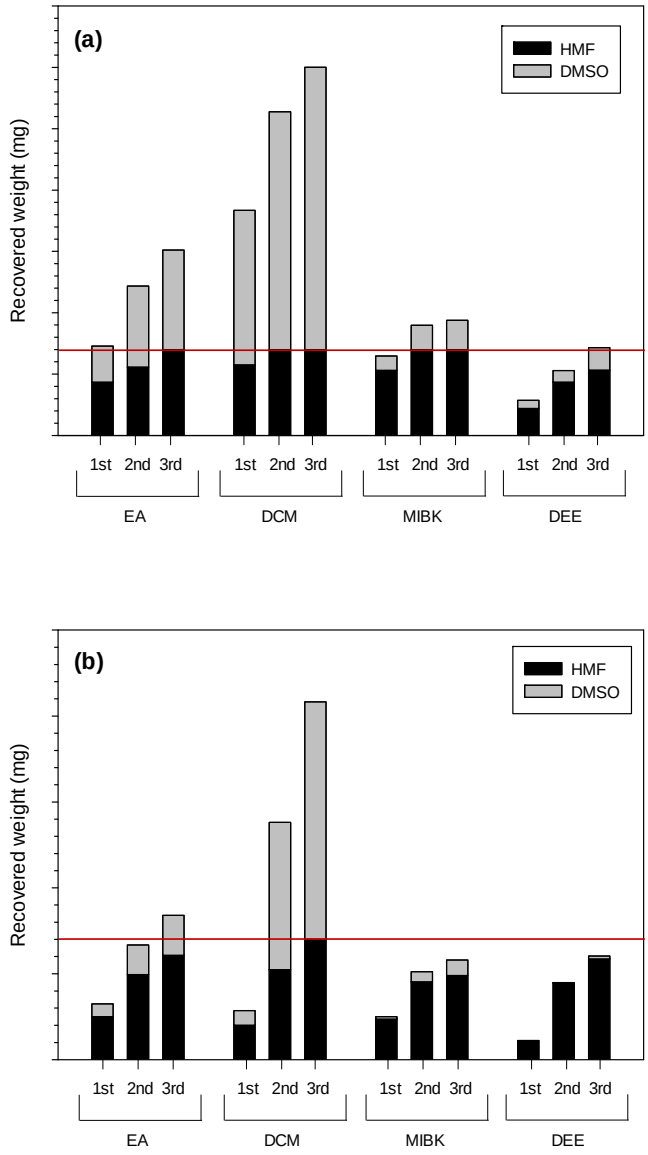

Figure 23. Recovery of HMF from DMSO using extraction method with various organic solvents after (a) 4 times and (b) 10 times dilution with distilled water (red line indicates the theoretical recovery yield of HMF at 100%).

3. Conclusion

In conclusion, polymer-supported NHC–metal catalysts were prepared and characterized with various analytical methods. The synthesized polymer-supported NHC–metal catalysts were successfully applied to the dehydration of fructose into HMF. In particular, PS–NHC–Fe^{III} catalyst afforded HMF in 73% yield and it could be reused 10 times without any significant loss of catalytic activity. Also GO–NHC–Fe^{III} catalyst was synthesized by IL grafting on GO surface and characterized various analytical methods. GO-NHC-Fe^{III} catalyst showed HMF in 90% yield, and it could be recycled 5 times without any significant loss of catalytic activity. Owing to strong metal bond of NHC ligand, supported NHC–Fe^{III} catalyst showed excellent catalytic performance compared to the conventional catalysts (99 % of fructose conversion and 90% of HMF yield). Both heterogeneous NHC–Fe^{III} catalysts were recyclable over 5 times without significant loss of catalytic activities. In addition, DEE was found to be an efficient solvent for the effective recovery of HMF from DMSO.

Chapter 2. Conversion of HMF to Value Added Chemicals

1. Experimental Section

1.1. Chemicals and Materials

$RuCl_3 \cdot xH_2O$, $Ru_3(CO)_{12}$, $Ru(bpy)_3Cl_2$, $RuCl_2$(*p*-cymene), $Ru(acac)_3$, Ru/C, RuO_2 anhydrous, RuO_2 hydrate, and 5-hydroxymethylfurfural (HMF) (99%), were purchased from Sigma Aldrich. Sodium hydroxide (reagent grade ≥98%) was gathered from Daejung Chemicals & Metals (S. Korea). Zirconium oxide (20-30 m^2/g) was obtained from STREM. All of NMR solvents were purchased from Cambridge Isotope Laboratories, Inc. All chemicals were used as received without further purification.

1.2. Characterization

The ^{1}H NMR was obtained on an Ascend^{TM} 400 (Bruker, USA) to analyze NHC ligand's structure. The X-ray photoelectron spectra (XPS) was obtained on a SIGMA PROBE (ThermoVG, U.K) equipped with a full 180 degree spherical sector analyzer to examine the chemical composition of the elements. The photon source was from an Al anode at 15 kV. The XRD patterns were measured with Bruker D8 DISCOVER (Bruker, Germany) (Cu Ka radiation, 3 kV 40 mA). Elemental analysis for transition metals was conducted using an inductively coupled plasma emission spectrometer (ICP, Shimadzu ICPS-7510). The X-ray photoelectron spectra (XPS) was obtained on a SIGMA PROBE (ThermoVG, U.K) equipped with a full 180 degree spherical sector analyzer to examine the chemical composition of the elements. The photon source was from an Al anode at 15 kV. The X-ray diffraction (XRD) patterns were obtained on a Bruker D8 DISCOVER (Bruker, USA) equipped with a full 180 degree spherical sector analyzer to examine the chemical composition of the elements. Elemental analysis was conducted using an elemental analyzer (LECO Corp US/CHNS-932). The transmission electron microscope (TEM) analysis was

performed on a JEM1010 (JEOL, Japan) operating at 80 kV, for which samples were deposited on a 300 mesh holey carbon grid.

1.3. Oxidation of HMF into FDCA Catalyzed by $Ru(OH)_x/ZrO_2$

The supported ruthenium hydroxide catalyst, $Ru(OH)_x/ZrO_2$, was prepared by the previously reported procedure.[107] HMF (51 μL, 0.5 mmol) was oxidized in water (2 mL) by using $Ru(OH)_x/ZrO_2$ (1 mol% of Ru) with molecular oxygen (1 bar). The reaction was carried out in a cylinder type of reactors, equipped with cross-shaped magnetic stirring bar, at 100 ^oC. After the reaction, the catalyst was removed by filtration and the filtrate was cooled to room temperature. The sample solution was diluted by water and analyzed by HPLC. The separated $Ru(OH)_x/ZrO_2$ catalyst was washed with aqueous sodium hydroxide (0.1 M) and dried in *vacuo* before being recycled.

1.4. Reduction of HMF into BHMF Catalyzed by $Ru(OH)_x/ZrO_2$

HMF (100 μL, 0.9 mmol) was reduced in 2-propanol (3 mL) by using $Ru(OH)_x/ZrO_2$ (0.3 μmol% of Ru) with hydrogen gas (30 bar). The reaction was carried out in a pressure vessel with Teflon liner (200 mL), equipped with glass vial (8 mL) at 40 ^oC. After the reaction, the catalyst was filtrated, and the filtrate was evaporated in *vacuo* to remove solvent. ^1H NMR of BHMF (400 MHz, DMSO-*d*6, TMS): δ (ppm) = 6.2 (s, 2H), 5.2 (s, 2H), 4.4 (s, 4H), (see Appendix A6). The conversion and selectivity of reaction were characterized by ^1H-NMR (DMSO-*d*6). The separated $Ru(OH)_x/ZrO_2$ catalyst was washed with aqueous sodium hydroxide (0.1 M) and dried in *vacuo* before being recycled.

2. Results and Discussion

2.1. Characterization of $Ru(OH)_x/ZrO_2$ Catalyst

Commercially available ZrO_2 was employed in the synthesis of the $Ru(OH)_x/ZrO_2$. The catalyst was fabricated by simple immersion of ZrO_2 to ruthenium precursor ($RuCl_3 \cdot xH_2O$) solution. The incorporation Ru on the surface of ZrO_2 was confirmed by inductively coupled plasma atomic emission spectroscopy (ICP–AES). As expected, $Ru(OH)_x/ZrO_2$ catalyst contained ~2 wt% Ru. The nature of the Ru and oxygen species on the surface of $Ru(OH)_x/ZrO_2$ was further analyzed by X-ray photoelectron spectroscopy (XPS). The surface morphological changes during the immobilization of ruthenium active sites were investigated by the high resolution transmission electron microscopy (HR-TEM) and X-ray diffractometry (XRD). As shown in Figure 24a, the crystal structure of ZrO_2 depicted that Ru immersion step did not affect the crystal structure of ZrO_2 and the value of *d*-spacing (0.29 nm). The lattice structure of solid support did not change, which was confirmed by comparing the freshly prepared $Ru(OH)_x/ZrO_2$ and the used $Ru(OH)_x/ZrO_2$ (Figure 24b, and Figure 24c). Additionally, any structural changes of ZrO_2 as well as the formation of

ruthenium metal or ruthenium oxide particles did not occur by the immobilization step of ruthenium active sites.

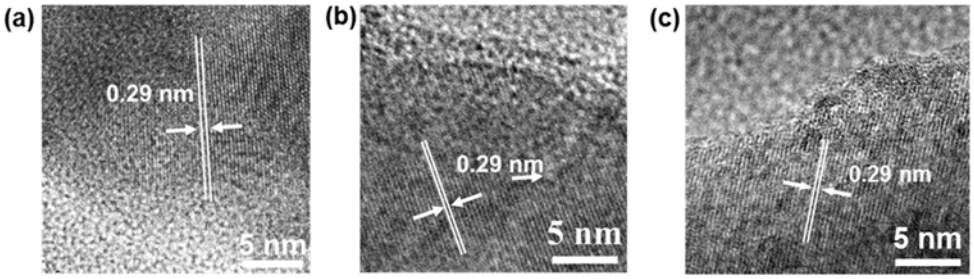

Figure 24. Surface morphologies of (a) ZrO2 (b) Ru(OH)x/ZrO2 and (c) used Ru(OH)x/ZrO2 obtained from high resolution transmission electon microscope (HR-TEM), which shows d-spacing of (a) 0.29 nm, (b) 0.29 nm (ZrO2 as a reference: 0.29 nm).

The powder X-ray diffraction (XRD) spectra on the ZrO_2 and the prepared catalyst exhibited strong peaks in the range from 10 ^{o} to 70 ^{o} (2θ) (Figure 25), which were attributed to the monoclinic phase of ZrO_2 (28.5 ^{o}, 34.5 ^{o}) and to the tetragonal phase (50.2 ^{o}).[108] From the XRD patterns of ZrO_2 and $Ru(OH)_x/ZrO_2$, the absence of ruthenium metal or ruthenium oxide particles on the catalyst was confirmed.

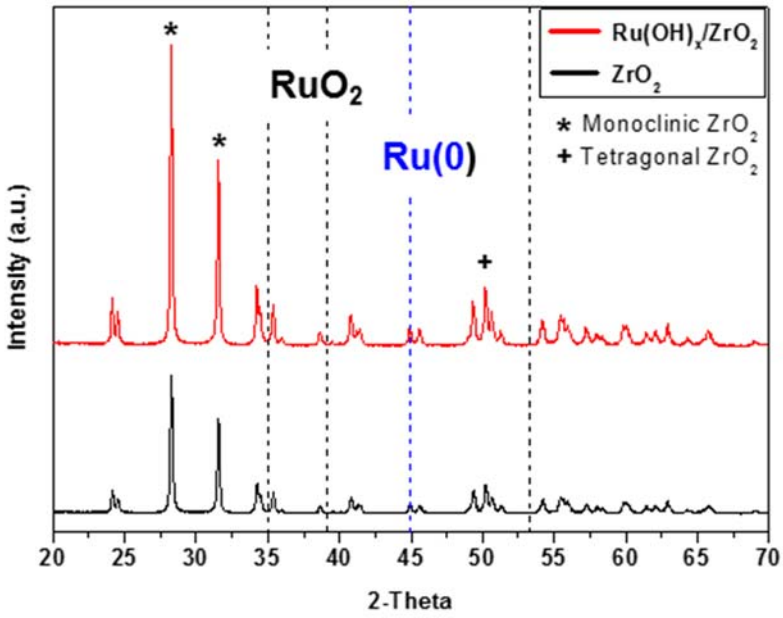

Figure 25. X-ray diffraction patterns (XRD) of Ru(OH)x/ZrO2 (red) and ZrO2 (black).

The Ru 3d XPS spectra in Figure 26a, consists of two asymmetric peaks assigned to Ru $3d_{5/2}$, Ru $3d_{3/2}$ and C 1s, which can be fitted with six curves. The binding energies of Ru $3d_{3/2}$ and Ru $3d_{5/2}$ were 281.6 eV and 286.7 eV, respectively, which were attributed to Ru(III) of Ru(OH) on $Ru(OH)_x/ZrO_2$.[109] The oxygen 1s XPS spectra contained oxygen bonding information, such as zirconium-oxygen, ruthenium-oxygen, and water (Figure 26b). The peak around 533 eV and 534 eV was attributed to ZrO_2, while the peak of 528.7 eV corresponded to ruthenium-oxygen from ruthenium–hydroxy bond.[109, 110] Based on this information, we can conclude that Ru active sites were well dispersed on the surface of ZrO_2 without forming RuO_2 or Ru (0) particles.

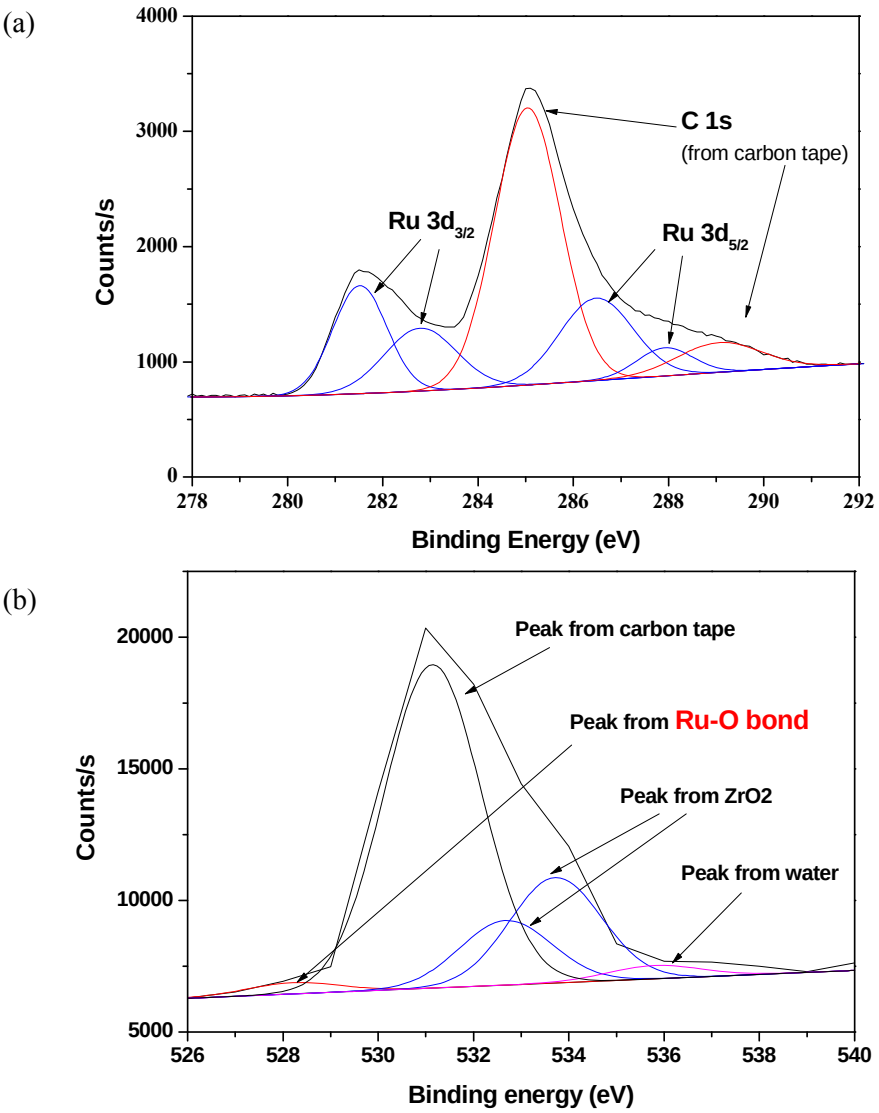

Figure 26. XPS spectra of $Ru(OH)_x/ZrO_2$. (a) Peaks of ruthenium 3d from $Ru(OH)_x/ZrO_2$, (b) peaks of oxygen 1s from $Ru(OH)_x/ZrO_2$. O 1s peak around 531 eV came from carbon tape background.

2.2. Oxidation HMF into FDCA Catalyzed by $Ru(OH)_x/ZrO_2$

As shown in Scheme 8, the oxidation of HMF to FDCA can occur by two routes. In route A, the aldehyde group of HMF is oxidized to the carboxylic acid, corresponding to HMFCA. Subsequently, HMFCA will turn into FFCA by the second oxidation and yield FDCA. In route B, the hydroxyl group of HMF is oxidized to the aldehyde group, yielding to DFF, followed by additional FFCA and FDCA.

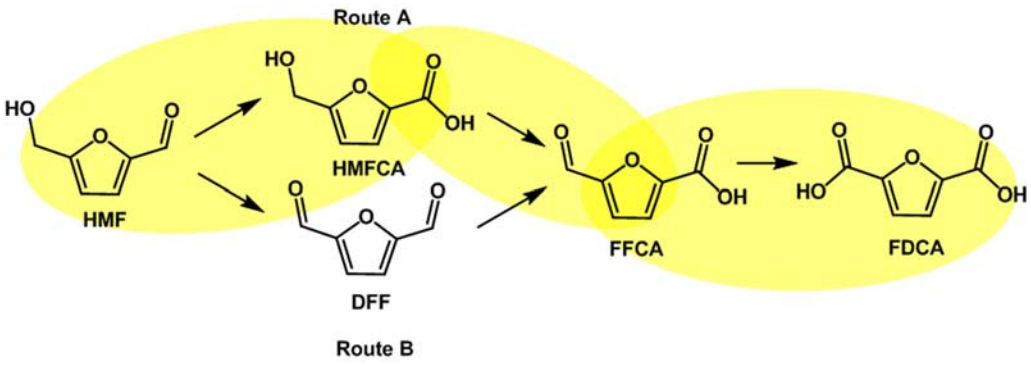

Scheme 8. The oxidation of HMF into the FDCA by two routes. Route A: the aldehyde group of HMF is oxidized to form a carboxylic acid. Route B: the hydroxyl group of HMF is oxidized to yield the dialdehyde.

To identify catalytic properties of $Ru(OH)_x/ZrO_2$, the conversion of HMF and its derivatives were monitored over time (Figure 27). During the reaction, HMFCA was found to be the main intermediates in first 6 hours of the reaction, whereas increasing amount of FDCA appeared from the 6th to 24th hour. The transformation of HMF to HMFCA occurred in the early stage of the reaction, whereas further oxidation of HMFCA to FFCA and FDCA was slowly proceeded. Thus, the reaction profile showed that $Ru(OH)_x/ZrO_2$ prefers the oxidation pathway route A rather than route B. To confirm whether route A is valid, the oxidation of furanic analogues mixture, furfuryl alcohol and furfural, was monitored. The yield of furan carboxylic acid was higher than that of furfural (100% vs. 6%). These results imply that $Ru(OH)_x/ZrO_2$ oxidize the aldehyde substituent first, instead of the hydroxyl group, and subsequently promotes hydroxyl oxidation yielding to aldehyde group as the next step. Based on the reaction time, it can be concluded that the oxidation of aldehyde substituent into carboxylic acid proceeded faster than that of the hydroxyl group. In agreement with the previous papers, oxidation of HMFCA to FFCA is reaction determining step.[50] Thus, $Ru(OH)_x/ZrO_2$ is far more efficient in the oxidation of aldehyde as evidenced

by the proportion of oxidized intermediates.

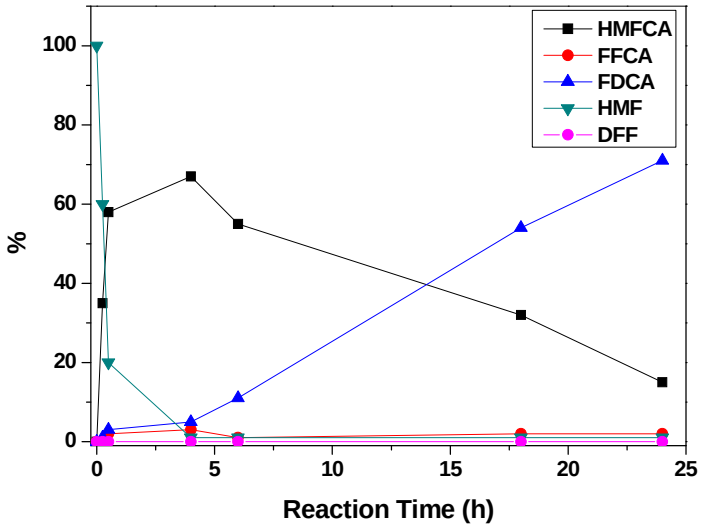

Figure 27. Time course of HMF conversion and product distribution during the aerobic oxidation of HMF using $Ru(OH)_x/ZrO_2$. Reaction conditions: HMF (0.5 mmol), water (3 mL), $Ru(OH)_x/ZrO_2$ (2 mol%), NaOH (2 mmol), O_2 1 bar.

The selective oxidation of HMF into FDCA with molecular oxygen in water is a green alternative of the stoichiometric oxidant in organic solvents. However, high pH condition is often required for the reaction to proceed.[111] Reaction optimization was carried out to decide the most suitable reaction condition including reaction solvent, base, and pressure of molecular oxygen. As shown in Table 10, the aerobic oxidation of HMF was performed in a variety of solvents using $Ru(OH)_x/ZrO_2$ catalyst under identical conditions. When the reactions were conducted in DMSO and DMF, which have strong polarities and high boiling points, very low FDCA yields were obtained under 1% (Entry 6 and Entry 7). In case of the other organic solvent (Entry 2–5), similar HMF conversions over 90% and non-furanic compound yields around 90% were obtained when the reactions were carried out in cyclopentyl methyl ether (CPME), toluene and 1,4-dioxane.

Table 10. The Effect of Reaction Solvent on The Aerobic Oxidation of HMF[a]

Entry	Solvent	Conversion (%)	Selectivity (%)[b]		
			FDCA	HMFCA	DFF
1	Water	99	71	15	<1
2	CPME	99	n.d.	n.d.	n.d.
3	Toluene	90	2	<1	70
4	1,4-dioxane	99	n.d.	n.d.	n.d.
5[c]	Ethanol	99	n.d.	n.d.	n.d.
6[b]	DMF	96	<1	n.d.	n.d.
7	DMSO	44	<1	<1	75

a: Reaction conditions: HMF (0.5 mmol), solvent (3 mL), $Ru(OH)_x/ZrO_2$ (2 mol%), NaOH (2 mmol), O_2 1 bar. b:byproduct was not furanic compounds. c: HMF was transformed to ethyl furandicarboxylate.

The reaction parameters such as base agent, reaction temperature, and catalyst loading were studied (Table 11). Inorganic bases generally exhibited superior performance in HMF oxidation into FDCA than other organic bases such as TEA, pyridine. And NaOH was the most suitable base agent for HMF oxidation into FDCA (Entry 1 vs. Entry 2–4). Because Cannizzaro reaction of HMF could generally occur in NaOH solution,[112] $Ru(OH)_x/ZrO_2$, can accelerate hydration of aldehyde group in HMF, subsequently oxidize to FDCA than Cannizzaro reaction of HMF.

Table 11. The Effect of Base on Aerobic Oxidation of HMF[a]

Entry	Base	Conversion (%)	Yield (%)[b]	
			FDCA	DFF
1	NaOH	99	71	<1
2	Na_2CO_3	99	54	32
3	DIPEA	67	<1	14
4	Pyridine	48	<1	36

a: Reaction conditions: HMF (0.5 mmol), water (3 mL), $Ru(OH)_x/ZrO_2$ (2 mol%), base (2 mmol), O_2 1 bar.

Obviously, the higher the reaction temperature, the higher the FDCA yield became. The HMF conversion and FDCA yield decreased dramatically when the reaction temperature dropped from 100 °C to 50 °C and 30 °C (Table 12). The conversion of HMF was observed to be 45% and 16% at the reaction temperature of 50 °C and 30 °C, respectively, which gave the corresponding HMFCA yields of 39% and 61%, respectively (Entries 2, 5 and 6). As expected, catalytic active sites were more available and participated in HMF oxidation reaction depending on an increase of catalyst amount. The conversion of HMF and FDCA yield was activated along with the increase of the catalyst amount (Entries 7-8 in Table 12).

Table 12. The Effect of Reaction Temperature, Pressure of Molecular Oxygen, and Catalyst Amount on The Aerobic Oxidation of HMF

Entry	Amount of Catalyst (mol%)	Temperature (°C)	Conversion (%)	Selectivity (%)	
				FDCA	HMFCA
1	2	100	>99	71	15
2[a]	2	100	>99	59	37
3[b]	2	100	>99	65	32
4[c]	2	100	>99	72	14
5	2	50	89	45	39
6	2	30	81	16	61
7	4	100	>99	77	18
8	0.5	100	>99	45	50
9	0.25	100	>99	54	45

Reaction conditions: HMF (0.5 mmol), water (3 mL), catalyst: $Ru(OH)_x/ZrO_2$, NaOH (2 mmol), O_2 1 bar. a under air condition. b: 0.5 bar of molecular oxygen, c: 10 bar of molecular oxygen.

To identify the catalytic active site, control tests were carried out using $Ru(OH)_x/ZrO_2$, ZrO_2, and based treated ZrO_2 (Table 13). Although HMF is not stable under alkaline conditions,[112, 113] HMF did not transform into any oxidized HMF derivatives in the presence of ZrO_2 or base treated ZrO_2 (Entry 12 and 13). Only $Ru(OH)_x/ZrO_2$ showed excellent catalytic activity in the oxidation of HMF with 71% yield (Entry 2). Although RuO_2 anhydrous, RuO_2 hydrate, and $Ru(OH)_x/ZrO_2$ contained Ru-OH active sites, they showed different catalytic performance (Entry 2 and Entry 3–5). The selectivity to FDCA was 71% for $Ru(OH)_x/ZrO_2$, 35% for RuO_2 anhydrous and 47% for RuO_2 hydrate, respectively. RuO_2 hydrate was clearly more active in producing more FDCA compared to RuO_2 anhydrous. As Ru-OH is more exposed on the surface of RuO_2 hydrate than that of RuO_2 anhydrous,[109] presence of Ru-OH is very important to produce FDCA. Because $Ru(OH)_x/ZrO_2$ catalyst showed highest catalytic activity in the oxidation of HMF to FDCA, these results indicate the importance of the support to enhance the overall catalytic activity and selectivity. In comparison with the conventional heterogeneous Ru catalyst, $Ru(OH)_x/ZrO_2$ showed superior catalytic performance (Entry 2 and Entry 11). The homogeneous Ru complex

such as $Ru(acac)_3$, $Ru_3(CO)_{12}$, $\{RuCl_2(p\text{-cymene})\}_2$, and $Ru(PPh_3)_3Cl_2$ indicated extremely poor catalytic activity for oxidation of HMF to FDCA (Entries 3–10). Less than 20% of FDCA yield with over 99% of HMF conversion was obtained in the presence of the homogeneous Ru catalysts. Levulinic acid was a mojor product catalyzed by $RuCl_3 \cdot xH_2O$ and $\{RuCl_2(p\text{-cymene})\}_2$, and yielded 61% and 65%, as respectively.

Table 13. The Results of The Aerobic Oxidation of HMF into HMF Derivatives Using Different Catalysts[a]

Entry	Catalyst	Conversion (%)	Selectivity (%)[a]	
			FDCA	HMFCA
1	None	<1	n.d.	n.d.
2	$Ru(OH)_x/ZrO_2$	>99	71	15
3	$Ru(OH)_x \cdot nH_2O$	>99	53	32
4	RuO_2 anhydrous	>99	35	27
5	RuO_2 hydrate	>99	47	25
6	$RuCl_3 \cdot xH_2O$	>99	18	<1
7	$Ru(acac)_3$	>99	14	<1
8	$Ru_3(CO)_{12}$	>99	19	<1
9	$Ru(PPh_3)_3Cl_2$	>99	7	<1
10	$\{RuCl_2(p\text{-cymene})\}_2$	>99	13	<1
11	Ru/C	>99	24	15
12	ZrO_2	>99	n.d.	n.d.
13	NaOH treated ZrO_2	>99	n.d.	n.d.

a: Reaction conditions: HMF (0.5 mmol), water (3 mL), $Ru(OH)_x/ZrO_2$ (2 mol%), NaOH (2 mmol), O_2 1 bar. b: byproducts were not furanic compounds.

The unsaturated oxygen on the ZrO_2 surface coordinated with ruthenium showed more covalent bond character through the immobilization of ruthenium active sites.[114, 115] In other word, ruthenium active sites on ZrO_2 might possess more Lewis acidic character than the homogeneous ones. Since Zr^{4+} ions of the surface of ZrO_2 are highly coordinative, electron-deficient, and have a high affinity for oxygen, an O−Zr bond can be easily formed.[116] This can accelerate selective oxidation of HMF into HMFCA rather than DFF. On the basis of the above discussions, a possible reaction mechanism can be proposed in the $Ru(OH)_x/ZrO_2$ catalyzed HMF oxidation as Scheme 9.

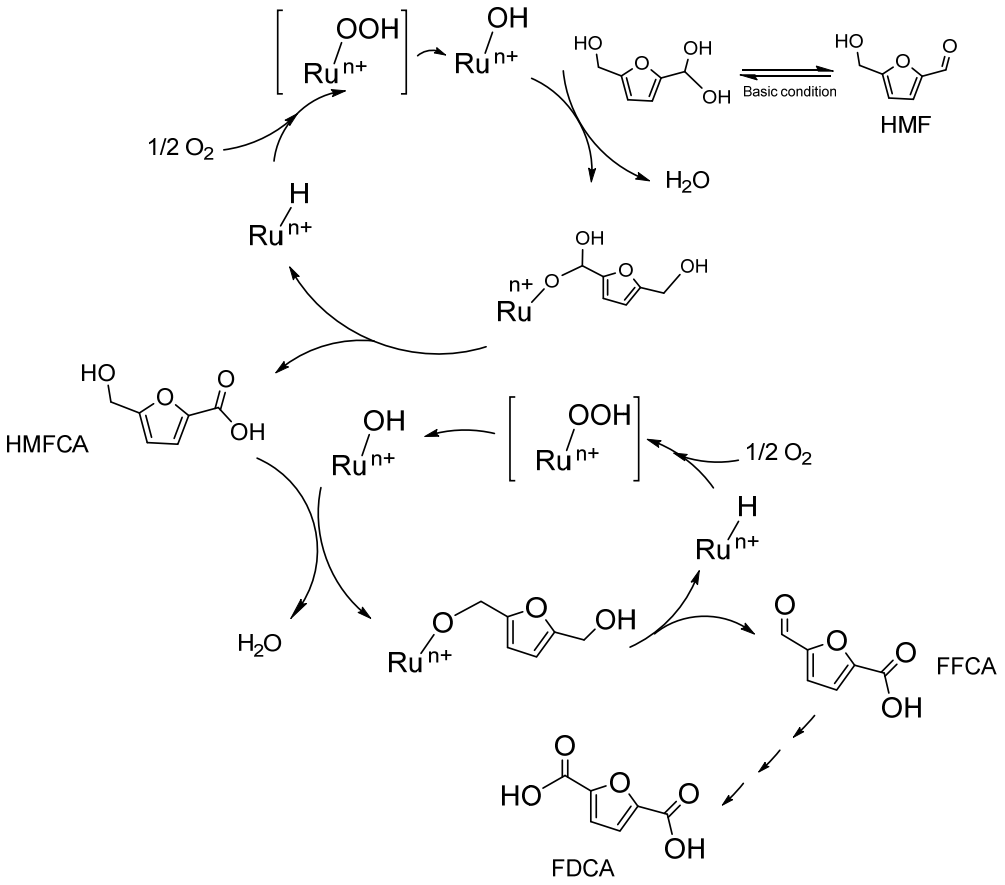

Scheme 9. A possible reaction mechanism for $Ru(OH)_x/ZrO_2$ catalyzed oxidation of HMF in water.

The highest HMF conversion of 99% and FDCA yield of 71% were obtained with TON= 36 and TOF=1.5 h^{-1}, when $Ru(OH)_x/ZrO_2$ catalyst (2 mol%) and NaOH (4 eq) were used. The TOF reached 1.5 h^{-1}, which is comparable or higher than those with previously reported heterogeneous catalysts as Au/TiO_2 (TOF = 1.6 h^{-1}),[117], Pt/C (TOF = 0.08 h^{-1}),[52] Au/C (TOF = 1.6 h^{-1})[118] and Au/CeO_2 (TOF = 0.31 h^{-1}).[119] The $Ru(OH)_x/ZrO_2$ catalyst was easily removed from the reaction solution by filtration, and recycled 10 times without significant any loss of its original catalytic activity (Table 14).

Table 14. Recycle Test of $Ru(OH)_x/ZrO_2$ in Oxidation of HMF

Cycle Number	HMF Conversion (%)	FDCA Yield (%)	ICP-AES (mmol 'Ru'/g)
1	>99	71	0.26
2	>99	70	0.26
3	>99	70	0.26
4	>99	69	0.26
5	>99	70	0.26
6	>99	67	0.25
7	>99	69	0.25
8	>99	68	0.25
9	>99	67	0.25
10	>99	66	0.25

Reaction conditions: HMF (0.5 mmol), $Ru(OH)_x/ZrO_2$ (2 mol%), water (3 mL), reaction temperature 100 ^oC, O_2 1 bar, 24 h.

2.3. Reduction HMF into BHMF Catalyzed by $Ru(OH)_x/ZrO_2$

2.3.1. Reaction Optimization in Reduction HMF into BHMF

Since HMF is composed of multifunctionalized compounds and highly oxidized organic molecules, many types of reaction can occur in the catalytic reaction.[120] In this aspect, HMF reduction condition is necessary in order to prevent any undesired side reactions with high selectivity. At first, HMF was reduced to BHMF under pressured hydrogen gas, which is a well-known hydrogenation condition for the reduction of HMF to BHMF. As shown in Table 15, various solvent systems were examined for the HMF reduction reaction using $Ru(OH)_x/ZrO_2$ catalyst under 30 bar pressured hydrogen. The catalyst showed excellent selectivity in most of the solvents, except for *tert*-butanol (Entry 11). The highest conversion was obtained in 2-propanol (Entry 1). In hydride transfer reaction, 2-propanol can take a role as a reducing agent in agreement with our result. The following HMF reduction result obviously showed the fact that 2-propanol had been enhancing the HMF reduction with regard to reaction temperature. Generally, the reduction reaction takes place in boiling 2-propanol with very chemoselectivity for aldehyde group.[121] As shown in Table 16,

hydrogenolysis of HMF simultaneously occurred to aliphatic substrate in high reaction temperature (Entry 3, and see Appendix A7). Meanwhile, HMF reduction reaction into BHMF was not favorable in low reaction temperatures (20 ^{o}C, Entry 1 in Table 16).

Table 15. Hydrogenation of HMF Result Depending on Various Solvent

Entry	Solvent	Conversion of HMF (%)	BHMF Selectivity (%)
1	2-Propanol	99	>99
2	Water	87	>99
3	Methanol	47	>99
4	Acetonitrile	17	>99
5	1,4-Dioxane	17	>99
6	Hexane	9	>99
7	Toluene	29	>99
8	Cyclopentyl metyl ether	60	>99
9[a]	*tert*-Butanol	99	<1
10	DMF	<1	<1

a: Reaction condition: HMF (100 uL, 0.97 mmol), $Ru(OH)_x/ZrO_2$ (15 mg, 3 μmol%), reaction temperature 40 ^{o}C, H_2 30 bar, solvent (3 mL), 3 h. Conversion and selectivity were analyzed by ^{1}H-NMR spectrum. a: Hydrogenolysis reaction occurred.

Table 16. Hydrogenation of HMF Result Depending on Reaction Temperature

Entry	Reaction temperature (°C)	Conversion (%)	BHMF Selectivity (%)
1	20	<1	<1
2	40	>99	>99
3	80	>99	<1

a: Reaction condition: HMF (100 uL, 0.97 mmol), $Ru(OH)_x/ZrO_2$ (15 mg, 3 μmol%), H_2 30 bar, 2-propanol (3 mL), 3 h. Conversion and selectivity were analyzed by ^{1}H-NMR spectrum.

Next, the pressure of hydrogen was varied in order to identify the pressure-dependence in HMF reduction reaction. As shown in Table 17, the conversion of HMF increased depending on the hydrogen pressure. Moreover, it showed that at least a certain level of hydrogen pressure was required to accelerate the reaction rate. In our case, the HMF reduction reaction was favorable over 30 bar of hydrogen pressure.

Table 17. Hydrogenation of HMF Result Depending on Various Hydrogen Pressure

Entry	Pressure of H_2 (bar)	Conversion (%)	BHMF Selectivity (%)
1	1	<1	<1
2	10	23	>99
3	20	44	>99
4	30	>99	>99
5	40	>99	>99

Reaction condition: HMF (100 uL, 0.97 mmol), $Ru(OH)_x/ZrO_2$ (15 mg, 3 μmol%), reaction temperature 40 ^oC, H_2 2-propanol (3 mL), 3 h. Conversion and selectivity were analyzed by ^1H-NMR spectrum.

To decide the amount of catalytic enough to carry out HMF reduction by $Ru(OH)_x/ZrO_2$, three versions (0.02 mol% to 0.3 mol %) of catalytic amount were used in the HMF reduction reaction (Table 18). 0.3 mol % of the catalyst was enough to hydrogenation of HMF into BHMF.

Table 18. Hydrogenation of HMF Result Depending on Amount of Catalyst

Entry	Amount of catalyst	Conversion (%)	BHMF Selectivity (%)
1	1 mg (0.02 mol %)	4	>99
2	5 mg (0.1 mol%)	27	>99
3	15 mg (0.3 mol%)	>99	>99

Reaction condition: HMF (100 uL, 0.97 mmol), $Ru(OH)_x/ZrO_2$, H_2 30 bar, reaction temperature 40 ^oC, 2-propanol (3 mL), 3 h. Conversion and selectivity were analyzed by ^1H-NMR spectrum.

2.3.2. Hydrogenation of HMF into BHMF

The hydrogenation of HMF was studied using various homogeneous, and heterogeneous Ru catalysts under 30 bar of H_2 at 40 ^oC (Table 19). Interestingly, $Ru(OH)_x/ZrO_2$ showed excellent catalytic activity in the selective hydrogenation of HMF compared to the conventional homogeneous Ru catalyst (Entry 2 vs. Entries 3−10). As shown in entry 3 and 6, the active site seems to be very important in the hydrogenation of HMF. Active site of $RuCl_3 \cdot nH_2O$ is Ru−Cl, and that of $Ru(OH)_x \cdot nH_2O$ is Ru-OH. Based on the result of HMF conversion, Ru−OH active site is more favorable for the hydrogenation of HMF than Ru−Cl (21% vs. 1%). The hydrogenation results in entry 4 and 5 were also in good agreement with this. Generally, RuO_2 hydrate can hold more hold Ru−OH active site than RuO_2 anhydrous because of crystal water, and thus RuO_2 hydrate shows superior catalytic ability than RuO_2 anhydrous.[109] As previously reported, RuO_2 hydrate showed higher hydrogenation activity as RuO_2 anhydrous (entry 4 and 5). When the catalytic performances are compared between $Ru(OH)_x/ZrO_2$ and $Ru(OH)_x \cdot nH_2O$, ZrO_2 support enhanced the catalytic activity as well as the selectivity in the hydrogenation

reaction (Entry 2 and 3). The ruthenium complexes such as $Ru(acac)_3$, $Ru_3(CO)_{12}$, $\{RuCl_2(p\text{-cymene})\}_2$, and $Ru(PPh_3)_3$ were inactive for the hydrogenation of HMF, and they could not be easily separated from the reaction mixture (entries 7−10). It is noteworthy that the use of commercially available heterogeneous Ru catalyst resulted in much lower yield of BHMF compared to $Ru(OH)_x/ZrO_2$. The hydrogenation reaction rarely took place in the presence of pristine ZrO_2, base-treated ZrO_2, and in the absence of the catalyst (Entries 12, 13, and 1). These results revealed that ZrO_2 supported Ru−OH is effective for the selective hydrogenation of HMF into BHMF under mild reaction conditions.

Based on the theory of electronic metal−support interactions, metal oxide support can enhance the catalytic activity of metal active site.[122] A number of studies have been devoted to study the interaction and behavior of oxide surfaces such as TiO_2, and Al_2O_3 with substrates, but only a few of the studies of ZrO_2 dealt with substrate absorptions and interactions.[123-126] The unsaturated oxygen on the ZrO_2 surface coordinated with ruthenium showed more covalent bond character through the immobilization of ruthenium active sites. In other words, electron density flows from

the Ru−O bond toward the Zr−O bond on the surface of ZrO_2. These phenomena indicate that ruthenium active sites on ZrO_2 might possess more Lewis acidic character than the homogeneous ones, which can accelerate the formation of Ru−H species. The Ru active site can favorably absorb oxygen atoms of organic molecule. Thus, the hydrogen can be easily spillover to form Ru-H, and the hydride can be transferred to the C=O bond to achieve selective hydrogenation. After calcination of $Ru(OH)_x/ZrO_2$ at 700 ^oC under inert atmosphere, the hydrogenation activity of the catalyst dramatically decreased. Only 1% of HMF was transformed to BHMF in the same hydrogenation condition. Because the calcination process can change the interface between metal oxide and metal active site, the above mentioned phenomena strongly proves that such electronic effects exhibit at the Ru−ZrO_2 interface. Based on these, a possible hydrogenation reaction mechanism by $Ru(OH)_x/ZrO_2$ in presence of 2-propanol is proposed (Scheme 10).

The TOF reached to 100 h^{-1} and 65 $mmol \cdot g^{-1} \cdot h^{-1}$, which is significantly higher than those with previously reported heterogeneous catalysts such as Ir-ReO_x/SiO_2 (TOF = 54 h^{-1}),[127] CeO_x (6.4 $mmol \cdot g^{-1} \cdot h^{-1}$),[66] Mg-Zr (7.5 $mmol \cdot g^{-1} \cdot h^{-1}$),[66] γ-

Alumina (6.4 $mmol \cdot g^{-1} \cdot h^{-1}$)[66] and Ni-Pd/$SiO_2$ (TOF = 61 h^{-1}).[128] The $Ru(OH)_x/ZrO_2$ catalyst was easily removed from the reaction mixture by filtration, and was recycled ten times without significant loss of its original catalytic activity (Table 20).

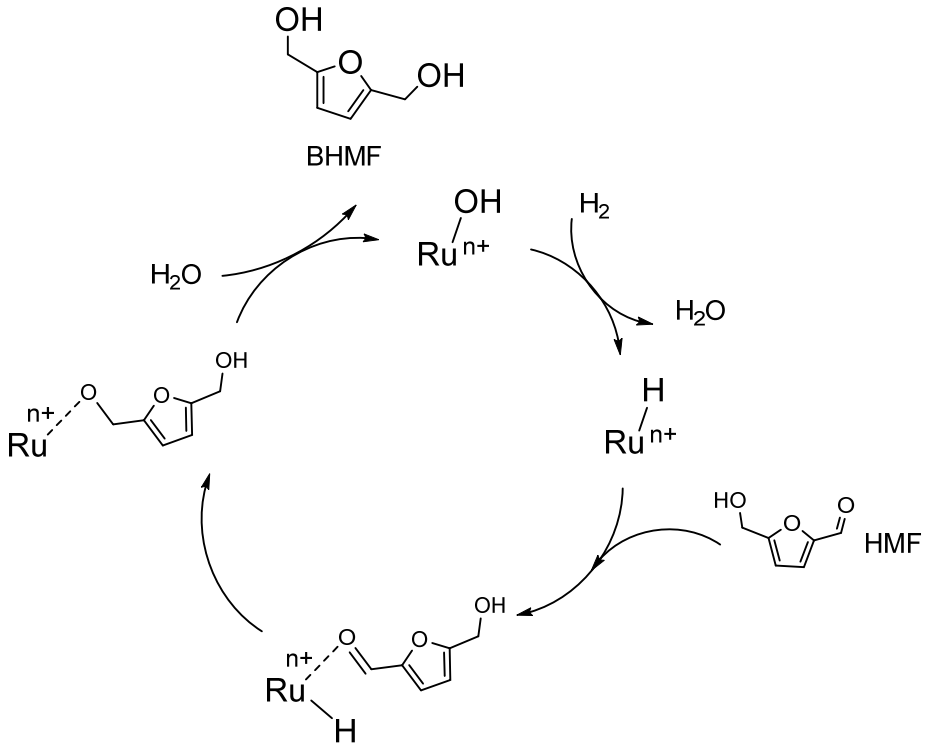

Scheme 10. A possible reaction mechanism for Ru(OH)x/ZrO2 catalyzed hydrogenation of HMF in presince of 2-propanol.

Table 19. The Results of The Aerobic Oxidation of HMF into HMF Derivatives Using Different Catalysts

Entry	Catalyst	Conversion of HMF (%)	BHMF Selectivity (%)
1	None	<1	n.d.
2	$Ru(OH)_x/ZrO_2$	>99	>99
3	$Ru(OH)_x \cdot nH_2O$	21	>99
4	RuO_2 anhydrous	9	>99[b]
5	RuO_2 hydrate	31	>99
6	$RuCl_3 \cdot xH_2O$	1	<1
7	$Ru(acac)_3$	<1	n.d.
8	$Ru_3(CO)_{12}$	<1	n.d.
9	$Ru(PPh_3)_3Cl_2$	23	>99
10	$\{RuCl_2(p\text{-cymene})\}_2$	7	>99
11	Ru/C	6	>99
12	ZrO_2	<1	n.d.
13	NaOH treated ZrO_2	<1	n.d.

Reaction condition: HMF (100 uL, 0.97 mmol), $Ru(OH)_x/ZrO_2$ (15 mg, 3 μmol%), reaction temperature 40 °C, H_2 30 bar, 2-propanol (3 mL), 3 h. Conversion and selectivity were analyzed by ^{1}H-NMR.

Table 20. Recycling Test of $Ru(OH)_x/ZrO_2$ in Hydrogenation of HMF

Cycle Number	Conversion of HMF (%)	BHMF Yield (%)	ICP-AES (mmol 'Ru'/g)
1	>99	>99	0.26
2	95	94	0.26
3	90	90	0.26
4	93	93	0.26
5	94	93	0.26
6	92	92	0.26
7	93	93	0.25
8	92	92	0.25
9	91	90	0.25
10	92	92	0.25

Reaction conditions: HMF (100 uL, 0.97 mmol), $Ru(OH)_x/ZrO_2$ (15 mg, 3 μmol%), reaction temperature 40 ^oC, H_2 30 bar, 2-propanol (3 mL), 3 h.

3. Conclusion

$Ru(OH)_x/ZrO_2$ is an efficient heterogeneous catalyst for selective HMF aerobic oxidation and hydrogenation. The highly active ruthenium active site, Ru−OH, was deposited on the surface of ZrO_2 without forming any ruthenium oxide or ruthenium metal NP, which was confirmed by TEM, XRD, and XPS. The ruthenium active site promoted excellent selective HMF aerobic oxidation reaction into FDCA, as well as selective hydrogenation of HMF into BHMF, because the surface chemical environment on ZrO_2 has unsaturated Lewis acid−base pairs. The catalyst can be separated easily and recycled 10 times without any loss of catalytic performance. Thus, $Ru(OH)_x/ZrO_2$ catalyst could be facilitated the development of new processes for the production of HMF derivatives.

References

1. Pilla, S., *Engineering Applications of Bioplastics and Biocomposites-an Overview*. Handbook of Bioplastics and Biocomposites Engineering Application, ed. S. Pilla, 2011, Salem, Massachusetts: Scrivener Publishing LLC, Wiley-VCH Verlag GmbH & Co. KGaA.

2. Anastas, P.T., Crabtree, Robert H., Leitner, Walter., Jessop, Philip G., Li, Chao-Jun., Wasserscheid, Peter., Stark, Annegret. , *Handbook of green chemistry,* 2009, Weinheim: Wiley-VCH.

3. Karinen, R., K. Vilonen, and M. Niemela, *Biorefining: Heterogeneously Catalyzed Reactions of Carbohydrates for the Production of Furfural and Hydroxymethylfurfural.* Chemsuschem, 2011. **4**(8): p. 1002-1016.

4. Paul, T.A.J.C.W., *Green Chemistry: Theory and Practice,* 1998, Oxford: Oxford University Press.

5. Poliakoff, M., et al., *Green chemistry: Science and politics of change.* Science, 2002. **297**(5582): p. 807-810.

6. Stocker, M., *Biofuels and Biomass-To-Liquid Fuels in the Biorefinery: Catalytic*

Conversion of Lignocellulosic Biomass using Porous Materials. Angewandte Chemie-International Edition, 2008. **47**(48): p. 9200-9211.

7. Alonso, D.M., J.Q. Bond, and J.A. Dumesic, *Catalytic conversion of biomass to biofuels.* Green Chemistry, 2010. **12**(9): p. 1493-1513.

8. Chheda, J.N., G.W. Huber, and J.A. Dumesic, *Liquid-phase catalytic processing of biomass-derived oxygenated hydrocarbons to fuels and chemicals.* Angewandte Chemie-International Edition, 2007. **46**(38): p. 7164-7183.

9. Initiative, B.R.a.D., *Vision for bioenergy and biobased products in the united states*, 2006.

10. Gallezot, P., *Conversion of biomass to selected chemical products.* Chemical Society Reviews, 2012. **41**(4): p. 1538-1558.

11. Elliott, D.C. and G.G. Neuenschwander, *Liquid Fuels by Low-Severity Hydrotreating of Biocrude*, in *Developments in Thermochemical Biomass Conversion*, A.V. Bridgwater and D.G.B. Boocock, Editors. 1997, Springer Netherlands. p. 611-621.

12. Hu, L., et al., *Catalytic conversion of biomass-derived carbohydrates into fuels and chemicals via furanic aldehydes.* Rsc Advances, 2012. **2**(30): p. 11184-11206.

13. Vyas, A.P., J.L. Verma, and N. Subrahmanyam, *A review on FAME production processes.* Fuel, 2010. **89**(1): p. 1-9.

14. Jawaid, M. and H.P.S. Abdul Khalil, *Cellulosic/synthetic fibre reinforced polymer hybrid composites: A review.* Carbohydrate Polymers, 2011. **86**(1): p. 1-18.

15. Zimmerman, P.T.A.J.B., *Innovations in Green Chemisgry and Green Engineering*, ed. P.T.A.J.B. Zimmerman2013, New York: Springer.

16. Balu, R.L.A.M., *Producing Fuels and Fine Chemicals from Biomass Using Nanomaterials*2014, Boca Raton: CRC Press Taylor & Francis Group.

17. Schmidt, L.D. and P.J. Dauenhauer, *Chemical engineering - Hybrid routes to biofuels.* Nature, 2007. **447**(7147): p. 914-915.

18. Laboratory, N.R.E., *Top Value Added Chemicals From Biomass Volume I: Results of Screening for Potential Candidates from Sugars and Synthesis Gas* 2004.

19. Bozell, J.J. and G.R. Petersen, *Technology development for the production of biobased products from biorefinery carbohydrates-the US Department of Energy's "Top 10" revisited.* Green Chemistry, 2010. **12**(4): p. 539-554.

20. Hu, L., et al., *Catalytic conversion of biomass-derived carbohydrates into fuels and*

chemicals via furanic aldehydes. Rsc Advances, 2012. **2**(30): p. 11184-11206.

21. Hansen, T.S., J.M. Woodley, and A. Riisager, *Efficient microwave-assisted synthesis of 5-hydroxymethylfurfural from concentrated aqueous fructose.* Carbohydrate Research, 2009. **344**(18): p. 2568-2572.

22. Moreau, C., M.N. Belgacem, and A. Gandini, *Recent catalytic advances in the chemistry of substituted furans from carbohydrates and in the ensuing polymers.* Topics in Catalysis, 2004. **27**(1-4): p. 11-30.

23. Qi, X.H., et al., *Sulfated zirconia as a solid acid catalyst for the dehydration of fructose to 5-hydroxymethylfurfural.* Catalysis Communications, 2009. **10**(13): p. 1771-1775.

24. Bicker, M., J. Hirth, and H. Vogel, *Dehydration of fructose to 5-hydroxymethylfurfural in sub- and supercritical acetone.* Green Chemistry, 2003. **5**(2): p. 280-284.

25. Despax, S., et al., *Fast and efficient DMSO-mediated dehydration of carbohydrates into 5-hydroxymethylfurfural.* Catalysis Communications, 2014. **51**: p. 5-9.

26. Wang, H.L., et al., *Graphene Oxide Catalyzed Dehydration of Fructose into 5-*

Hydroxymethylfurfural with Isopropanol as Cosolvent. Chemcatchem, 2014. **6**(3): p. 728-732.

27. Chen, J.Z., et al., *Conversion of fructose into 5-hydroxymethylfurfural catalyzed by recyclable sulfonic acid-functionalized metal-organic frameworks.* Green Chemistry, 2014. **16**(5): p. 2490-2499.

28. Roman-Leshkov, Y., J.N. Chheda, and J.A. Dumesic, *Phase modifiers promote efficient production of hydroxymethylfurfural from fructose.* Science, 2006. **312**(5782): p. 1933-1937.

29. Pagan-Torres, Y.J., et al., *Production of 5-Hydroxymethylfurfural from Glucose Using a Combination of Lewis and Bronsted Acid Catalysts in Water in a Biphasic Reactor with an Alkylphenol Solvent.* Acs Catalysis, 2012. **2**(6): p. 930-934.

30. Lansalot-Matras, C. and C. Moreau, *Dehydration of fructose into 5-hydroxymethylfurfural in the presence of ionic liquids.* Catalysis Communications, 2003. **4**(10): p. 517-520.

31. Qi, X.H., et al., *Efficient process for conversion of fructose to 5-hydroxymethylfurfural with ionic liquids.* Green Chemistry, 2009. **11**(9): p. 1327-

1331.

32. Binder, J.B. and R.T. Raines, *Simple Chemical Transformation of Lignocellulosic Biomass into Furans for Fuels and Chemicals.* Journal of the American Chemical Society, 2009. **131**(5): p. 1979-1985.

33. Zhao, H.B., et al., *Metal chlorides in ionic liquid solvents convert sugars to 5-hydroxymethylfurfural.* Science, 2007. **316**(5831): p. 1597-1600.

34. Hu, S., et al., *Efficient conversion of glucose into 5-hydroxymethylfurfural catalyzed by a common Lewis acid SnCl4 in an ionic liquid.* Green Chemistry, 2009. **11**(11): p. 1746-1749.

35. Yong, G., Y.G. Zhang, and J.Y. Ying, *Efficient Catalytic System for the Selective Production of 5-Hhydroxymethylfurfural from Glucose and Fructose.* Angewandte Chemie-International Edition, 2008. **47**(48): p. 9345-9348.

36. Qi, X.H., et al., *Fast Transformation of Glucose and Di-/Polysaccharides into 5-Hydroxymethylfurfural by Microwave Heating in an Ionic Liquid/Catalyst System.* Chemsuschem, 2010. **3**(9): p. 1071-1077.

37. Ilgen, F., et al., *Conversion of carbohydrates into 5-hydroxymethylfurfural in highly*

concentrated low melting mixtures. Green Chemistry, 2009. **11**(12): p. 1948-1954.

38. Qi, X.H., et al., *Efficient one-pot production of 5-hydroxymethylfurfural from inulin in ionic liquids.* Green Chemistry, 2010. **12**(10): p. 1855-1860.

39. King II, J.L.K., A. W., Benecke, H. P.; Mitchell, K. P.; Clingerman, M. C., 2008.

40. Ma, J.P., et al., *The copolymerization reactivity of diols with 2,5-furandicarboxylic acid for furan-based copolyester materials.* Journal of Materials Chemistry, 2012. **22**(8): p. 3457-3461.

41. Wilsens, C.H.R.M., et al., *Thermotropic Polyesters from 2,5-Furandicarboxylic Acid and Vanillic Acid: Synthesis, Thermal Properties, Melt Behavior, and Mechanical Performance.* Macromolecules, 2014. **47**(10): p. 3306-3316.

42. Bing, L., Z.H. Zhang, and K.J. Deng, *Efficient One-Pot Synthesis of 5-(Ethoxymethyl)furfural from Fructose Catalyzed by a Novel Solid Catalyst.* Industrial & Engineering Chemistry Research, 2012. **51**(47): p. 15331-15336.

43. Chheda, J.N., Y. Roman-Leshkov, and J.A. Dumesic, *Production of 5-hydroxymethylfurfural and furfural by dehydration of biomass-derived mono- and poly-saccharides.* Green Chemistry, 2007. **9**(4): p. 342-350.

44. Duan, Z.Q. and F. Hu, *Highly efficient synthesis of phosphatidylserine in the eco-friendly solvent gamma-valerolactone.* Green Chemistry, 2012. **14**(6): p. 1581-1583.

45. Bermudez, J.M., et al., *Continuous flow nanocatalysis: reaction pathways in the conversion of levulinic acid to valuable chemicals.* Green Chemistry, 2013. **15**(10): p. 2786-2792.

46. Alonso, D.M., S.G. Wettstein, and J.A. Dumesic, *Gamma-valerolactone, a sustainable platform molecule derived from lignocellulosic biomass.* Green Chemistry, 2013. **15**(3): p. 584-595.

47. Roman-Leshkov, Y., et al., *Production of dimethylfuran for liquid fuels from biomass-derived carbohydrates.* Nature, 2007. **447**(7147): p. 982-986.

48. Kunkes, E.L., et al., *Catalytic Conversion of Biomass to Monofunctional Hydrocarbons and Targeted Liquid-Fuel Classes.* Science, 2008. **322**(5900): p. 417-421.

49. Pan, T., et al., *Catalytic conversion of biomass-derived levulinic acid to valerate esters as oxygenated fuels using supported ruthenium catalysts.* Green Chemistry, 2013. **15**(10): p. 2967-2974.

50. Tong, X., Y. Ma, and Y. Li, *Biomass into chemicals: Conversion of sugars to furan derivatives by catalytic processes.* Applied Catalysis A: General, 2010. **385**(1–2): p. 1-13.

51. Vuyyuru, K.R. and P. Strasser, *Oxidation of biomass derived 5-hydroxymethylfurfural using heterogeneous and electrochemical catalysis.* Catalysis Today, 2012. **195**(1): p. 144-154.

52. Ait Rass, H., N. Essayem, and M. Besson, *Selective aqueous phase oxidation of 5-hydroxymethylfurfural to 2,5-furandicarboxylic acid over Pt/C catalysts: influence of the base and effect of bismuth promotion.* Green Chemistry, 2013. **15**(8): p. 2240-2251.

53. Vinke, P., H.E. van Dam, and H. van Bekkum, *Platinum Catalyzed Oxidation of 5-Hydroxymethylfurfural.* Studies in Surface Science and Catalysis, 1990. **Volume 55**: p. 147-158.

54. Lilga, M., R. Hallen, and M. Gray, *Production of Oxidized Derivatives of 5-Hydroxymethylfurfural (HMF).* Topics in Catalysis, 2010. **53**(15-18): p. 1264-1269.

55. Davis, S.E., B.N. Zope, and R.J. Davis, *On the mechanism of selective oxidation of*

5-hydroxymethylfurfural to 2,5-furandicarboxylic acid over supported Pt and Au catalysts. Green Chemistry, 2012. **14**(1): p. 143-147.

56. Pasini, T., et al., *Selective oxidation of 5-hydroxymethyl-2-furfural using supported gold-copper nanoparticles.* Green Chemistry, 2011. **13**(8): p. 2091-2099.

57. Casanova, O., S. Iborra, and A. Corma, *Biomass into chemicals: One pot-base free oxidative esterification of 5-hydroxymethyl-2-furfural into 2,5-dimethylfuroate with gold on nanoparticulated ceria.* Journal of Catalysis, 2009. **265**(1): p. 109-116.

58. Davis, S.E., et al., *Oxidation of 5-hydroxymethylfurfural over supported Pt, Pd and Au catalysts.* Catalysis Today, 2011. **160**(1): p. 55-60.

59. Gupta, N.K., et al., *Hydrotalcite-supported gold-nanoparticle-catalyzed highly efficient base-free aqueous oxidation of 5-hydroxymethylfurfural into 2,5-furandicarboxylic acid under atmospheric oxygen pressure.* Green Chemistry, 2011. **13**(4): p. 824-827.

60. Taarning, E., et al., *Chemicals from renewables: Aerobic oxidation of furfural and hydroxymethylfurfural over gold catalysts.* Chemsuschem, 2008. **1**(1-2): p. 75-78.

61. Hansen, T.S., et al., *One-pot reduction of 5-hydroxymethylfurfural via hydrogen*

transfer from supercritical methanol. Green Chemistry, 2012. **14**(9): p. 2457-2461.

62. Chidambaram, M. and A.T. Bell, *A two-step approach for the catalytic conversion of glucose to 2,5-dimethylfuran in ionic liquids.* Green Chemistry, 2010. **12**(7): p. 1253-1262.

63. Buntara, T., et al., *Caprolactam from Renewable Resources: Catalytic Conversion of 5-Hydroxymethylfurfural into Caprolactone.* Angewandte Chemie-International Edition, 2011. **50**(31): p. 7083-7087.

64. Hales, R.A., 1962.

65. Lilga, M., et al., *Hydroxymethylfurfural Reduction Methods and Methods of Producing Furandimethanol*, 2007, Google Patents.

66. Alamillo, R., et al., *The selective hydrogenation of biomass-derived 5-hydroxymethylfurfural using heterogeneous catalysts.* Green Chemistry, 2012. **14**(5): p. 1413-1419.

67. Wang, Z., et al., *Cooperativity of Brønsted and Lewis Acid Sites on Zeolite for Glycerol Dehydration.* Acs Catalysis, 2014. **4**(4): p. 1144-1147.

68. Acharya, D.P., et al., *Site-Specific Imaging of Elemental Steps in Dehydration of*

Diols on TiO2(110). Acs Nano, 2013. **7**(11): p. 10414-10423.

69. Sheldon, R.A., *Green and sustainable manufacture of chemicals from biomass: state of the art.* Green Chemistry, 2014. **16**(3): p. 950-963.

70. Sheldon, R.A., *Fundamentals of green chemistry: efficiency in reaction design.* Chemical Society Reviews, 2012. **41**(4): p. 1437-1451.

71. Davis, S.E., M.S. Ide, and R.J. Davis, *Selective oxidation of alcohols and aldehydes over supported metal nanoparticles.* Green Chemistry, 2013. **15**(1): p. 17-45.

72. Sheldon, R.A.R.A.v.S.E., *Catalytic Oxidation: Principles and Applications*1995, Singapore: World Scientific.

73. Sheldon, R.A.A., Isabel; Hanefeld, Ulf, *Green Chemistry and Catalysis*2007, Weinheim: WILEY-VCH Verlag GmbH & Co. KGaA.

74. Shi, Z., et al., *Recent advances in transition-metal catalyzed reactions using molecular oxygen as the oxidant.* Chemical Society Reviews, 2012. **41**(8): p. 3381-3430.

75. Nerozzi, F., *Heterogeneous Catalytic Hydrogenation Platinum group metals as hydrogenation catalysts in a two-day course.* Platinum Metals Review, 2012. **56**(4):

p. 236-241.

76. Huheey, J.E.K., E. A.; Keiter, R. L.; Medhi, O. K.;, *Inorganic Chemistry: Principles of Structure and Reactivity*2006, Upper Saddle River, NJ: Pearson Education.

77. Lippard, S.J.B., J. M., *Principles of Bioinorganic Chemistry*1994, Mill Valley, CA: University Science Books.

78. Lloyd, L., *Handbook of Industrial Catalysts* 2011, Berlin, Germany: Springer:.

79. Plietker, B.B., M., *Iron Catalysis: Fundamentals and Applications*2011, Berlin, Germany: Springer.

80. Hopkinson, M.N., et al., *An overview of N-heterocyclic carbenes.* Nature, 2014. **510**(7506): p. 485-496.

81. Riener, K., et al., *Chemistry of Iron N-Heterocyclic Carbene Complexes: Syntheses, Structures, Reactivities, and Catalytic Applications.* Chemical Reviews, 2014.

82. Cotton, F.A.W., G.; Murille, C. A.; Bochmann, M., *Advanced Inorganic Chemistry*. 6th Edition ed1999: Wiley-Interscience.

83. Climent, M.J., A. Corma, and S. Iborra, *Heterogeneous Catalysts for the One-Pot Synthesis of Chemicals and Fine Chemicals.* Chemical Reviews, 2010. **111**(2): p.

1072-1133.

84. Murahashi, S.-I. and D. Zhang, *Ruthenium catalyzed biomimetic oxidation in organic synthesis inspired by cytochrome P-450.* Chemical Society Reviews, 2008. **37**(8): p. 1490-1501.

85. Sheldon, R.A.K., J. K., *Metal-Catalyzed Oxidations of Organic Compounds*1981, New York: Academic Press.

86. Yamaguchi, K. and N. Mizuno, *Supported ruthenium catalyst for the heterogeneous oxidation of alcohols with molecular oxygen.* Angewandte Chemie-International Edition, 2002. **41**(23): p. 4538-+.

87. Bavykin, D.V., et al., *TiO2 nanotube-supported ruthenium(III) hydrated oxide: A highly active catalyst for selective oxidation of alcohols by oxygen.* Journal of Catalysis, 2005. **235**(1): p. 10-17.

88. Yu, H., et al., *Capacitance dependent catalytic activity of RuO2[middle dot]xH2O/CNT nanocatalysts for aerobicoxidation of benzyl alcohol.* Chemical Communications, 2009(17): p. 2408-2410.

89. Marcano, D.C., et al., *Improved Synthesis of Graphene Oxide.* Acs Nano, 2010. **4**(8):

p. 4806-4814.

90. Yoon, H.J., et al., *Polymer-supported gadolinium triflate as a convenient and efficient Lewis acid catalyst for acetylation of alcohols and phenols.* Tetrahedron Letters, 2008. **49**(19): p. 3165-3171.

91. Van Doorslaer, C., et al., *Immobilization of molecular catalysts in supported ionic liquid phases.* Dalton Transactions, 2010. **39**(36): p. 8377-8390.

92. Hara, K., et al., *Construction of self-assembled monolayer terminated with N-heterocyclic carbene-rhodium(I) complex moiety.* Surface Science, 2007. **601**(22): p. 5127-5132.

93. Deng, T., et al., *Conversion of carbohydrates into 5-hydroxymethylfurfural catalyzed by ZnCl2 in water.* Chemical Communications, 2012. **48**(44): p. 5494-5496.

94. Yamaguchi, K., et al., *Tin-Tungsten Mixed Oxide as Efficient Heterogeneous Catalyst for Conversion of Saccharides to Furan Derivatives.* Chemistry Letters, 2011. **40**(5): p. 542-543.

95. Dutta, A., et al., *Synthesis of 5-Hydroxymethylfurural from Carbohydrates using Large-Pore Mesoporous Tin Phosphate.* Chemsuschem, 2014. **7**(3): p. 925-933.

96. Kourieh, R., et al., *Relation between surface acidity and reactivity in fructose conversion into 5-HMF using tungstated zirconia catalysts.* Catalysis Communications, 2013. **30**(0): p. 5-13.

97. Fan, C.Y., et al., *Conversion of fructose and glucose into 5-hydroxymethylfurfural catalyzed by a solid heteropolyacid salt.* Biomass & Bioenergy, 2011. **35**(7): p. 2659-2665.

98. Cardoso, J.M.S. and B. Royo, *Unprecedented synthesis of iron-NHC complexes by C-H activation of imidazolium salts. Mild catalysts for reduction of sulfoxides.* Chemical Communications, 2012. **48**(41): p. 4944-4946.

99. Tong, X., et al., *Defunctionalization of fructose and sucrose: Iron-catalyzed production of 5-hydroxymethylfurfural from fructose and sucrose.* Catalysis Today, 2011. **175**(1): p. 524-527.

100. Xin, B. and J. Hao, *Imidazolium-based ionic liquids grafted on solid surfaces.* Chemical Society Reviews, 2014. **43**(20): p. 7171-7187.

101. Han, L., et al., *Ionic liquids grafted on carbon nanotubes as highly efficient heterogeneous catalysts for the synthesis of cyclic carbonates.* Applied Catalysis A:

General, 2012. **429–430**(0): p. 67-72.

102. Han, L., et al., *Ionic liquids containing carboxyl acid moieties grafted onto silica: Synthesis and application as heterogeneous catalysts for cycloaddition reactions of epoxide and carbon dioxide.* Green Chemistry, 2011. **13**(4): p. 1023-1028.

103. Lozano, P., et al., *Immobilised Lipase on Structured Supports Containing Covalently Attached Ionic Liquids for the Continuous Synthesis of Biodiesel in scCO2.* Chemsuschem, 2012. **5**(4): p. 790-798.

104. Wang, Z., et al., *Enhancing lithium–sulphur battery performance by strongly binding the discharge products on amino-functionalized reduced graphene oxide.* Nature Communications, 2014. **5**.

105. Amarasekara, A.S., L.D. Williams, and C.C. Ebede, *Mechanism of the dehydration of D-fructose to 5-hydroxymethylfurfural in dimethyl sulfoxide at 150 degrees C: an NMR study.* Carbohydrate Research, 2008. **343**(18): p. 3021-3024.

106. Sidhpuria, K.B., et al., *Supported ionic liquid silica nanoparticles (SILnPs) as an efficient and recyclable heterogeneous catalyst for the dehydration of fructose to 5-hydroxymethylfurfural.* Green Chemistry, 2011. **13**(2): p. 340-349.

107. Kim, Y.H., et al., *Zirconia-Supported Ruthenium Catalyst for Efficient Aerobic Oxidation of Alcohols to Aldehydes.* Industrial & Engineering Chemistry Research, 2014. **53**(31): p. 12548-12552.

108. Boudjennad, E., et al., *Experimental and theoretical study of the Ni-(m-ZrO2) interaction.* Surface Science, 2012. **606**(15-16): p. 1208-1214.

109. Giang, T.P.L., T.N.M. Tran, and X.T. Le, *Preparation and characterization of titanium dioxide nanotube array supported hydrated ruthenium oxide catalysts.* Advances in Natural Sciences: Nanoscience and Nanotechnology, 2012. **3**(1): p. 015008.

110. Kim, M.S., et al., *Characteristics and processing effects of ZrO2 thin films grown by metal-organic molecular beam epitaxy.* Applied Surface Science, 2004. **227**(1-4): p. 387-398.

111. Vinke, P.v.D., H. E.; van Bekkum, H. , *New Developments in Selective Oxidation*1990, New York: Elsevier.

112. Kang, E.-S., et al., *Efficient preparation of DHMF and HMFA from biomass-derived HMF via a Cannizzaro reaction in ionic liquids.* Journal of Industrial and

Engineering Chemistry, 2012. **18**(1): p. 174-177.

113. Mascal, M. and E.B. Nikitin, *High-yield conversion of plant biomass into the key value-added feedstocks 5-(hydroxymethyl)furfural, levulinic acid, and levulinic esters via 5-(chloromethyl)furfural.* Green Chemistry, 2010. **12**(3): p. 370-373.

114. Sokol, A.A., et al., *Point defects in ZnO.* Faraday Discussions, 2007. **134**: p. 267-282.

115. Ganduglia-Pirovano, M.V., A. Hofmann, and J. Sauer, *Oxygen vacancies in transition metal and rare earth oxides: Current state of understanding and remaining challenges.* Surface Science Reports, 2007. **62**(6): p. 219-270.

116. Han, Y. and J. Zhu, *Surface Science Studies on the Zirconia-Based Model Catalysts.* Topics in Catalysis, 2013. **56**(15-17): p. 1525-1541.

117. Gorbanev, Y.Y., et al., *Gold-Catalyzed Aerobic Oxidation of 5-Hydroxymethylfurfural in Water at Ambient Temperature.* Chemsuschem, 2009. **2**(7): p. 672-675.

118. Villa, A., et al., *Pd-modified Au on Carbon as an Effective and Durable Catalyst for the Direct Oxidation of HMF to 2,5-Furandicarboxylic Acid.* Chemsuschem, 2013.

6(4): p. 609-612.

119. Cai, J., et al., *Gold Nanoclusters Confined in a Supercage of Y Zeolite for Aerobic Oxidation of HMF under Mild Conditions.* Chemistry – A European Journal, 2013. **19**(42): p. 14215-14223.

120. Nakagawa, Y., M. Tamura, and K. Tomishige, *Catalytic Reduction of Biomass-Derived Furanic Compounds with Hydrogen.* Acs Catalysis, 2013. **3**(12): p. 2655-2668.

121. Czako, L.K.B., *Strategic Apllications of Named Reactions in Organic Synthesis* 2005, Burlington: Elsevier Inc.

122. Herrmann, J.M., *Electronic Effects in Strong Metal Support Interactions on Titania Deposited Metal-Catalysts.* Journal of Catalysis, 1984. **89**(2): p. 404-412.

123. Scott, C.E., et al., *Interaction between Ruthenium and Molybdenum in Rumo/Al2o3 Catalysts.* Applied Catalysis a-General, 1995. **125**(1): p. 71-79.

124. Benvenutti, E.V., et al., *FTIR study of hydrogen and carbon monoxide adsorption on Pt/TiO2, Pt/ZrO2, and Pt/Al2O3.* Langmuir, 1999. **15**(23): p. 8140-8146.

125. Bitter, J.H., K. Seshan, and J.A. Lercher, *On the contribution of X-ray absorption*

spectroscopy to explore structure and activity relations of Pt/ZrO2 catalysts for CO2/CH4 reforming. Topics in Catalysis, 2000. **10**(3-4): p. 295-305.

126. Wang, F., et al., *Catalytic behavior of supported Ru nanoparticles on the (101) and (001) facets of anatase TiO2.* Rsc Advances, 2014. **4**(21): p. 10834-10840.

127. Tamura, M., et al., *Rapid synthesis of unsaturated alcohols under mild conditions by highly selective hydrogenation.* Chemical Communications, 2013. **49**(63): p. 7034-7036.

128. Nakagawa, Y. and K. Tomishige, *Total hydrogenation of furan derivatives over silica-supported Ni-Pd alloy catalyst.* Catalysis Communications, 2010. **12**(3): p. 154-156.

Appendix

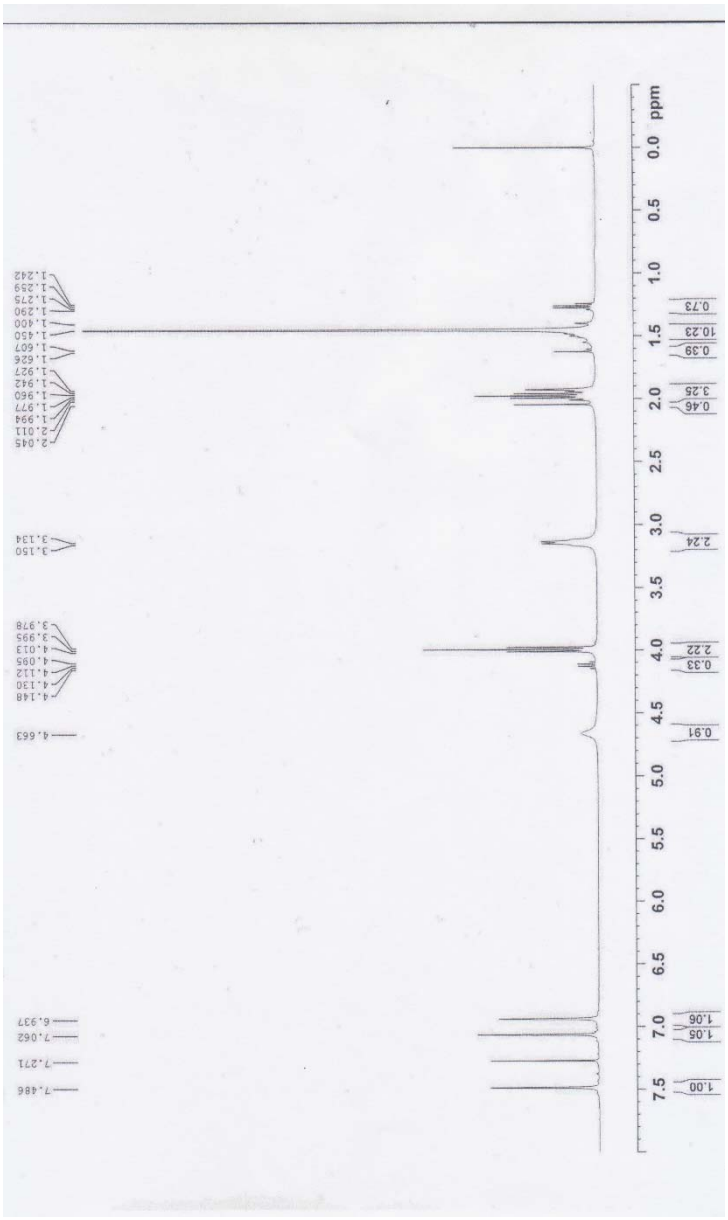

Figure A1. ^{1}H-NMR of 1-[(*N*-tert-butoxycarbonyl)aminopropyl] imidazole

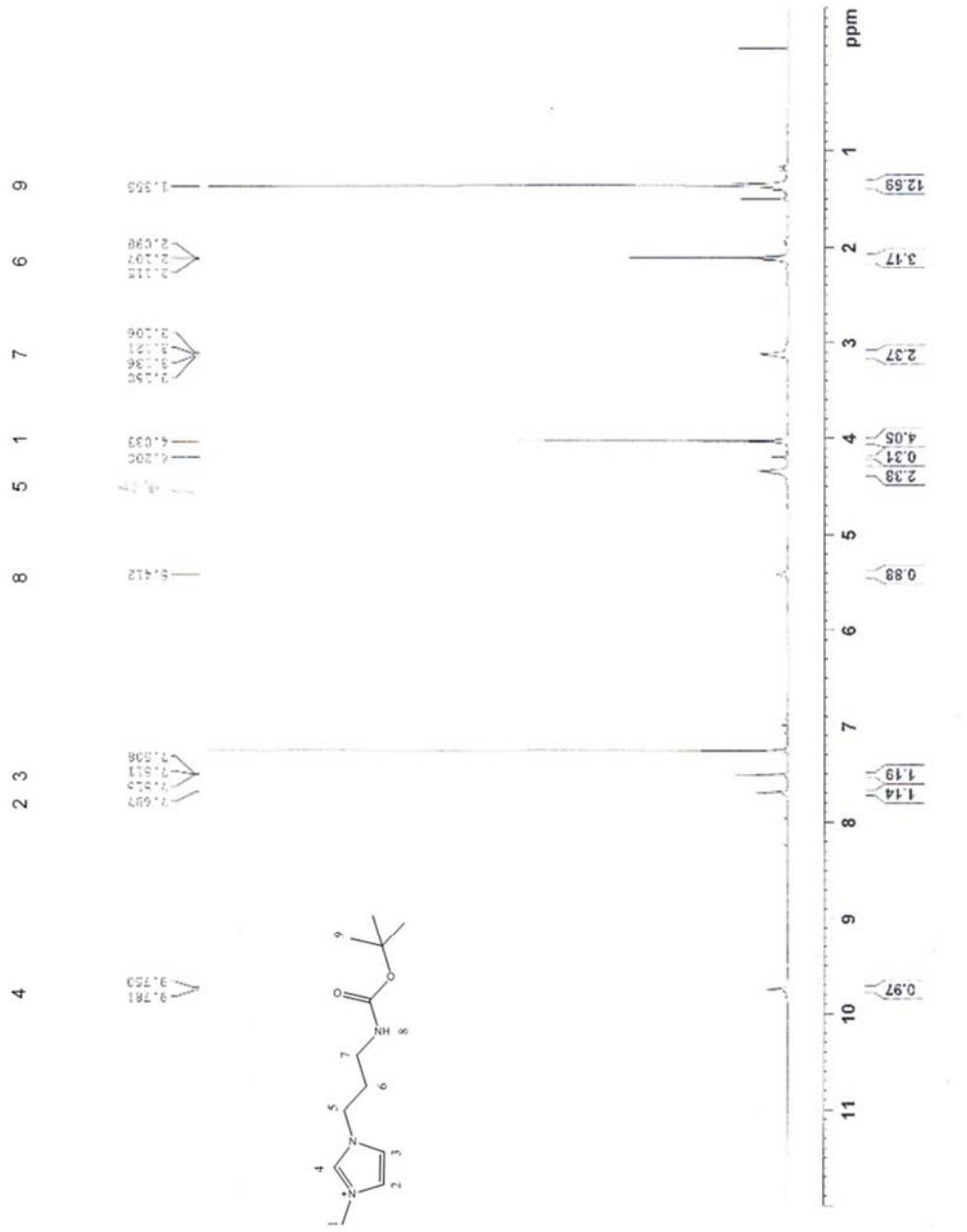

Figure A2. [1]H-NMR of methyl 1-[(*N*-tert-butoxycarbonyl)aminopropyl] imidazolium iodide

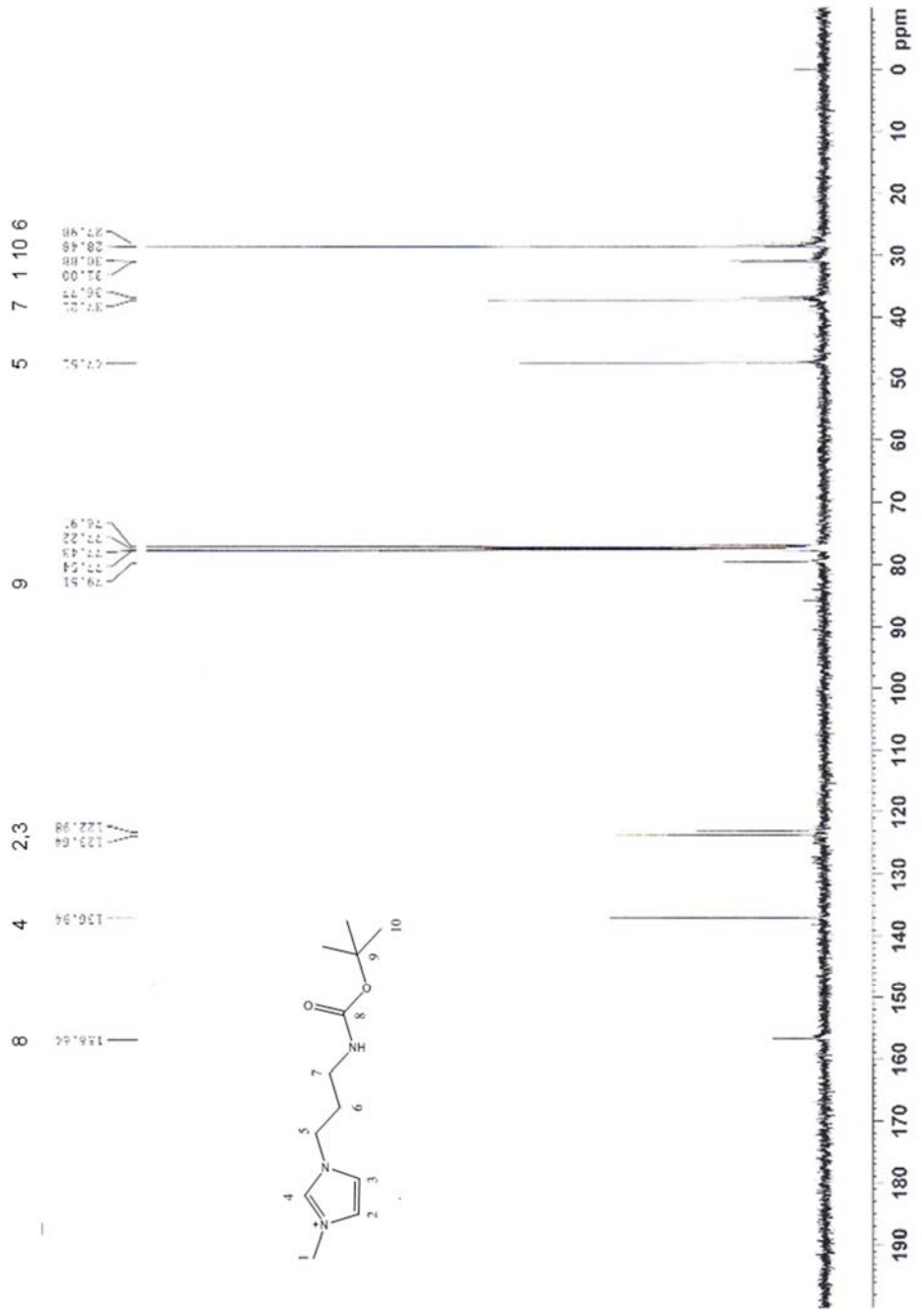

Figure A3. ^{13}C-NMR of methyl 1-[(*N*-tert-butoxycarbonyl)aminopropyl] imidazolium iodide

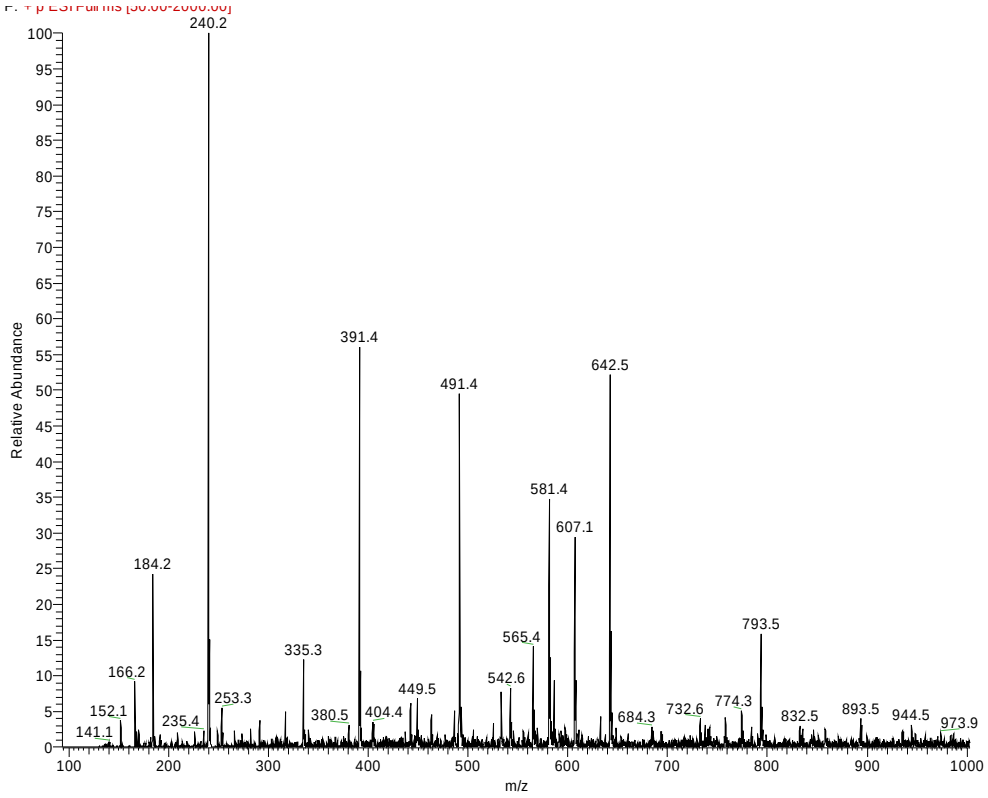

Figure A4. Mass spectrum of methyl 1-[(*N*-tert-butoxycarbonyl)aminopropyl] imidazolium iodide

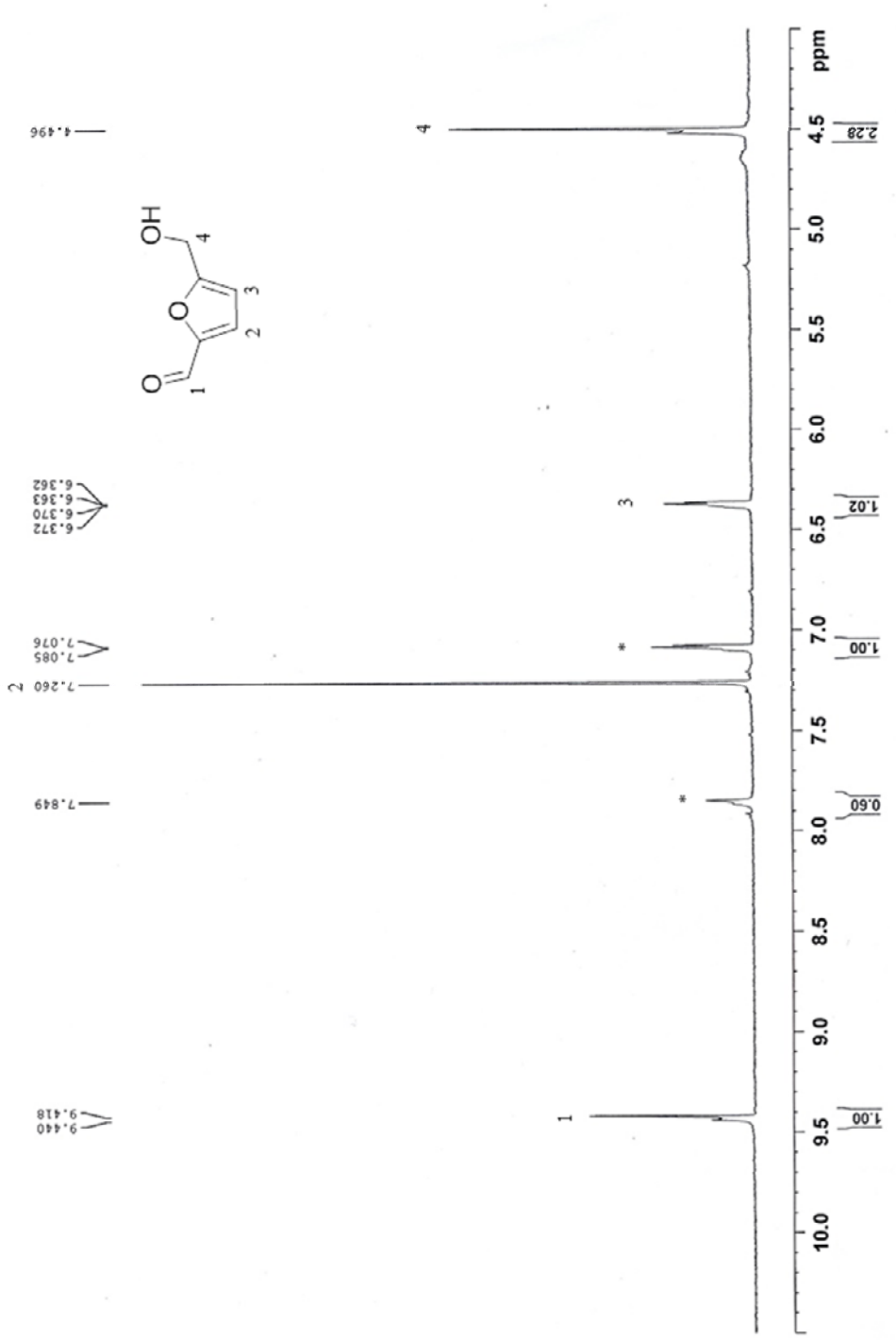

Figure A5. H-NMR of extracted HMF in $CDCl_3$, star was residue of remaining DMSO.

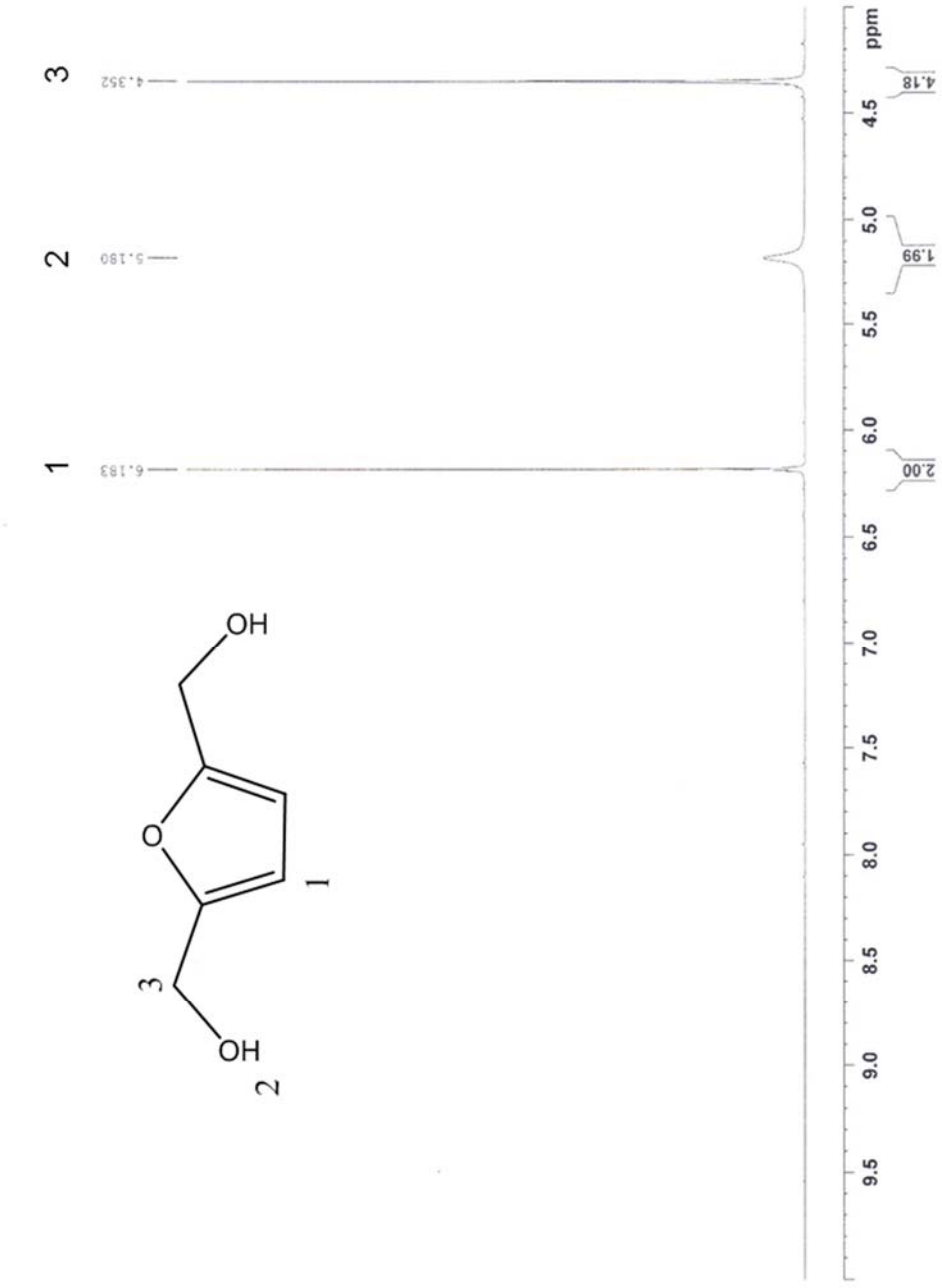

Figure A6. ^{1}H-NMR spectrum of 2,5-bis(hydroxymethyl) furan (400 MHz, CDCl3, TMS).

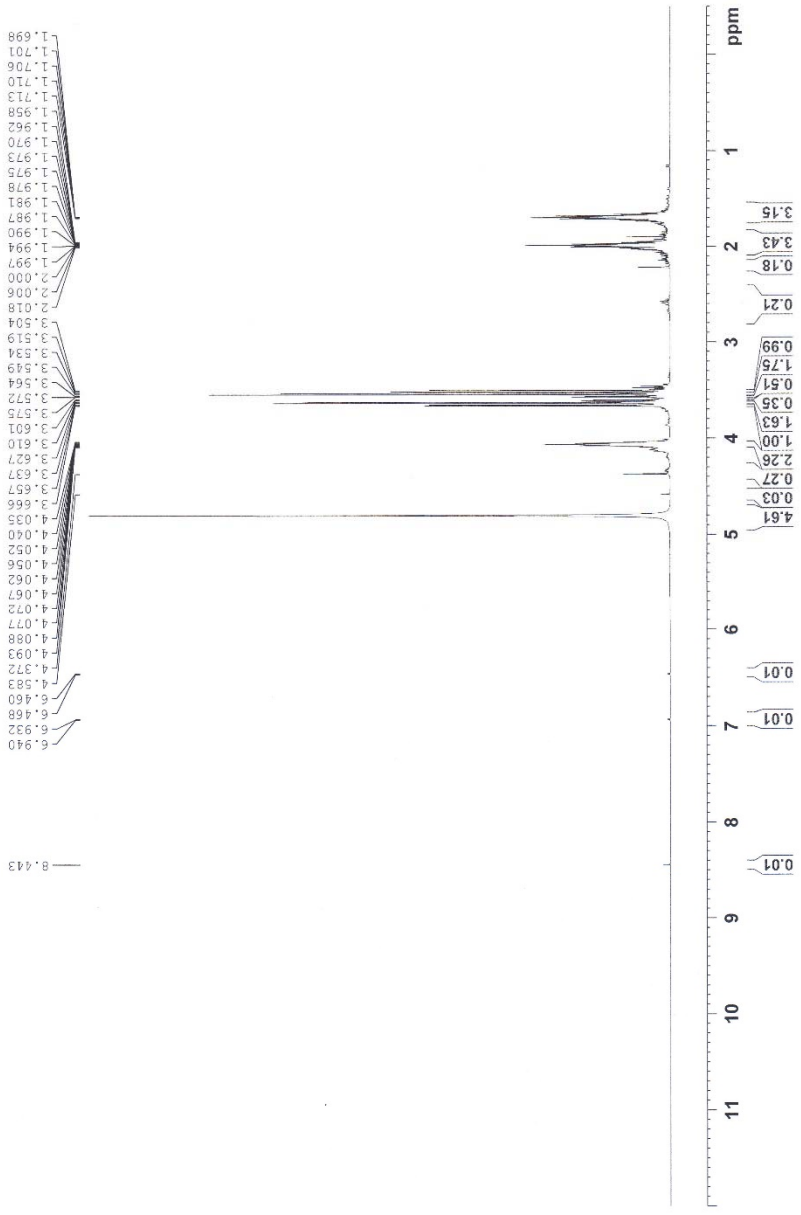

Figure A7. [1]H-NMR spectrum of overhydrogenation reaction mixture of HMF.

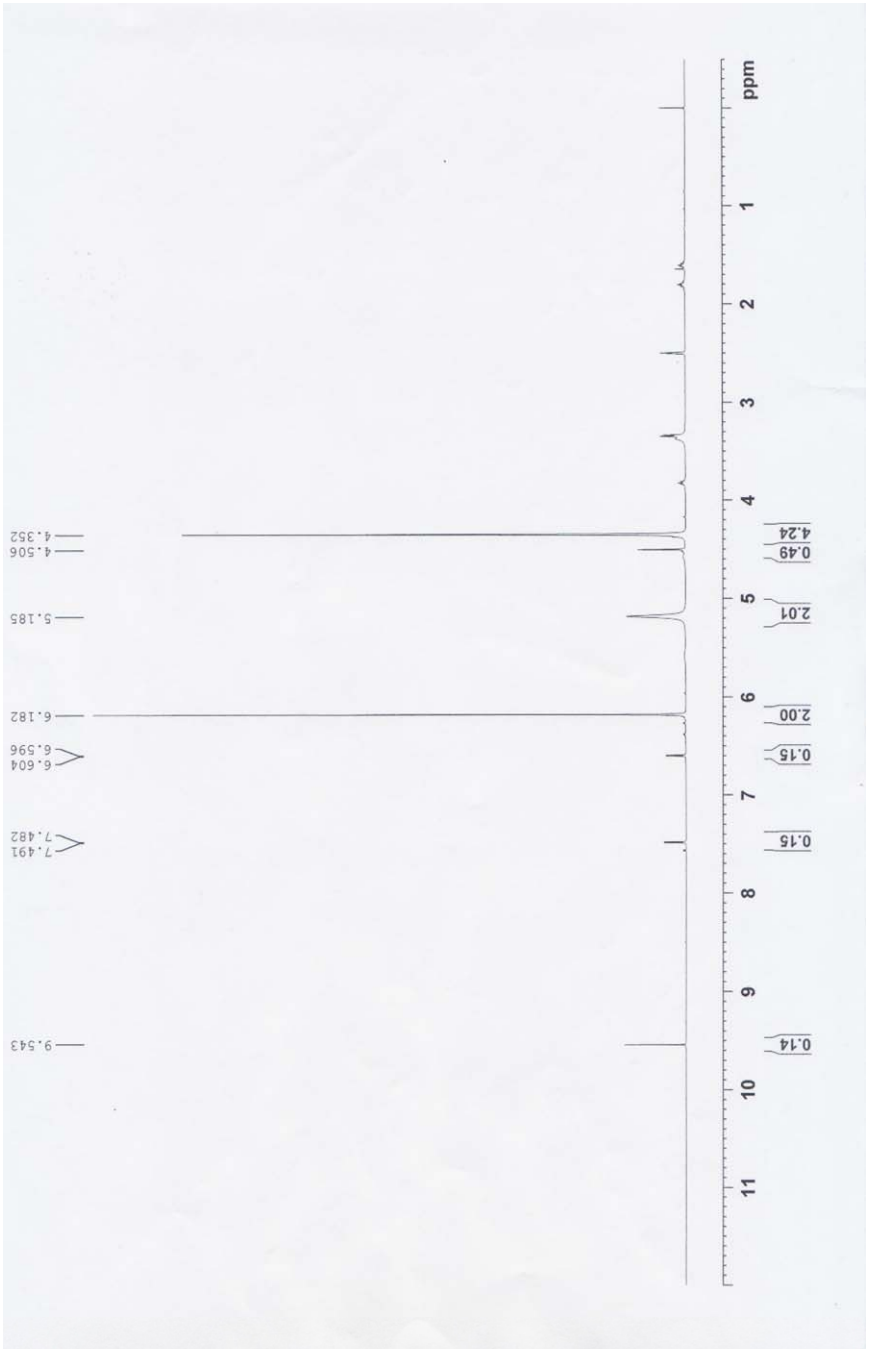

Figure A8. [1]H-NMR spectrum of hydrogenation reaction mixture of HMF after 10 time reused.

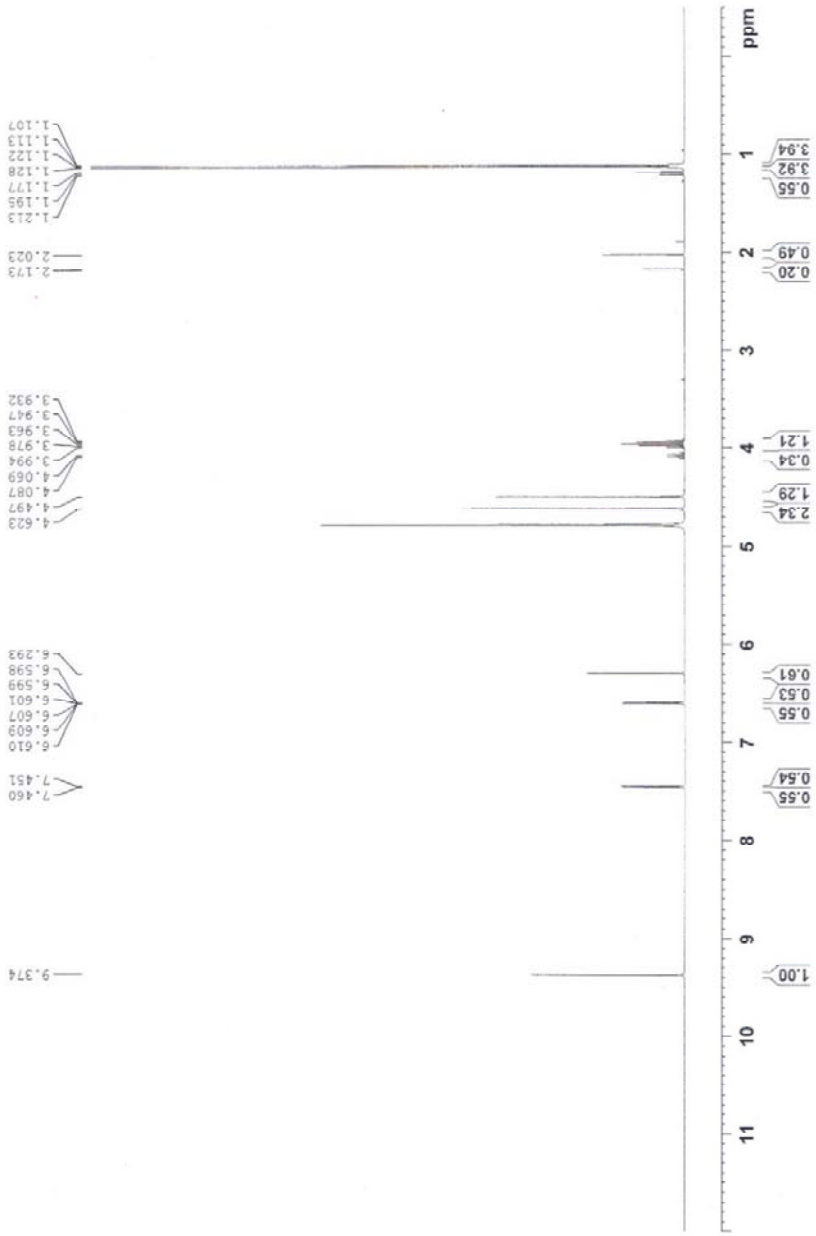

Figure A9. ^{1}H-NMR spectrum of hydrogenation reaction mixture of HMF using normal $Ru(OH)_x/ZrO_2$.

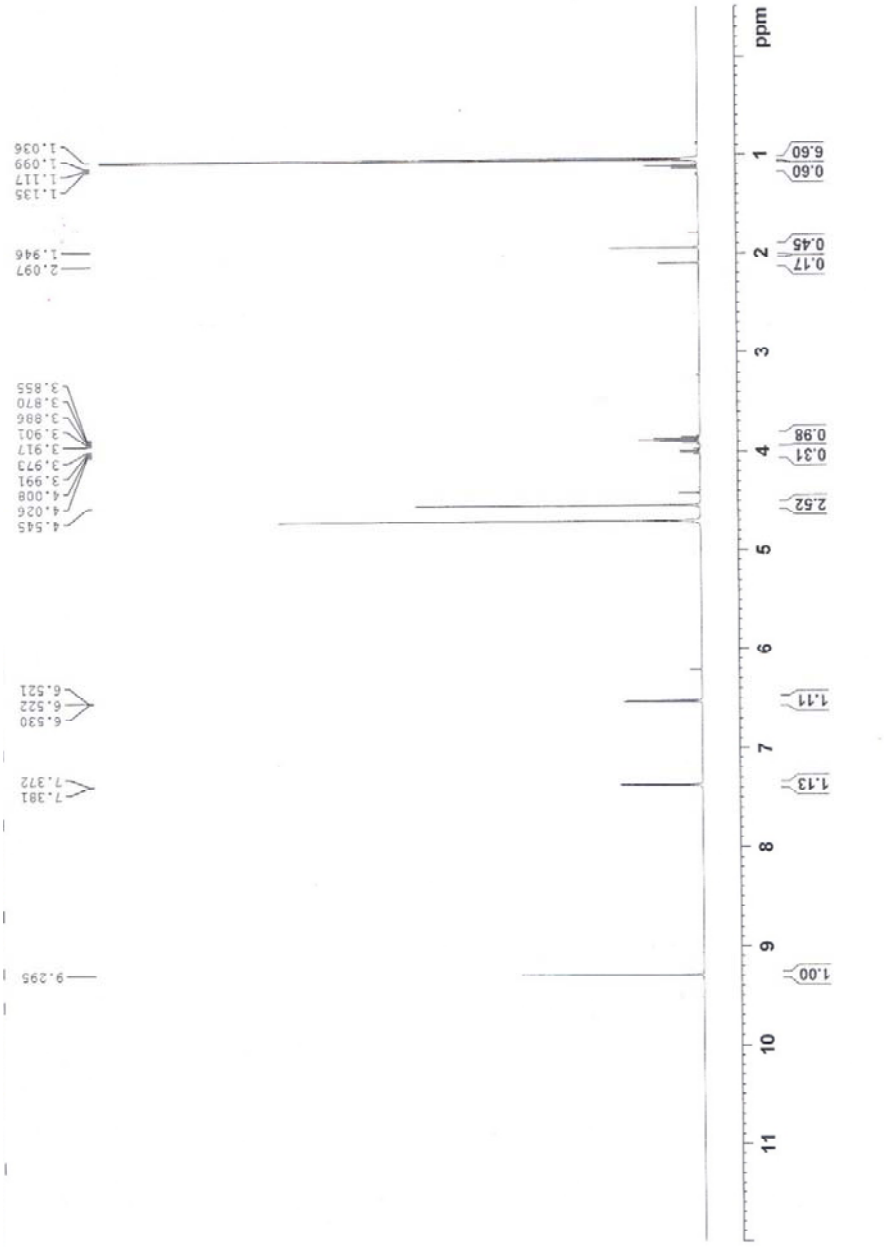

Figure A10. ^{1}H-NMR spectrum of hydrogenation reaction mixture of HMF using thermal treated $Ru(OH)_x/ZrO_2$.

Abstract in Korean

최근, 그린 화학분야에서 불균일계 촉매의 활용은 많은 관심을 받는 주제이다. 고분자, 산화금속 그리고 탄소 물질은 불균일계 촉매를 만드는데 있어서 범용적으로 쓰이는 지지체이다. 일반적으로 불균일계 촉매는 용매에 녹지 않으므로 쉽게 반응물로부터 분리할 수 있으며, 이로 인해 많은 횟수만큼 재사용이 가능하다. 게다가 불균일계 촉매는 화학적 과정을 통해 원하는 촉매의 특성을 디자인 할 수 있는 강점이 있다. 이러한 장점에도 불구하고 균일계 촉매보다 낮은 활성 때문에 불균일계 촉매는 바이오매스 전환을 통한 고부가가치 화합물의 합성에 크게 활용되지 못하였다. 따라서 높은 활성을 지니는 불균일계 촉매의 개발은 바이오매스 전환분야에서 도전적인 분야이다.

본 논문은 두 가지 불균일계 전이금속 촉매를 이용한 효율적인 탄수화물 전환에 대해 기술하였다. 철 촉매는 프록토오스의 탈수화반응에 적용하였고, 루테늄 촉매는 5-하이드록시메틸 푸르푸랄의

수소첨가 및 산화반응에 적용하였다.

첫번째 장에서는 프록토오스의 탈수화반응을 통한 5-하이드록시메틸 푸르푸랄 생산에 활용하는 불균일계 NHC (*N*-heterocyclic carbene)-Fe 촉매에 대해 기술하였다. 5-하이드록시메틸 푸르푸랄 생산 과정 개발은 6탄당 기반 바이오매스 전환에서 가장 중요한 반응이다. 이러한 관점에서 브뢴스테드 산, 루이스 산 및 이온성 액체를 촉매로 사용한 수많은 5-하이드록시 푸르푸랄의 생산 방법이 보고되었다. 기술된 촉매들의 단점을 해결하기 위해 폴리스티렌과 그래핀 옥사이드에 각각 NHC-Fe 활성점을 고정하여 철 촉매를 합성하였다. 안정적이고 강한 금속-리간드 결합을 가지는 NHC-Fe 복합체는 매우 효과적인 활성점으로 작용할 수 있다. 폴리스티렌에 고정된 NHC-Fe 촉매는 상용 촉매에 비해 우수한 프록토오스 탈수화 활성을 보였다 (Turnover frequency,= 15 h^{-1}). 그래핀 옥사이드에 고정된 NHC-Fe 촉매는 폴리스티렌에 고정된 NHC-Fe 촉매보다 더 뛰어난 활성을 보여주었다 (Turnover frequency,= 15 h^{-1}). 게다가 이 NHC-Fe 촉매들은 촉매 활성의 손실 없이 최소 5회 이상의 재사용

이 가능하였다.

두번째 장에서는 불균일계 루테늄 촉매를 이용한 5-하이드록시메틸 푸르푸랄 유도체의 합성에 대해 기술하였다. 2,5-퓨란디카르복실산, 2,5-bis(하이드록시메틸)퓨란과 같은 5-하이드록시메틸 푸르푸랄의 유도체는 높은 활용도로 인해 많은 주목을 받고 있다. 기술한 유도체의 효과적인 합성하고자 금속의 촉매적 성능을 향상시키는 독특한 표면 성질을 가지는 산화지르코늄을 고체상 지지체로 선택하였다. 표면에 고르게 분포되어있는 루테늄 활성점을 가지는 산화지르코늄 촉매는 루테늄(0) 이나 산화루테늄(RuO_2) 나노입자의 형성 없이 성공적으로 합성되었다. 합성된 촉매는 5-하이드록시메틸 푸르푸랄의 수소첨가 및 산화 반응에 매우 뛰어난 활성을 보여주었다. 루테늄 활성점이 고정된 산화지르코늄 촉매는 분자 산소를 산화제로 사용하여 5-하이드록시메틸 푸르푸랄을 높은 수율로 2,5-퓨란디카르복실 산으로 전환하였다 (71%). 또한 수소가스 가압 조건에서 5-하이드록시메틸 푸르푸랄을 매우 뛰어난 수율로 2,5-bis(하이드록시메틸)퓨란으로 전환하였다 (99 %). 게다가 이 촉매는 10번

의 재사용과정에서 촉매활성의 손실을 보이지 않았다.

주요어: 그린 화학, 바이오매스 전환, 불균일계 촉매, 프록토오스 탈수화, 불균일계 철 촉매, 불균일계 루테늄 촉매 5-하이드록시메틸 푸르푸랄 산화반응, 5-하이드록시메틸 푸르푸랄 수소첨가반응, 분자 산소, 2,5-퓨란디카르복실 산, 2,5-bis(하이드록시메틸)퓨란

학번: 2010-20985